



**Development of an Equation for Evaluating Hydraulic Erosive Parameter of Unlined Dam
Spillways Considering Surface Irregularities and Geometrical Parameters**

By

Yavar Jalili Kashtiban

**Under supervision of Prof. Ali Saeidi and co-supervision of Prof. Marie-Isabelle Farinas and Dr.
Marco Quirion**

**Thesis presented to the University of Quebec at Chicoutimi with a view to obtaining the degree
of Doctor of Philosophy (PhD) in engineering (Civil)**

Defended on 1st December 2023

BOARD OF EXAMINERS:

Prof. Romain Chesnaux, Department of Applied Sciences at UQAC, President of the Board

Prof. Saad Bennis, Department of Construction Engineering at ÉTS, External Member of the Board

Prof. Eric Villeneuve, Department of Applied Sciences at UQAC, Internal Member of the Board

Québec, Canada
© Yavar Jalili Kashtiban, 2023

RÉSUMÉ

L'érosion des massifs rocheux en aval des barrages et des structures hydrauliques est devenue une préoccupation majeure en matière de sécurité des barrages. Cette étude offre une revue complète des mécanismes d'érosion et des méthodes d'évaluation dans le contexte de l'érosion potentielle des massifs rocheux. Diverses approches théoriques, semi-théoriques, semi-analytiques et numériques sont examinées, avec des méthodes semi-théoriques établissant des corrélations entre l'intensité de l'écoulement des fluides et la capacité de résistance des roches, et des méthodes semi-analytiques se concentrant sur l'interaction entre les massifs rocheux et l'eau. Bien que les méthodes numériques fournissent des informations précieuses, elles présentent des défis dans la définition du paramètre érosif et l'application des paramètres hydrauliques aux surfaces des évacuateurs. Notamment, l'effet des irrégularités de la surface rocheuse n'est pas pris en compte dans la définition du paramètre érosif hydraulique pour combler cette lacune, l'étude examine l'influence des irrégularités de surface dans les évacuateurs de barrages sans revêtement sur les paramètres hydrauliques. La dynamique des fluides numérique (CFD) est utilisée pour analyser 25 configurations d'irrégularités de surface d'évacuateurs et leur impact sur la pression, la contrainte de cisaillement, la vitesse d'écoulement et l'énergie. Les résultats révèlent que les irrégularités affectent ces paramètres hydrauliques, avec une hauteur d'irrégularité accrue entraînant une diminution de la vitesse maximale, de la pression totale et de la contrainte de cisaillement, tandis que la perte d'énergie totale et la vulnérabilité à l'érosion augmentent. Après avoir examiné les effets des irrégularités, l'étude se concentre sur l'exactitude de l'équation de dissipation de puissance spécifique (USPD) existante pour prédire les taux de dissipation d'énergie dans les évacuateurs de barrages sans revêtement. Une équation améliorée pour l'USPD est proposée, en tenant compte des irrégularités de surface et de la géométrie des évacuateurs sans revêtement. Il est constaté que les paramètres géométriques et les irrégularités de surface influencent l'exactitude de l'équation, et des modifications sont suggérées pour améliorer ses capacités prédictives, ce qui se traduit par des estimations améliorées des taux de dissipation d'énergie. Ces avancées ont des implications pratiques pour la conception et la maintenance des évacuateurs, favorisant le développement de systèmes de gestion de l'eau plus sûrs et plus efficaces. En résumé, cette étude offre des perspectives précieuses sur les mécanismes d'érosion, les méthodes d'évaluation, l'influence des irrégularités de surface et les améliorations apportées à l'équation USPD pour évaluer l'érosion des masses rocheuses dans les évacuateurs sans revêtement. Ces résultats améliorent notre compréhension des processus d'érosion et facilitent des évaluations plus précises pour la conception et la gestion des structures hydrauliques.

Mots clés: barrage, structures hydrauliques, érodibilité, les évacuateurs sans revêtement, dynamique des fluides numérique (CFD), unité de puissance hydraulique spécifique (USPD), massif rocheux.

ABSTRACT

Rock mass erosion downstream of dams and hydraulic structures has been as a significant concern for dam safety. This study offers a comprehensive review of erosion mechanisms and assessment methods in the context of potential rock mass erosion. Various theoretical, semi-theoretical, semi-analytical, and numerical approaches are examined, with semi-theoretical methods establishing correlations between fluid flow intensity and rock resistive capacity, and semi-analytical methods focusing on the interaction between rock mass and water. While numerical methods provide insights, they present challenges in defining the erosive parameter and applying hydraulic parameters to spillway surfaces. Notably, the consideration of rock surface irregularities' effect on the hydraulic erosive parameter has been lacking. To address this gap, the study investigates the influence of surface irregularities in unlined dam spillways on hydraulic parameters. Computational fluid dynamics (CFD) is used to analyze 25 configurations of spillway surface irregularities and their impact on pressure, shear stress, flow velocity, and energy. Findings reveal that irregularities affect these hydraulic parameters, with increased irregularity height leading to decreased maximum velocity, total pressure, and shear stress, while total energy loss and vulnerability to erosion increase. Following the examination of irregularity effects, the study focuses on the accuracy of the existing unit stream power dissipation (USPD) equation for predicting energy dissipation rates in unlined dam spillways. An improved equation for USPD is proposed, considering surface irregularities and the geometry of unlined spillways. Geometrical parameters and surface irregularities are found to influence the equation's accuracy, and modifications are suggested to enhance its predictive capabilities, resulting in improved estimates of energy dissipation rates. These advancements have practical implications for spillway design and maintenance, promoting the development of safer and more efficient water management systems. In summary, this study provides valuable insights into erosion mechanisms, assessment methods, the influence of surface irregularities, and enhancements to the USPD equation for evaluating rock mass erosion in unlined spillways. These findings enhance our understanding of erosion processes and facilitate more accurate assessments for the design and management of hydraulic structures.

Keywords: dam, hydraulic structures, erodibility, scour, unlined spillways, plunge pools, computational fluid dynamics, USPD, rock mass

TABLE OF CONTENTS

RÉSUMÉ	ii
ABSTRACT.....	iii
TABLE OF CONTENTS.....	iv
LIST OF TABLES	vii
LIST OF FIGURES	viii
LIST OF SYMBOLS	x
LIST OF ABBREVIATIONS.....	xv
DEDICATION.....	xvi
ACKNOWLEDGMENTS	xvii
CHAPTER 1	1
INTRODUCTION.....	1
1.1 Statement of the problem	1
1.2 Research objectives.....	3
1.3 Research methodology.....	3
1.4 Originality and contribution.....	5
1.5 Thesis outline	7
CHAPTER 2	8
Article 1: A Review on Existing Methods to Assess Hydraulic Erodibility Downstream of Dam Spillways.....	8
2.1 Highlights.....	9
2.2 Abstract.....	9
2.3 Introduction.....	10
2.4 Scour prediction approaches	12
2.4.1 Comparative Methods based on Resistance of Materials for Erosion and Rate of Energy Dissipation.....	12
2.4.1.1 Background of the Comparative Methods Base on Kirsten’s Index.....	16
2.4.1.2 Background of Pells’ Methods.....	18
2.4.1.3 Discussion of EIM and Pells’ Methods.....	19
2.4.2 Semi-Theoretical Methods for Computing Scour of the Plunge Pools.....	19
2.5 Semi-Analytical methods.....	21
2.5.1 CFM.....	26
2.5.2 DI Method.....	30
2.5.3 QSI Method.....	36

2.6 Scouring at the Multiblock System with Numerical Methods	41
2.7 Critical Analysis and Application of Different Approaches on Real Cases	45
2.8 Summary and Discussion.....	47
2.9 Conclusions and Potential Future Research Direction.....	50
CHAPTER 3	51
Article 2: Evaluation of the effect of surface irregularities on the hydraulic parameters within unlined dam spillways.....	51
3.1 Abstract.....	52
3.2 Highlights.....	52
3.3 Introduction.....	53
3.4 Materials and Methods.....	57
3.4.1 Determining model geometry	59
3.4.1.1 Step 1: Blasting effect on the profile of surface irregularities	59
3.4.1.2 Step 2: Selection of geometries for unlined surface profiles	60
3.4.2 Numerical modeling.....	62
3.4.2.1 Step 1: Model geometry and boundary conditions	64
3.4.2.2 Step 2: Meshing and convergence analysis.....	64
3.4.2.3 Step 3: Model setup (VOF method, turbulence model, control equation)	65
3.5 Results.....	66
3.5.1 Effect of irregularities on velocity	67
3.5.2 Effect of irregularities on total pressure (P_T)	70
3.5.3 Effect of irregularities on shear stress.....	73
3.5.4 Effect of irregularities on the energy gradient	74
3.6 Discussion.....	78
3.7 Conclusions.....	79
CHAPTER 4	80
Article 3: Modification of the unit stream power dissipation (USPD) equation for unlined spillways considering geometrical parameters and surface irregularities.....	80
4.1 Abstract.....	81
4.2 Highlights.....	81
4.3 Introduction.....	81
4.4 Methodology	85
4.4.1 Identification and selection of effective geometric parameters	86
4.4.2 Model geometry	87

4.4.3 Numerical modeling.....	88
4.5 Results and modification of the USPD equation	89
4.5.1 Effects of irregularities on maximum and average velocities	91
4.5.2 Effects of irregularities on maximum velocity head ($H_{V, \max}$).....	92
4.5.3 Effects of irregularities on average velocity head ($H_{V, \text{ave}}$).....	93
4.5.4 Effects of irregularities on pressure head and position head ($H_p + Z$)	94
4.5.5 Sequential approach for modifying the USPD: A stepwise approach	95
4.5.5.1 Development of $H_{V, \max}$, $H_{V, \text{ave}}$, and (H_p+Z) equation as functions of α_1 , h , and x , respectively	95
4.5.5.2 Effects of the spillway slope (β) on developed equations for $H_{V, \max}$, $H_{V, \text{ave}}$, V_{\max} , V_{ave} , and ($H_p + Z$).....	99
4.6 Cross validation, comparison, and practicality	102
4.7 Conclusions.....	103
CHAPTER 5	105
Discussion and conclusion.....	105
5.1 Discussion.....	105
5.2 Conclusion	107
5.3 Perspectives for future research	109
REFERENCES	111
PUBLICATIONS	120
Appendix A: Supplementary data of article 1	121

LIST OF TABLES

Table 2-1. Classification of the erosion extent	16
Table 2-2. Scour threshold equations by different researchers.....	17
Table 2-3. Classification of erosion proposed by Pells [1].....	18
Table 2-4. General scour formulae.....	20
Table 2-5. Coefficients of five simplified scour formulae.....	20
Table 2-6. Symbol notation list of the plunge pool semi-theoretical method.....	21
Table 2-7. The range of T_u due to the type of outlet structure (left side) [61]; polynomial and regression coefficients for various T_u (right side) [62].....	25
Table 2-8. Input and output parameters of the falling jet and plunge pool modules [59].	25
Table 2-9. Conditions for computing the amplification factor ($\Gamma +$) [63].....	26
Table 2-10. Parameters of Equations (2-22) and (2-23) for the in situ fracture toughness value $K_{I,ins}$ [59].....	28
Table 2-11. Net uplift stagnation pressures for the various setups of block projection and joint points [82].....	39
Table 2-12. Upstream and downstream strayed pieces of the absolute discharge rate for various points of impingement δ ..	40
Table 2-13. Hydraulic geometrical characteristics of the experiments.....	41
Table 2-14. Advantages and disadvantages of the various approaches.....	48
Table 2-15. Detailed information references about erosion or scour in spillways, plunge pools, rivers, and gullies.	49
Table 3-1. Existing hydraulic erosive indices.....	55
Table 3-2. Input parameters used in the computational fluid dynamics (CFD) modeling.....	63
Table 3-3. Grid independence study at the last irregularity	64
Table 4-1. Existing hydraulic erosion indices	84
Table 4-2. Input parameters used in the computational fluid dynamics (CFD) modeling.....	89
Table 4-3. Grid independence study at the last irregularity	89
Table 4-4. Angle factors of the HV, max graphs	96
Table 4-5. New y-intercepts produced on the basis of a_{ave}	96
Table 4-6. The coefficients of various normalized angles on the basis of the tangent function of the slope angle, β	100
Table 4-7. Comparison of the energy results as determined using our novel equation and those of the Pells equation.....	102
Table 5-1. Advantages and disadvantages of the various approaches.	106
Table A1. Result of the application of various semi-theoretical approaches on several case studies.....	121

LIST OF FIGURES

Fig. 1-1. The methodology for reaching to the main and sub-objectives of this thesis.....	5
Fig. 2-1. Main mechanical processes of rock erosion and the occurrence timescale [3].	10
Fig. 2-2. Classifications of the scour prediction methods	12
Fig. 2-3. (a) Variation of properties over a differential flow section in an open channel. (b) Cross-sectional view of the flow channel [19].....	14
Fig. 2-4. (a) Original dataset as presented in the study of Van Schalkwyk [24]; (b) after inclusion of data from Moore [24]; (c) scour threshold line presented by Annandale; (d) comparison of scour threshold lines.	17
Fig. 2-5. (a) Erosion classes determined according to the eGSI index; (b) erosion classes determined according to the RMEI index [39].....	18
Fig. 2-6. Scheme of scour in semi-theoretical methods [50].	21
Fig. 2-7. Description of CSM.	23
Fig. 2-8. Main physical processes used for computation of rock scour (CSM) [59,60].	24
Fig. 2-9. (a) Diversity of the mean dynamic pressure coefficient (along the jet centre line) as a performance of the dimensionless ratio of YD_j [55]; (b) nondimensional root-mean-square dynamic pressure coefficient for jet velocities higher than 20 m/s [62]......	25
Fig. 2-10. Encountered rock mass layer circumstances for (a) irregularly and (b) totally jointed rocks; (c) proposed structure for the essential geometrical designs of the discontinuously jointed rock [59]......	27
Fig. 2-11. CFM flowchart.....	30
Fig. 2-12. DI flowchart	31
Fig. 2-13. Conceptualisation of impulse dynamics on a block, based on the Bollaert DI method [59].	32
Fig. 2-14. Proposed criteria to evaluate the rock scour potential by DI [63,70].	35
Fig. 2-15. (a) Plane jet deflection on a flat bottom and wall jet velocity profiles; (b) effective forces on block uplift.....	37
Fig. 2-16. QSI flowchart	38
Fig. 2-17. Flowchart of the numerical approach.	42
Fig. 2-18. Two-dimensional ejectable blocks in an unlined spillway [88]......	43
Fig. 2-19. Numerical simulation of plunge pool scour [91]......	44
Fig. 2-20. Schematic of the spillway and removable block geometry for reliability analysis [83]......	45
Fig. 2-21. (a) The percentage of poorly estimated cases for each approach. (b) Committed errors of various methods according to different erosion classes. (c) Over- and underestimation rates of various semi-theoretical approaches.....	46
Fig. 3-1. Mechanisms of rock mass erosion [118, 119]......	53
Fig. 3-2. Flowchart presenting the steps of modeling spillway for assessing the effect of irregularity geometry on hydraulic parameters	58
Fig. 3-3. (a) Diagram of an unlined dam spillway; (b) channel view from above; (c) controlled-blasting pattern of the channel showing spacing and burden; and (d) channel surface profile after blasting	60
Fig. 3-4. The assumed spillway geometry used in our model of irregularities along an unlined rock spillway	62
Fig. 3-5. Configurations of the various modeled spillway surface irregularities	62
Fig. 3-6. Diagram of the numerical modeling and the applied meshing	65
Fig. 3-7. The volume fraction of water, dynamic pressure contour, and total pressure contour.....	67
Fig. 3-8. Maximum velocity profiles of the flow along the unlined spillway; (a) $\alpha_1 = 12^\circ$; (b) $\alpha_1 = 19^\circ$; (c) $\alpha_1 = 26^\circ$; (d) $\alpha_1 = 33^\circ$; (e) $\alpha_1 = 40^\circ$	68
Fig. 3-9. Velocity profiles as a function of flow depth for various irregularity heights; a flow depth of 0 m refers to the channel bottom; (a) $\alpha_1 = 12^\circ$; (b) $\alpha_1 = 19^\circ$; (c) $\alpha_1 = 26^\circ$; (d) $\alpha_1 = 33^\circ$; (e) $\alpha_1 = 40^\circ$; (f) the analyzed section of the channel profile (red line)	69
Fig. 3-10. Total pressure (sum of dynamic and static pressures) profile along the water–rock interface for the configuration $\alpha_1 = 19^\circ$ and $h = 10$ cm; red line describes the upper bound of the graph	71
Fig. 3-11. Total pressure (static and dynamic pressure) profiles on water–rock interface as a function of spillway length for various irregularity heights and angles; (a) $\alpha_1 = 12^\circ$; (b) $\alpha_1 = 19^\circ$; (c) $\alpha_1 = 26^\circ$; (d) $\alpha_1 = 33^\circ$; and (e) $\alpha_1 = 40^\circ$; (f) the analyzed section of the channel profile (red line).....	72
Fig. 3-12. Total pressure profiles on the water surface as a function of spillway length for various irregularity heights; (a) $\alpha_1 = 12^\circ$; (b) $\alpha_1 = 19^\circ$; (c) $\alpha_1 = 26^\circ$; (d) $\alpha_1 = 33^\circ$; and (e) $\alpha_1 = 40^\circ$	73
Fig. 3-13. Shear stress along the water–rock interface for an irregularity angle of $\alpha_1 = 12^\circ$	74
Fig. 3-14. Calculation of energy at the water–rock interface and water surface.....	75
Fig. 3-15. Energy gradient profiles at the water–rock interface; (a) $\alpha_1 = 12^\circ$; (b) $\alpha_1 = 19^\circ$; (c) $\alpha_1 = 26^\circ$; (d) $\alpha_1 = 33^\circ$; and (e) $\alpha_1 = 40^\circ$	76

Fig. 3-16. Energy gradient profiles along the water surface; (a) $\alpha_1 = 12^\circ$; (b) $\alpha_1 = 19^\circ$; (c) $\alpha_1 = 26^\circ$; (d) $\alpha_1 = 33^\circ$; and (e) $\alpha_1 = 40^\circ$.	77
Fig. 4-1. Fundamental basis of hydraulic erodibility	82
Fig. 4-2. Flowchart of the modification of USPD equation taking into account irregularity geometry	86
Fig. 4-3. Assumed spillway geometry used in our model of irregularities along an unlined rock spillway, and boundary conditions of the computational fluid dynamics (CFD) modeling	88
Fig. 4-4. Configurations of the various modeled spillway surface irregularities	88
Fig. 4-5. Calculation of energy at the water surface and location of the average velocity measurement	90
Fig. 4-6. Maximum velocity profiles of flow along the unlined spillway	92
Fig. 4-7. Maximum velocity head profiles of flow along the unlined spillway	93
Fig. 4-8. Average velocity head profiles of the flow along the unlined spillway	94
Fig. 4-9. Profiles of the (HP+Z) along the unlined spillway	95
Fig. 4-10. Relationship between $c\alpha_1$, h and irregularity height (h)	96
Fig. 4-11. Correlation between $\tan(\alpha_1)$ and the new y-intercepts of the angle factor graphs	97
Fig. 4-12. Methodology for modifying the USPD on the basis of irregularity height and angle (α_1 and h)	98
Fig. 4-13. Simulation results for $H_{V,max}$ as a function of distance	99
Fig. 4-14. Relationship between the coefficient of the normalized angle factors of $H_{V,max}$ and the unlined spillway slope (β)	100
Fig. 4-15. Methodology to modify the USPD for application on an unlined spillway slope (β)	101
Fig. 4-16. Comparison of model outputs run using heterogeneous and homogeneous irregularities	103

LIST OF SYMBOLS

- a_a : Volume fraction of air
- a_w : Volume fraction of water
- a_{ave} : Average angle factors of the Fig. 4-10 graphs
- a_{α_1} : Angle factors of the Fig. 4-10 graphs
- α_1 : Angle between the front face of the irregularity and the channel's overall slope ($^\circ$)
- α_2 : Angle between the irregularity's back surface and the channel's overall slope ($^\circ$)
- B: Burden (m)
- b_{α_1} : Y-intercepts of the Fig. 4-10 graphs
- $b_{\alpha_{1,n}}$: Normalized intercepts of the Fig. 4-10 graphs
- B_f : Width of the spillway surface (m)
- c: Mean pressure wave celerity ($m \cdot s^{-1}$)
- c_{α_1} : Angle factors of the Fig. 4-9 graphs
- C_1 : Nondimensional dynamic impulsion coefficient
- C_{1c} : Constant (1) in the turbulence model equation
- C_{2c} : Constant (2) in the turbulence model equation
- C_{uplift} : Uplift pressure coefficient
- D: Disturbance factor
- d: Water depth (m)
- D_i : Jet diameter at issuance from the dam (m)
- D_j : Jet diameter at impacting point of plunge pool (m)
- D_{50} : Median grain size (m)
- $\frac{dE}{dx}$: Energy gradient
- e_f : The length of the block against the direction of the flow (m)
- e_b : The length of the block in the direction of the flow (m)

E: Energy (m)

$E_{\text{Annandale}}$: Energy used in the Annandale equation (in the SP equation) (m)

E_i : Young's modulus of intact rock (GPa)

E_{modified} : Energy used in the current study (in the USPD equation) (m)

E_{Pells} : Energy used in the Pells equation (in the USPD equation) (m)

E_{rm} : Rock mass deformation modulus (GPa)

$E_{\text{water surface}}$: Energy at the water surface (m)

$E_{\text{water-rock interface}}$: Energy at the channel bottom (at the water-rock interface) (m)

f: Frequency or boundary correction factor (Hz)

F_L : Lifting Force (N)

F_O : Force over the block (kN)

F_{QSL} : Quasi-steady lifting force (N)

βR : Dimensionless coefficient related to energy dissipation by turbulence

Fr: Froude number

F_{sh} : Shear force (kN)

F_u : Force of the fluid particle in the x direction (N)

F_{un} : Force under the block (kN)

F_y : Force of the fluid particle in the y direction (N)

g: Gravitational acceleration ($\text{m}\cdot\text{s}^{-2}$)

G_b : Submerged weight (kN)

G_k : Turbulent kinetic energy production

h: Irregularity height (m)

H_f : Friction energy loss (m)

H_p : Pressure head at the channel bottom (at the water-rock interface) (m)

H_{p_i} : Initial pressure head at the (m)

$H_{p,\text{WRI}}$: Pressure head at the channel bottom (at the water-rock interface) (m)

$H_{P,WS}$: Pressure head at the water surface (m)

$H_{V,ave}$: Average velocity head along water depth (m)

$H_{Vi,ave}$: Initial average velocity head along water depth (m)

$H_{V,max}$: Maximum velocity head within the water depth (m)

$H_{Vi,max}$: Initial maximum velocity head within the water depth (m)

$H_{V,WRI}$: Velocity head at the channel bottom (at the water–rock interface) (m)

$H_{V,WS}$: Velocity head at the water surface (m)

$I_{impulse}$: Dynamic impulse ($kg \cdot m \cdot s^{-1}$)

J_a : Joint surface alteration number

J_n : Joint set number

J_o : Joint opening (mm)

J_r : Joint roughness number

J_s : Relative block structure

k : Turbulent kinetic energy ($m^2 \cdot s^{-2}$)

K_b : Rock block size number

K_d : Joint shear strength number

K_I : Stress intensity ($MPa \cdot m^{-1/2}$)

L : Spillway length (m)

L_f : Total length of fracture (m)

q : Unit discharge, the volumetric discharge per unit width of the channel ($m^2 \cdot s^{-1}$)

l : Irregularity length (m)

L_{Block} : Rock block length (m)

m : Rock mass (kg)

M_s : Compressive strength number

N : Kirsten's index

n : Manning's n

P_a : Available hydraulic stream power (kW/m^2)
 P_D : Dynamic pressure (Pa)
 $P_{D, \text{ channel bottom}}$: Dynamic pressure at the channel bottom (at water–rock interface) (m)
 $P_{D, \text{ water surface}}$: Dynamic pressure at the water surface (m)
 P_{max} : Maximum instantaneous fluctuating head (m)
 P_S : Static pressure (Pa)
 $P_{S, \text{ channel bottom}}$: Static pressure at the channel bottom (at the water–rock interface) (m)
 P_T : Total pressure (Pa)
 $P_{T, \text{ max}}$: Maximum total pressure (m)
 $P_{(b)}, P_{(w)}$: Wetted perimeter of the bed and side walls of the flow channel
 Q : Water flow rate ($\text{m}^3 \cdot \text{s}^{-1}$)
 Q_c : Critical discharge ($\text{m}^3 \cdot \text{s}^{-1}$)
 R_H : Hydraulic radius (m)
 S : Spacing (m)
 S_f : Friction slope, the gradient of the total hydraulic energy line
 T : Uniaxial tensile strength of rock (MPa)
 T_u : Longitudinal jet turbulence intensity (%)
 T_{up} : Nondimensional time coefficient
 u_i : Velocity components of fluid particle in the x direction ($\text{m} \cdot \text{s}^{-1}$)
 V : Flow velocity ($\text{m} \cdot \text{s}^{-1}$)
 V_{ave} : Average flow velocity ($\text{m} \cdot \text{s}^{-1}$)
 V_b : Rock block volume (m^3)
 V_i : Mean jet velocity at issuance from the dam ($\text{m} \cdot \text{s}^{-1}$)
 V_j : Mean jet velocity at impacting point of plunge pool ($\text{m} \cdot \text{s}^{-1}$)
 V_{max} : Maximum flow velocity ($\text{m} \cdot \text{s}^{-1}$)

$V_{x,max}$: Maximum flow velocity in the x direction ($m \cdot s^{-1}$)

$V_{\Delta t pulse}$: Block uplift velocity ($m \cdot s^{-1}$)

x: Distance (m)

X_i : Coordination

Y: Total plunge pool water depth (m)

Z: Elevation above a datum (m)

Z_b : Block uplifting height (m)

Z_{WRI} : Elevation above a datum up to the channel bottom (m)

Z_{WS} : Elevation above a datum up to the water surface (m)

(% SF_w): Percentage of the shear force

β : Spillway slope ($^\circ$)

δ_o : Boundary layer thickness (m)

σ_{ci} : Uniaxial compressive strength (MPa)

τ_o : Shear stress at threshold velocity (Pa)

τ_b : Shear stress (Pa)

θ : Angle between the side wall and the water surface ($^\circ$)

ν : Kinematic viscosity ($m \cdot s^{-1}$)

ϵ : Energy dissipation rate ($kg \cdot m^2 \cdot s^{-2}$)

μ : Hydrodynamic viscosity coefficient ($N \cdot s \cdot m^{-2}$)

μ_{eff} : Effective dynamic viscosity coefficient ($N \cdot s \cdot m^{-2}$)

ρ : Water density ($kg \cdot m^{-3}$)

γ : Specific weight ($kN \cdot m^{-3}$)

γ_s : Unit weight of rock or particle ($N \cdot m^{-3}$)

LIST OF ABBREVIATIONS

XML: Extensible Markup Language

E_{doa} : Adjustment erosion, discontinuity orientation

eGSI: Erodibility geological strength index

GSI: Geological strength index

LF: Likelihood factor

NPES: Nature of the potentially eroding surface

RF: Relative importance factor

RMEI: Rock mass erosion index

RMR: Rock mass rating system

RMSE: Root mean square error

RQD: Rock quality designation

UCS: Unconfined compressive strength (MPa)

USPD: Unit stream power dissipation of water ($\text{kW}\cdot\text{m}^{-2}$)

$\text{USPD}_{\text{equation}}$: Unit stream power dissipation of water (based on the modified equation) ($\text{kW}\cdot\text{m}^{-2}$)

$\text{USPD}_{\text{software}}$: Unit stream power dissipation of water (based on the software results) ($\text{kW}\cdot\text{m}^{-2}$)

DEDICATION

To My Pillar of Strength, Laya,

In appreciation of Laya, whose love and strength have sustained me through this academic journey. Your presence has made the impossible feel achievable.

“À Mon Pilier de Force, Laya,

En appréciation de Laya, dont l'amour et la force m'ont soutenu tout au long de ce parcours académique. Ta présence a rendu l'impossible réalisable.”

ACKNOWLEDGMENTS

I am deeply grateful to all those who have contributed to the completion of this research journey, providing guidance, support, and encouragement along the way.

Foremost, I extend my heartfelt gratitude to my PhD supervisor, Prof. Ali Saeidi, whose expert guidance, unwavering patience, and insightful feedback have been invaluable in shaping the trajectory of this work. His mentorship has been pivotal in my academic growth.

I also wish to acknowledge my co-supervisors, Prof. Marie-Isabelle Farinas and Dr. Marco Quirion, whose collaborative expertise and constructive insights enriched the depth and quality of this study. Their combined mentorship played a significant role in broadening my perspectives.

A special note of appreciation goes to my industrial advisor, Mr. Javier Patarroyo, whose real-world insights and industry experience provided a practical dimension to my research.

I would like to express my gratitude to the members of the examination board for their valuable comments and assistance in enhancing the quality of this project. Special thanks to Prof. Saad Bennis from ETS, Prof. Romain Chesnaux and Prof. Éric Villeneuve from UQAC, as well as Prof. Duygu Kocaefe, also from UQAC.

I would like to express my gratitude to the members of the examination board for their valuable comments and assistance in enhancing the quality of this project. Special thanks to Prof. Saad Bennis from ETS, Prof. Romain Chesnaux and Prof. Éric Villeneuve from UQAC, as well as Prof. Duygu Kocaefe, also from UQAC.

This research project would not have been possible without the generous financial support from UQAC, Hydro-Quebec, NSERC, the Canadian Geotechnical Society, and UNIPER. Their funding and scholarships not only facilitated the progress of this research but also highlighted their commitment to advancing academic exploration.

I extend my gratitude to my family and friends for their unwavering support and encouragement. Your belief in me and your patience during the challenging times were a constant source of strength.

In conclusion, the completion of this research stands as a testament to the collaborative efforts and support of many individuals and organizations. Your contributions have been vital in transforming this endeavor from a mere idea to a tangible reality.

With profound appreciation,
Yavar Jalili Kashtiban

CHAPTER 1

INTRODUCTION

1.1 STATEMENT OF THE PROBLEM

Since the 1930s, numerous methods have been proposed to predict the hydraulic erodibility of materials, with a focus on soils, granular materials, and diving jet cases. However, the assessment of hydraulic erodibility for rock masses in unlined spillways (open channels) has received limited attention. The study of erodibility in spillways and scour in plunge pools involves two crucial aspects: geomechanical and hydraulic considerations. An unlined spillway is a spillway structure devoid of a protective lining, depending on natural materials to guide upstream water away from a dam or reservoir. The absence of a man-made coating distinguishes it from lined spillways, exposing it to potential erosion. Scour, on the other hand, describes the erosion of sediment from a spillways or riverbed caused by the force of flowing water. It commonly occurs around structures like bridge piers, abutments or other hydraulic structures, influencing the stability of these features. A plunge pool, in contrast, is a basin that forms at the base of a waterfall or downstream of a dam spillway due to the erosive forces of falling water. This basin helps dissipate the energy of the descending water, preventing further erosion and contributing to the overall geomorphology of the watercourse. A review of the literature reveals that various parameters have been used in erosion studies, including the velocity of flowing water (V), shear stress on the rock surface (τ_b), unit stream power dissipation of water (Π_{UD}), stress intensity (K_I), and lifting force (F_L). However, there is a lack of a unified method to determine the erosive parameter of water for evaluating rock mass erodibility. Existing methods also suffer from limitations, as they are applicable only in specific cases. For instance, equations exist to determine the unit stream power dissipation of water (Π_{UD}), which is based on internal flow conditions. However, the application of these equations to unlined spillways remains uncertain. Stress intensity (K_I), initially developed for metallurgical cases, is solely used to assess crack propagation in intact rocks, rather than rock masses. Additionally, the stress intensity (K_I) employed in Bollaert's method relies on the maximum pressure in pool bottoms, but it cannot accurately determine the pressure applied to joint tips. Furthermore, there is a lack of developments specific to unlined spillway structures. Considering previous studies, it is evident that comprehensive evaluations of the geometrical parameters of rock masses and unlined spillways are lacking. In engineering, a comprehensive grasp of geometric parameters is indispensable for assessing both stability and functionality. When examining discontinuities, critical parameters such as orientation, spacing, persistence, and roughness provide valuable insights into the behavior of geological formations. Additionally, understanding the geometric parameters of surface irregularities, including irregularity length, height, and angle, further contributes to this assessment. Simultaneously, the design and analysis of water management infrastructure, exemplified by unlined spillways, necessitate considerations of

slope, length, width, and crest elevation. These parameters collectively guide the engineering process, ensuring not only the stability of geological formations but also effective water conveyance. Understanding the effect of various unlined spillway geometries, including water-rock interface and channel bottom profiles, on hydraulic parameters is crucial. Additionally, the influence of surface irregularities on erosive forces and the overall behavior of water flow in unlined spillways needs to be explored.

To address these gaps, several key questions must be explored:

- 1) What impact do surface irregularities in unlined spillways have on hydraulic parameters such as pressures, stress, flow velocity, and energy?
- 2) How do the geometric characteristics of irregularities relate to the hydraulic parameters?
- 3) How do these irregularities influence the unit stream power dissipation (USPD) equation?

By addressing these questions, we can gain valuable insights into the influence of surface irregularities on erosive forces and the overall behavior of water flow in unlined spillways. This knowledge is crucial for enhancing our understanding of hydraulic erodibility and optimizing the design and management of hydraulic structure considering geometrical parameters of the unlined spillways and rock surface. Moreover, this research seeks to enhance the design of unlined spillways by accounting for the geometric features of both the rock surface and the unlined spillways themselves. This is crucial because the irregularities in the rock surface geometry can directly impact hydraulic parameters and, consequently, influence the design process. Ultimately, the intention is to elevate the overall design quality and performance of unlined dam spillways. The objective of this thesis is to investigate the influence of surface irregularities on unlined spillways' hydraulic parameters and develop an equation for unit stream power dissipation, considering geometrical parameters. Unlined spillways play a critical role in ensuring dam stability and human safety by facilitating controlled water discharge. The presence of surface irregularities on these spillways can impact hydraulic performance. This research seeks to address the current gap in understanding the effects of such irregularities on hydraulic parameters, aiming to enhance the accuracy of hydraulic erodibility analyses. By developing a comprehensive equation for unit stream power dissipation, incorporating relevant geometrical parameters, this study aims to provide dam engineers with a more accurate tool for assessing and managing the hydraulic performance of unlined spillways. Through these efforts, the importance of considering geometric parameters in spillway design and analysis is emphasized, contributing to the broader goal of enhancing dam safety and reliability.

1.2 RESEARCH OBJECTIVES

To improve the prediction of hydraulic erodibility in dam spillways, this thesis focuses on determining a representative hydraulic erosive parameter and developing an equation that incorporates the geometric parameters of unlined spillways and surface irregularities. The specific objectives of this study are as follows:

- a) Identify the key parameters that exert the most effect on the erosive forces of water in dam spillways.
- b) Evaluate the impact of surface irregularities on the hydraulic parameters of flowing water, with a particular emphasis on the erosive parameter.
- c) Establish a representative hydraulic erosive parameter for spillways by comprehensively considering the effects of surface irregularities.
- d) Develop an equation that accurately represents the hydraulic erosive parameter as a function of spillway surface irregularities.

By accomplishing these specific objectives, this research aims to advance our understanding of hydraulic erodibility in dam spillways within an academic framework. The identification of the primary parameter and the comprehensive analysis of surface irregularities will contribute to more precise assessments and predictions of erosive forces. Furthermore, the development of an equation for the hydraulic erosive parameter will provide a robust tool for engineers and designers to optimize spillway design and implement effective maintenance practices. Ultimately, this academic work will contribute to the advancement of knowledge in the field of dam engineering, enabling the development of safer and more efficient hydraulic structures.

1.3 RESEARCH METHODOLOGY

The specific methodology used to achieve the principal and sub-objectives of this study is briefly illustrated in Fig. 1-1.

This thesis is devoted to the comprehensive assessment of rock scouring phenomena occurring downstream of dams, aiming to develop an equation for evaluating the hydraulic erosive parameter (USPD) while accounting for the presence of rock surface irregularities. The methodology employed in this study is structured into three distinct steps, which are outlined as follows:

- 1) Literature Review and Evaluation of Existing Methods:

- The study begins with a comprehensive literature review to understand the existing methods for assessing and predicting hydraulic erodibility.
- Various theoretical, semi-theoretical, semi-analytical, and numerical approaches are examined and their advantages and disadvantages are analyzed.
- The limitations of the current methods are identified, particularly in terms of their applicability to different situations and their failure to consider important factors such as spillway geometry.
- The need for a unified parameter to measure the erosive capacity of water and account for rock mass erodibility is emphasized.

2) Incorporating Irregularities of Spillway Surfaces:

- A key aspect of this research is to address the irregularities of spillway surfaces and their impact on hydraulic parameters.
- Computational fluid dynamics (CFD) 2D simulations are used to analyze the effects of irregularities on pressure, shear stress, flow velocity, and energy.
- Various spillway surface geometries, including irregularity height and angle, are studied using ANSYS-Fluent software to obtain relevant 2D flow simulation results.
- Correlations between velocity head, pressure head, position head, irregularity angle, irregularity height, and spillway slope are established.

3) Modification of the Unit Stream Power Dissipation (USPD) Equation:

- Building upon the insights gained from the literature review and the analysis of spillway surface irregularities, a modified approach to the USPD equation is proposed.
- Available effective data is analyzed to identify influential geometric parameters of spillways and irregularities.
- An equation is developed to calculate maximum velocity head, average velocity head, maximum velocity, average velocity, pressure head, and position head as functions of distance, irregularity angle, irregularity height, and unlined spillway slope.
- The modified USPD equation is derived based on the developed equations, and the error of the modified equation is determined.

By following this methodology, this thesis aims to contribute to the field of hydraulic erodibility assessment by addressing the limitations of existing methods and incorporating the effects of spillway surface irregularities.

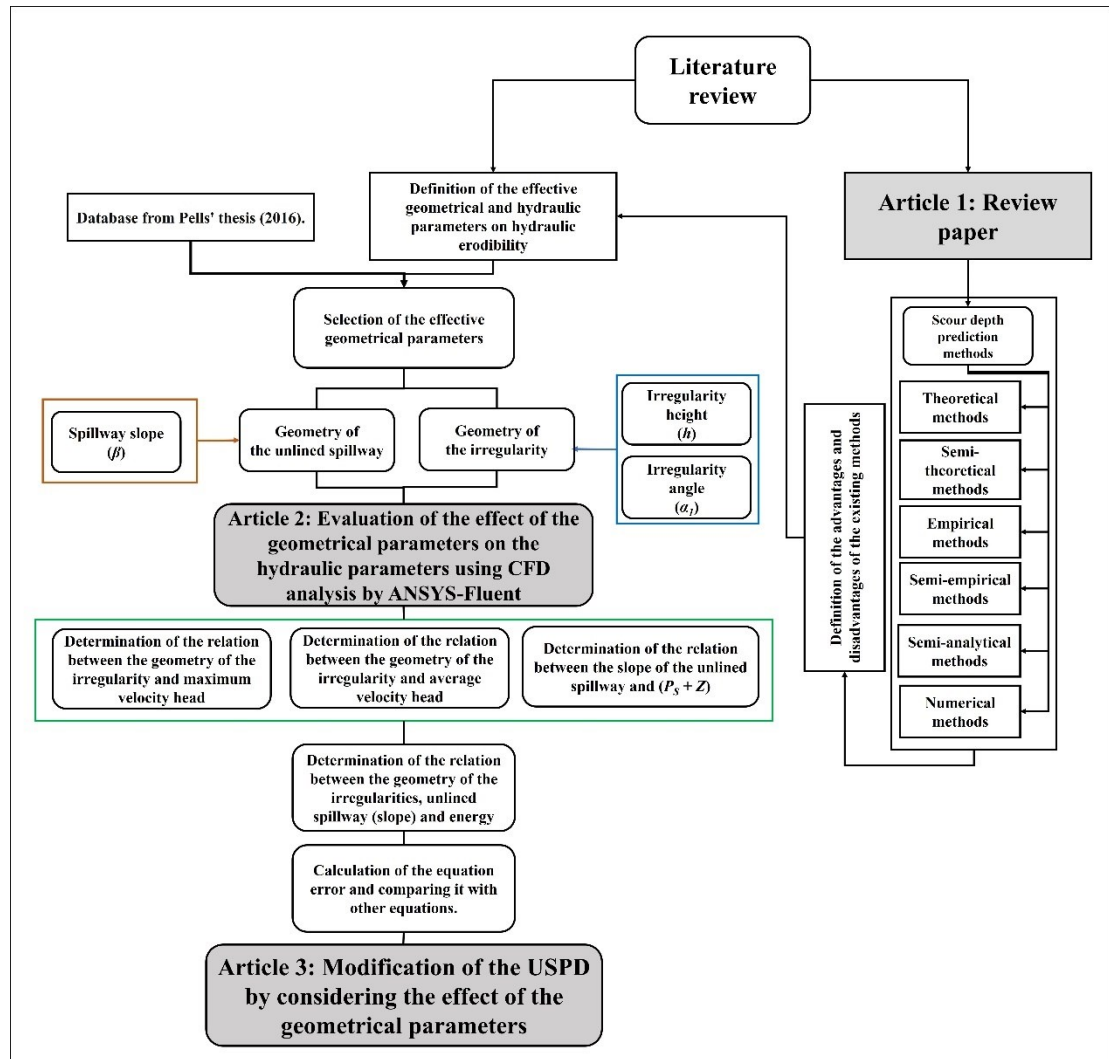


Fig 1-1. The methodology for reaching to the main and sub-objectives of this thesis

1.4 ORIGINALITY AND CONTRIBUTION

The main objective of this thesis is to enhance the accuracy of hydraulic erodibility predictions in dam spillways. This is achieved through the determination of a representative hydraulic erosive parameter and the development of an equation that effectively incorporates the geometric parameters of unlined spillways as well as surface irregularities. The focus of this research is to address the limitations of existing methodologies by refining the estimation of hydraulic erosive behavior, thereby providing more reliable and comprehensive assessments in the context of dam spillways. By considering the geometric characteristics of unlined spillways and incorporating surface irregularities, the proposed equation aims to improve the prediction accuracy of hydraulic erodibility, ultimately contributing to a more robust understanding of erosion processes and facilitating informed decision-making in spillway design and management. The specific contributions of this thesis are outlined as follows:

- The present study makes contributions to the understanding and assessment of hydraulic erodibility in unlined dam spillways. Through a comprehensive review of existing methodologies, the research identifies gaps and limitations in current approaches. By exploring theoretical, semi-theoretical, semi-analytical, and numerical methods, the study provides a comprehensive overview of the advantages and disadvantages associated with each method for evaluating erosion and scouring phenomena.
- One of the key contributions of this research lies in the investigation of the geomechanical and hydraulic aspects of hydraulic erosional phenomena in unlined dam spillways. By recognizing the importance of considering surface irregularities in hydraulic erodibility, the study utilizes computational fluid dynamics (CFD) with ANSYS-Fluent software to analyze various 2D configurations of spillway surface irregularities and their impact on hydraulic parameters.
- The findings reveal that surface irregularities influence hydraulic parameters such as maximum velocity, static pressure, dynamic pressure, total pressure, shear stress, and energy.
- Building upon these findings, the study proposes modifications to the unit stream power dissipation (USPD) equation to enhance its accuracy when applied to unlined dam spillways. By incorporating geometrical parameters and surface irregularities, the equation of the USPD has been modified.
- Comparing computational results for irregular surfaces with the actual scenarios of irregularities presents challenges, primarily due to the prevailing omission of rock surface irregularities in most analytical assessments. The absence of these irregularities in existing analyses hinders straightforward comparisons. In this context, our confidence in the reliability of our findings is substantiated by a comprehensive cross-validation of our computational models and simulations. Rigorous scrutiny was applied to our model inputs through a comparative analysis of smooth surfaces in both computational and real-world contexts. This systematic evaluation revealed discernible deviations between these cases, indicating the impact of irregularities on hydraulic parameters.
- In conclusion, this research contributes to the enhancement of safety in hydraulic structural design, addressing it as the paramount concern in engineering. By incorporating surface irregularities and considering both geometrical and hydraulic parameters, the findings of this thesis enable more accurate design of structures, thereby reducing potential safety hazards downstream of dams. Moreover, the methodology proposed in this study has the potential to yield cost savings in the design process, offering a more efficient and economical approach. The thesis provides a methodology and equations for designers to easily calculate hydraulic parameters, streamlining the design process and further contributing to safety and budget optimization. Ultimately, the outcomes of this thesis have the potential to revolutionize current design practices, providing a pathway for more optimized and cost-effective designs in the field of hydraulic structures.

1.5 THESIS OUTLINE

Three journal papers are the outcome of this thesis, and they are presented separately in Chapters 2 to 4. The general structure of the articles comprises the Abstract, Introduction, Methodology, Discussion, and Conclusion.

CHAPTER 1 describes the overall structure of the thesis by explaining the statement of the problems first. On this basis, the objectives of the research are presented. Then, the methodology used to achieve the principal and sub-objectives of the study are described, and the originality and novelty of the thesis are explained.

CHAPTER 2 reviews the methods used to assess rock erosion in hydraulic structures, including theoretical, semi-theoretical, semi-analytical, and numerical approaches. It highlights the challenges and limitations associated with these methods, particularly in relation to spillways. The study emphasizes the need for further research in understanding erosion mechanisms and proposes future research directions in the field of rock mass erosion downstream of dams and hydraulic structures.

CHAPTER 3 includes an increased awareness of rock mass erosion in unlined dam spillways, an examination of the geomechanical and hydraulic aspects of erosion, and the identification of the impact of surface irregularities on hydraulic parameters. The findings highlight the importance of considering 2D surface irregularities in erosion management for unlined spillways..

CHAPTER 4 focuses on improving the accuracy of energy dissipation rate predictions for water flowing over unlined spillways. By modifying the unit stream power dissipation (USPD) equation to incorporate geometrical parameters and surface irregularities, the study demonstrates enhanced predictions of energy dissipation rates. These findings have important implications for spillway design and maintenance, highlighting the need to consider these factors in estimating USPD for unlined spillways.

CHAPTER 5 presents the most important outcomes of the present work and the directions for future research.

Supplementary data related to CHAPTER 2 are presented in Appendix .

CHAPTER 2

Article 1: A Review on Existing Methods to Assess Hydraulic Erodibility Downstream of Dam Spillways

Yavar Jalili Kashtiban ^{a *}, Ali Saedi ^a, Marie-Isabelle Farinas ^a, Marco Quirion ^b

^a Department of Applied Sciences, University of Quebec at Chicoutimi, Saguenay, G7H 2B1, QC, Canada

^b Hydro-Québec Production Unité Expertise en barrages, 75 Boulevard René-Lévesque Ouest, Montréal, QC
H2Z 1A4, Canada

Published in *Water* 2021, 13(22), 3205; <https://doi.org/10.3390/w13223205>

Submitted: 31 October 2021 / Revised: 9 November 2021 / Accepted: 9 November 2021 / Published: 12
November 2021

AUTHOR CONTRIBUTIONS: Conceptualization, Y.J.K.; methodology, Y.J.K., A.S.; software, Y.J.K.; validation, Y.J.K., A.S., M.-I.F. and M.Q.; formal analysis, Y.J.K.; investigation, Y.J.K.; resources, Y.J.K. and A.S.; writing—original draft preparation, Y.J.K.; writing—review and editing, Y.J.K., A.S., M.-I.F. and M.Q.; visualization, Y.J.K., A.S., M.-I.F. and M.Q.; supervision, A.S., M.-I.F. and M.Q.; project administration, A.S., M.-I.F. and M.Q.; funding acquisition, A.S. All authors have read and agreed to the published version of the manuscript.

FUNDING: This research was funded by: Natural Sciences and Engineering Research Council of Canada and Hydro-Québec (NSERC, Hydro-Quebec) [CRDPJ 537350-18]. Natural Sciences and Engineering Research Council of Canada (NSERC) [RGPIN-2019-06693].

ACKNOWLEDGEMENT: The authors would like to thank the Natural Sciences and Engineering Research Council of Canada (NSERC) and Hydro-Quebec for funding this project (CRDPJ 537350 - 18, NSERC-RGPIN-2019-06693) and all those who helped us to improve the quality of this paper.

CONFLICTS OF INTEREST: The authors declare that they have no conflict of interest regarding the content of this document.

*Email: Yavar.jalilikashtiban1@uqac.ca

2.1 HIGHLIGHTS

- Existing methodologies for investigating the hydraulic erodibility of rock in dam spillways and plunge pools are reviewed comprehensively.
- Hydraulic erodibility or scouring downstream of dams can be assessed by theoretical, semi-theoretical, semi-analytical, and numerical methods.
- The advantages and disadvantages of existing methods for evaluating erosion and scouring are summarized.
- Future directions for assessing the hydraulic erodibility of rock in hydraulic structures (dams) are discussed.

2.2 ABSTRACT

In recent years, rock scouring or erosion downstream of dams has become an increasing dam safety concern. Several theoretical, semi-theoretical, semi-analytical and numerical methods can be used to assess the rock erosion in hydraulic structures. Semi-theoretical approaches determine the correlation between the erosive intensity of fluid flow and the resistive capacity of rock. Such approaches establish the scour thresholds as a function of erosive intensity of water and several rock mass indices by using in situ data and a curve-fitting approach. In some studies, the ex-cavatability index, initially developed for rock mass stability analysis, was used to analyse the rock mass resistance in hydraulic erodibility analysis. The effectivity and weight of the geomechanical parameters used are yet to be determined on the basis of the erodibility phenomenon. The semi-analytical methods are developed on the basis of the mechanical and hydraulic interaction of rock mass and water. Four methods developed by Bollaert et al. are important in determining the erodibility in the plunge pool, but they are not applicable in the case of spillways. They used the comprehensive fracture mechanics for closed-end joints, quasi-steady impulsion, and dynamic impulsion (DI) for blocky rock erosion. The application of these methods to each site is necessary to identify constants that are difficult to determine. Few numerical methods are available to assess the rock mass erosion in hydraulic structures. In the case of numerical methods, the erosive agent is indistinct, and the hydraulic hazard parameter on the spillway surface is almost challenging to apply. This study comprehensively reviews the mechanism of erosion and the methods for assessing the risk of potential rock mass erosion downstream of dams and hydraulic structures. The advantages and disadvantages of all methods are discussed and the potential future research directions in this domain are proposed.

Keywords: erodibility, scour, spillways, plunge pools, dam, hydraulic, rock mass

2.3 INTRODUCTION

In recent years, the risk of rock scouring or erosion in hydraulic structures increased the concern about dam safety. The terms ‘erodibility’, ‘scour’, and ‘hydraulic erosion’ are considered synonymous technical words to explain critical centralised erosion that occurs when the erosive intensity of fluid surpasses the resistive capacity of the rock mass. The design of dam spillways that can discharge a wide range of floods with the minor scouring of material is one of the important challenges in designing hydraulic structures [1,2]. Rock scouring is a complicated mechanism. Rock scour basically occurs by four principal mechanical processes as revealed by its occurrence near engineering structures:

- 1) Rock block abrasion (long term);
- 2) Intact rock fracturing (brittle failure and fatigue failure);
- 3) Single block deletion (uplift pressures in fractures and shear forces);
- 4) Rock block peeling off.

These mechanisms of rock erosion are presented in Fig. 2-1.

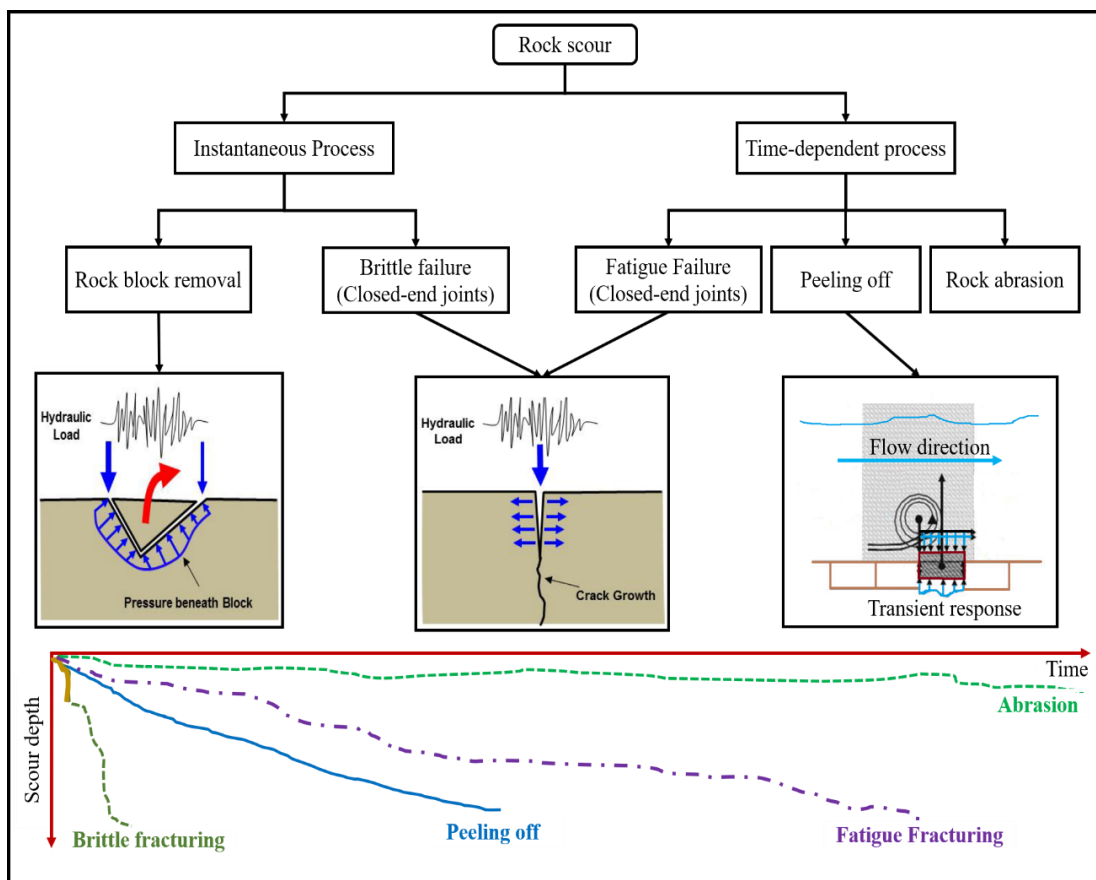


Fig. 2-1. Main mechanical processes of rock erosion and the occurrence timescale [3].

The instantaneous processes consist of rock block removal and brittle failure. In the case of block removal mechanism, single rock blocks can be lifted by horizontal and vertical pressures. Along these lines, the stream turbulence, block size, block dimensions, bulge of the blocks, surrounding rock mass, joint roughness, and cohesion of filling as a shear destabilised force are relevant and effective parameters that straightforwardly characterise the lifting forces.

The breaking of rock in fractured media is scientifically explained by the hypothesis of linear elastic fracture mechanics and may occur by abrupt or progressive hydraulic-driven fracturing. The stress intensity at the tip of shut-end cracks and fracture toughness of the rock play important roles in identifying the types of fracturing; if the stress intensity surpasses the fracture toughness, then brittle failure will occur; otherwise, dynamic fracturing of rock or fatigue failure will occur [4]. Fatigue failure spreads a current fracture on the basis of the intensity and the number of pressure pulses and stops when fracture formation is finished.

In the case of the block peeling-off mechanism, quasi-steady pressure forces play an important role. This type of erosion ordinarily occurs in thin rock layers with protruded open-end rock blocks. The block protrusion causes the stream deviation. The deviation of the stream creates the lifting and drag forces on the block because of the quasi-steady stream velocity, which causes block ejection [3].

Fig. 2-1 demonstrates the other time-dependent rock mass scouring mechanism that occurs on the rock surface by abrasion phenomenon. Abrasion, occasionally referred to as ball-milling or bedrock wear, alludes to gradual grinding resulting from the repeated impacts due to different particles, such as sands or cobbles that are carried by flowing fluid. The occurrence of scouring because of abrasion commonly requires a large amount of time. Thus, dam overtopping or spillway erodibility evaluations are rarely conducted. These mechanisms are used for the development of the methods for the prevision of rock mass erosion.

This review paper attempts to provide an extensive survey of the existing methods to assess the rock mass erosion in several types of hydraulic structures. We extract the advantages and disadvantages of the existing semi-theoretical, semi-analytical, and numerical approaches. A comparison between the semi-theoretical methods is conducted on the basis of the committed error of each method by considering real datasets and the prediction of each methodology. To efficiently explain the existing methods, we present the algorithm of each methodology in various flowcharts. Some potential future research directions are presented on the basis of this review. Finally, the limitations of the application of some methods in erosion prediction are defined, and the new necessary research in this domain is established.

In this work, the semi-theoretical methods are first explained. Thereafter, the semi-analytical methodologies are explained by mainly focusing on the comprehensive scour model (*CSM*). The scouring at the multiblock system with numerical methods is explained. The summary of the paper and conclusion of the authors are presented in the last two sections of this work.

2.4 SCOUR PREDICTION APPROACHES

Many authors have studied scour hole development below plunging spillway jets [5–8]. The disintegration capability of soil along inclines or unlined spillway channels is also considered in several studies [9–12]. Amongst the approaches used for assessing rock mass erosion, the most common are semi-theoretical methods according to the correlation between the resistive capacity of rock and the erosive intensity of fluid, such as Annandale’s and Pells’ approach [1]. Some classical equations can be used for computing the final scour depth in plunge pools. The flowchart in Fig. 2-2 shows the classifications of the empirical, theoretical, and semi-theoretical methods.

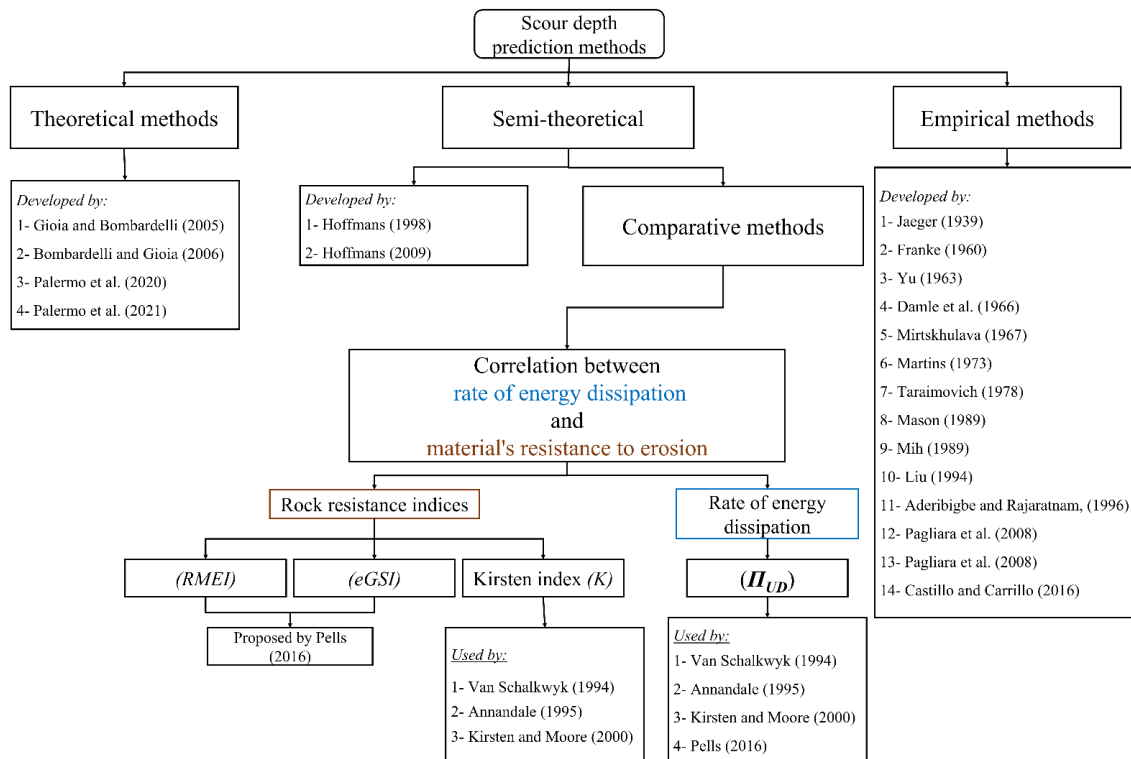


Fig. 2-2. Classifications of the scour prediction methods.

2.4.1 Comparative Methods based on Resistance of Materials for Erosion and Rate of Energy

Dissipation

A certain form is considered in the design of a dam spillway to evaluate the potential of hydraulic erosion of dams. The scour threshold is an erodibility index and a function of P that is widely used in the industry [13–15]. This function is calculated for different comparative methods on the basis of the interpreted erosion

obtained from various case studies. A threshold line with a specific scour condition that distinguishes case studies can be identified in the plotted data. The correlation between the resistance of material for erosion and the energy dissipation rate P is calculated as in Equation (2-1):

$$P = f(K_h), \quad (2-1)$$

where P is the total water erosive intensity that is released on or over the material. The resistance of a material to erosion is contingent upon its strength and can be elucidated through established methods that assess the overall component commitment, such as the Kirsten index (K_h). In $P < f(K_h)$, the limit of erodibility is not surpassed, while $P > f(K_h)$ indicates that the values above the erodibility threshold are exceeded; accordingly, erosion will occur, and the material will scour [16–18].

Equation (2-1) is a two-part equation representing the erosive force and the material resistance threshold to scouring, which is determined by the erodibility index, rock mass erosion index ($RMEI$), or geological strength index (GSI) ($eGSI$). In this work, an improved strategy is needed to find an agent that is easy to be determined while explaining the overall strength of the fluctuating turbulence. Hydraulic water energy (kW/m^2) denotes the erosive force of stream water and is represented as hydraulic stream power (P_a) or unit stream power dissipation Π_{UD} . The favoured agent for this purpose is the rate of energy dissipation. Hydraulic turbulence is the main cause of energy loss and pressure fluctuations. Increased turbulence intensity leads to a great energy dissipation rate and high levels of water pressure fluctuations. Erosive force and pressure fluctuations of flowing water are evaluated and calculated, as in the following equations [19], in energy dissipation rate analysis:

$$\Pi_{UD} = \gamma q \Delta E \quad (2-2)$$

$$\Pi_{UD} = \rho g \frac{Q}{\beta_f} \frac{dE}{dx} = \rho g \frac{Q}{\beta_f} \frac{dh_l}{dx} \quad (2-3)$$

$$\Pi_{UD} = \rho g q (S_f) \quad (2-4)$$

where Π_{UD} is the unit stream power dissipation and the change in unit stream power between two locations along a flow path (kW/m^2); γ = unit weight of water (kN/m^3); q = unit discharge rate (m^2/s); ΔE = energy loss ($\text{J} = \text{kg} \cdot \text{m}^2 \cdot \text{s}^{-2}$); h_l = head loss; x = horizontal direction of flow; y = depth of water; Z_b = the vertical distance of the bottom surface from the reference datum; ρ = water density (kg/m^3); V = velocity of flowing water; g = gravitational acceleration (m/s^2); Q = total discharge amount (m^3/s); β_f = width of a flow section measured at the water surface (m); and $S_f = \frac{dh_l}{dx}$ and presents the friction slope or the gradient of the total hydraulic energy line. Fig. 2-3a shows the variation of properties over a differential flow section in an open channel. Fig. 2-3b shows the cross-sectional view of the flow channel.

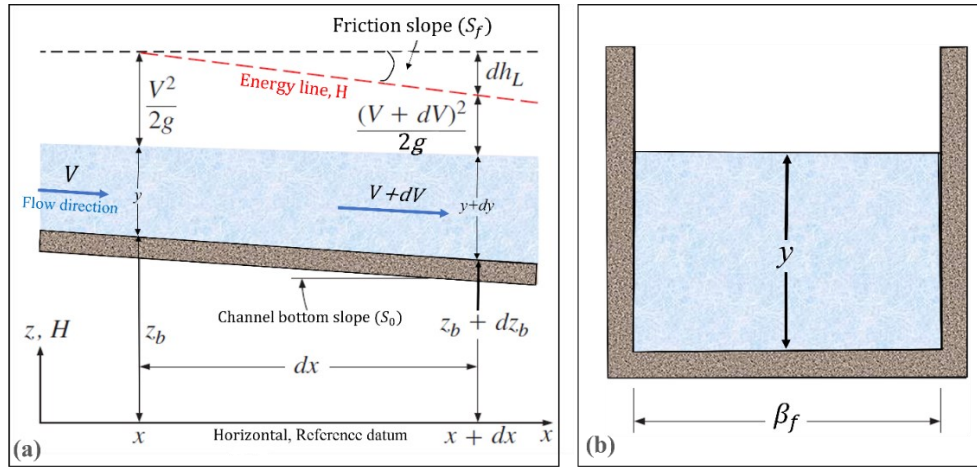


Fig. 2-3. (a) Variation of properties over a differential flow section in an open channel. (b) Cross-sectional view of the flow channel [19]

This equation was used for evolving equations to assess the energy dissipation rate for a characteristic manner of erosion [1,20]. Annandale provided alternate forms of Equation (2-3) to decide the erosive limit concerning an assortment of flow cases, including open channels, plunge pools, hydraulic jumps, knick-points, and head cuts [21].

Part two of Equation (2-1) shows the rock resistance capacity, which is calculated by using the rock mass parameters and forms an index when inserted into the equation. In this regard, different categories of engineering rock mass that are used in evaluating the rock mechanical excavatability apply a large number of agents that modify the rock hydraulic erodibility [22,23]. Van Schalkwyk used some rock mass indices for this purpose, including the rock mass rating (*RMR*) classification of Bieniawski; the *Q*-classification of Barton, which was primarily suggested for underground space designs; and the index suggested by Kirsten for evaluating the excavatability of earth materials [24–28]. The authors reported similar results for all these indices. However, the highest accuracy was found for the Kirsten index (*N*), which is used to evaluate the erosion of rock mass [29–31].

Equation (2-5) is determined by using certain rock mass parameters, such as uniaxial compressive strength (*UCS*), mass strength (M_s), joint shear strength (K_d), relative block structure (J_s), and rock block size (K_b). The proposed system applies across the full range of natural materials from the weakest soils to the hardest rocks.

$$N = M_s \cdot K_b \cdot K_d \cdot J_s \quad (2-5)$$

In 1982, Kirsten used the classifications and charts of Jennings to propose a descriptive chart with M_s ranging from 0.87 to 280 [27,32]. In 1970, Cecil combined the *RQD* index with the joint set (J_n) and introduced

the K_b factor ranging from 1 to 100 [33]. The corresponding changes for RQD and J_n were 5–100% and 1–5, which were proposed by Barton and Kirsten, respectively [26–28]. The K_b factor was later adopted in the N index. The J_r/J_a ratio represents the joint shear strength for the K_d factor, where J_r is the joint roughness, ranging from 0.5 to 4, and J_a is the joint surface change ranging from 0.75 to 18 [27]. The K_d changes from 0.03 to 5.33. J_s is the effect of rock block shape and the path by which related joints are arranged to flow. In 1982, Kirsten proposed the rating for orthogonal fractured systems, which ranges from 0.37 to 1.5. The author also used the orthogonal case as the measuring standard because it was simple and effective, maintaining that the jointing angle was correct in most cases, even though slight errors exist. However, this notion was rejected by Boumaiza et al. in 2019. The finding of Boumaiza et al. in 2019 encouraged a proposed new rating from 0.09 to 1.38 for nonorthogonal fractured systems. In 2018, Kamali stressed that the number and connectivity of blocks increase and have considerable effects on erodibility under orthogonal joint conditions [34,35].

The following are the two other indices recently proposed by Pells to evaluate the limit of rock resistance to erosive power of water: geological strength index (GSI) ($eGSI$) and $RMEI$. The $eGSI$ was developed on the basis of the GSI of Hoek and previously suggested to define and classify the rock mass [1,36].

Bieniawski concluded that the joint orientation parameter is not considered in the RMR system, when the GSI system is identified utilising the RMR system [37]. In this regard, Pells suggested the $eGSI$ index for illustrating the importance of the joint orientation relative to the flow direction and a rock block shape by considering the recently proposed discontinuity orientation adjustment parameter (E_{doa}) (Equation (2-6)) [1].

$$eGSI = GSI + E_{doa} \quad (2-6)$$

The $RMEI$ index is the other index suggested by Pells [1]. This index may be noted on the basis of the likelihood factor (LF) and relative significance factor (RF) (Equation (2-7)). Prefixes P_1 to P_5 in Equation (2-7) are various sets of parameters introduced in the classification system. P_1 to P_5 indicate the kinematically viable system for isolation, the feature of the potentially eroding surface, the feature of joints, the joint spacing, and the rock block shape, respectively [1].

$$RMEI = [(RF_{P1}.LF_{P1}).(RF_{P2}.LF_{P2})].[(RF_{P3}.LF_{P3}) + (RF_{P4}.LF_{P4}) + (RF_{P5}.LF_{P5})] \quad (2-7)$$

Pells argued that the erosion mechanism in this field is poorly represented by existing indices, including Kirsten's index. The $RMEI$ systems represent the rock mass parameters that gain significance from studies on eroded rocky spillways to control this mechanism. A high RF is used to measure the relative importance of the rock mass parameters. The RF measures the isolation and eroding surface by using three values: joints ($RF = 2$), joint spacing ($RF = 1$), and rock block shape ($RF = 1$).

The $RMEI$ system designed by Pells for hydraulic erosion is structurally similar to the Q -system of Barton that was initially designed for field investigations. The size of the rock blocks determined by joint spacing and

dip is indirectly included in *RMEI*. However, the joint shear strength is not considered in the *RMEI* system. The joint nature that maintains the natural conditions of joints can be used as an alternative for determining the rock block size. Joint spacing is a less significant factor ($RF = 1$) in the *RMEI* system compared with joint factor ($RF = 2$). The K_b rating factor as an indicator of the rock block size is given more importance in the *Q*-system compared with the K_d factor representing the joint shear strength [26]. This phenomenon shows that the field evaluation to determine the importance of the rock mass parameters is highly influenced by the individual judgement of the analyst. Pells assumed that the existing indices, including Kirsten's index, do not indicate the erosion mechanism in the field. Accordingly, the *RMEI* system attempts to represent the rock mass parameters controlling the erosion mechanism. The relative importance of these parameters is assumed to be due to the field observations of the eroded rocky spillways. A high RF weights the important rock mass parameters. The kinematically viable system for isolation and the feature of the potentially eroding surface are weighted with a high RF value of three compared with the nature of joints ($RF = 2$), joint spacing ($RF = 1$), and rock block shape ($RF = 1$). The structure of the *RMEI* system for hydraulic erosion is considered similar to that of the *Q*-system, which was also developed on the basis of the field investigation. In the *RMEI* system of Pells, the rock block size is indirectly included. However, the joint spacing and dip could provide an idea about the rock block size given that the wide spacing of joints produces a more important rock block volume than the close spacing of joints. The joint shear strength is not included in the *RMEI* classification. Nevertheless, the nature of the joint factor is the same given that it incorporates the natural conditions of joints. The *RMEI* classification considers the joint spacing factor as a less important factor ($RF = 1$) compared with the nature of the joint factor, which is weighted with $RF = 2$. The *Q*-system provides a more important rating to the K_b factor, which is an indicator of the rock block size, compared with the K_d factor, which represents the joint shear strength [26]. The discordance of the relative importance of the parameters included in these two classification systems demonstrates how the field evaluation can be highly affected by analyst judgement. Consequently, the relative importance of the rock mass parameters is difficult to determine by using an accurate alternative.

2.4.1.1 Background of the Comparative Methods Base on Kirsten's Index

Van Schalkwyk assumed the erosion condition as a function of erosion depth (Table 2-1) [29]. They also used recent data from Moore, Kirsten's index limitations, and scale effects to update their findings [38]. Accordingly, the scour threshold lines were changed (Table 2-1).

Table 2-1. Classification of the erosion extent.

Van Schalkwyk et al. (1994a) [24]		Van Schalkwyk et al. (1994b) [29]		Kirsten et al. (2000) [18] and Annandale (1995) [21]	
Depth of Erosion (m)	Erosion Class	Depth of Erosion (m)	Erosion Class	Depth of Erosion (m)	Erosion Class
0	None	<0.2	None	<2	No scour or erosion
0-1	Little	0.2-0.5	Little	>2	Scour
1-5	Moderate	0.5-2	Moderate		
>5	Extensive	>2	Extensive		

Annandale analysed the findings of Moore, Van Schalkwyk, and other scour data using Kirsten's index to offer a scour threshold related to unit stream power dissipation (Π_{UD}) (Table 2-1) [21,29,31]. Table 2-1 illustrates that the erosion depth beyond two leads to scour occurrence, while the values below two are insignificant and might be the outcome of loose rock blocks being removed from the surface [21]. In 2000, Kirsten adopted a similar approach for determining the scour threshold to show the scour and no-scour conditions by using data from the study of Dooge and Moore [18,30,31]. A comparison of the scouring onset values for Kirsten's index versus Π_{UD} is presented in Fig 2-4, and the corresponding equations are shown in Table 2-2.

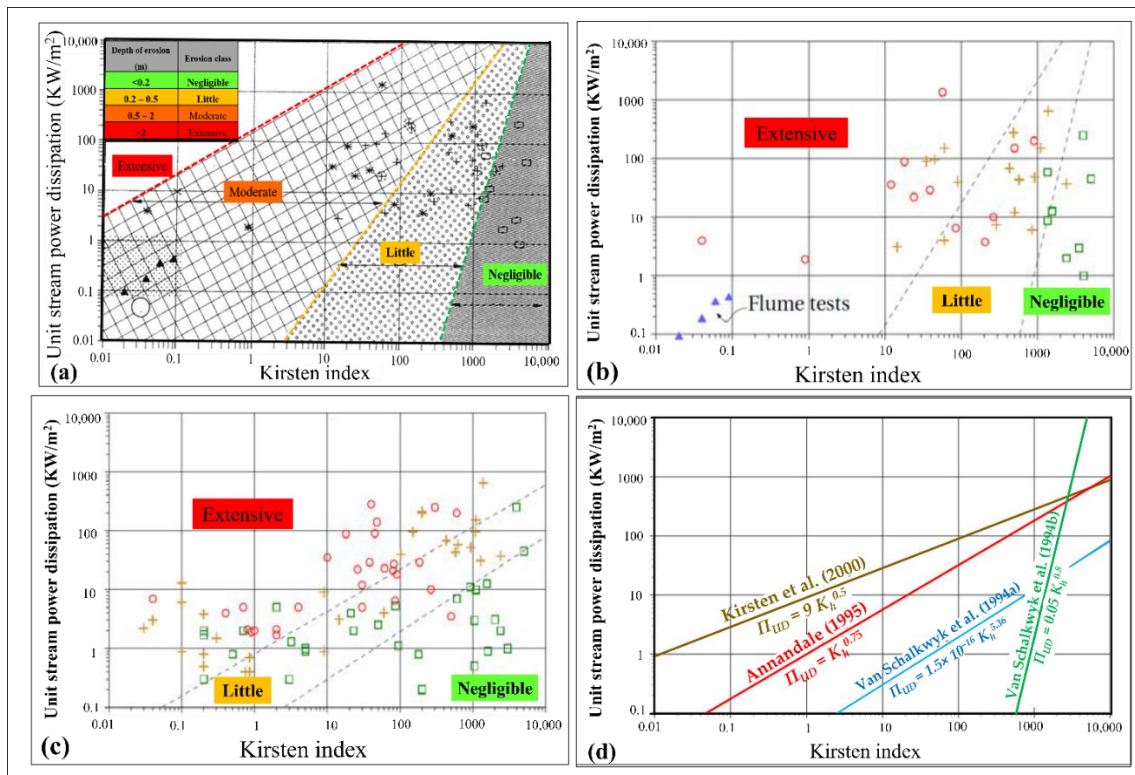


Fig. 2-4. (a) Original dataset as presented in the study of Van Schalkwyk [24]; (b) after inclusion of data from Moore [24]; (c) scour threshold line presented by Annandale; (d) comparison of scour threshold lines.

Table 2-2. Scour threshold equations by different researchers.

Analyst	Equations
Van Schalkwyk et al. (1994b) [29]	$\Pi_{UD} = 0.05 K_h^{0.8}$
Van Schalkwyk et al. (1994a) [24]	$\Pi_{UD} = 1.5 \times 10^{-16} K_h^{5.36}$
Annandale (1995) [21]	$\Pi_{UD} = K_h^{0.75}$
Kirsten et al. (2000) [18]	$\Pi_{UD} = 9 K_h^{0.5}$

2.4.1.2 Background of Pells' Methods

Pells classified the erosion condition in certain classes with minor modifications on the depth of eroded area according to the same concept of the study of Van Schalkwyk and added information on the extent of the eroded area (Table 2-3). Neither depth nor volume is a complete descriptor of the erosion severity. However, whether the conditions in the first and second columns of Table 2-3 should be simultaneously or separately considered is ambiguous in this classification. Thus, if the conditions should be simultaneously considered, then it might result in a problem, for example, whether class 1 or 2 should be considered for the maximum depth of 0.5 m and the general extent of 8 m³/100 m².

Table 2-3. Classification of erosion proposed by Pells [1].

Maximum Depth of Erosion (m)	General Extent (m ³ /100 m ²)	Erosion Class	Erosion Condition
<0.3	<10	1	Negligible
0.3–1	1–30	2	Minor
1–2	30–100	3	Moderate
2–7	100–350	4	Large
>7	>350	5	Extensive

Pells plotted the calculated index values versus Π_{UD} by using the *eGSI* index (Equation (2-6)) and the *RMEI* index (Equation (2-7)) to manually determine the selected erosion classes. These values were separated by scour threshold lines (Fig. 2-5a,b) and were originally proposed by Pells and recently modified by Douglas [39]. However, no finding has been obtained on the optimisation introduced into the original scour threshold lines.

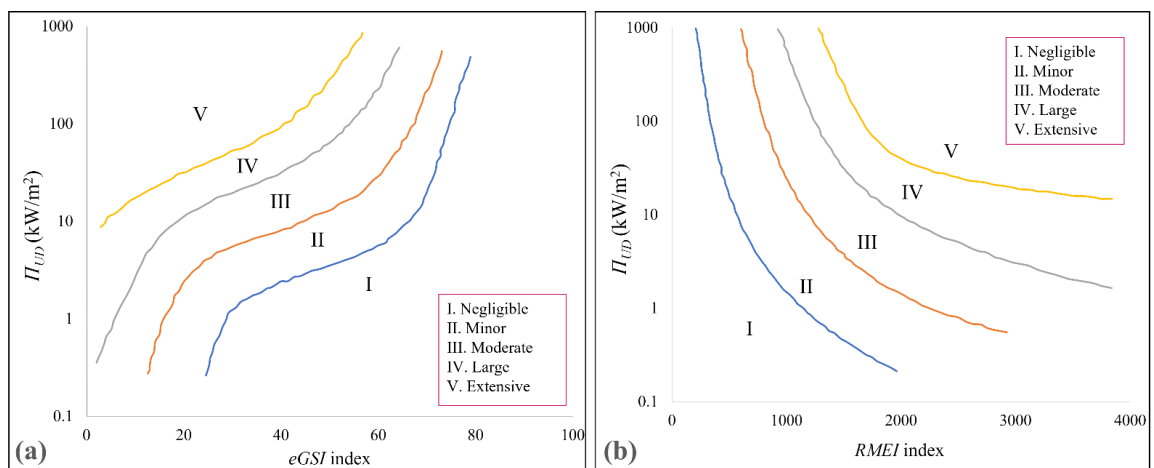


Fig. 2-5. (a) Erosion classes determined according to the *eGSI* index; (b) erosion classes determined according to the *RMEI* index [39].

2.4.1.3 Discussion of EIM and Pells' Methods

The easiness and wide pertinence to different stream conditions make the erodibility index method (*EIM*) especially alluring for practice. In any case, this approach is not without confinement. As the name of this approach suggests, it consolidates an empirical index to classify and identify the rock. Along these lines, the *EIM* cannot reveal various erosion mechanisms (i.e., fatigue failure, block removal, or brittle failure). The results of *EIM* are general and do not incorporate the erosion mechanisms. The geometry of rock is considered 2D, and the 3D nature of the discontinuity orientations is not accounted. However, this method can illustrate the discontinuity structure relative to the flow direction.

The data analysed by Annandale consider several types of flow conditions (137 case studies), while Pells used the predominant channel flow in spillways. Under the channel flow conditions, block removal is considered to be the dominant mechanism for scour to occur; thus, the analysis of variables representing blocks (e.g., K_b) in those cases would be expected to show great importance. Under the jet conditions wherein fracturing of the rock can be more dominant, the other variables may be shown to be more relevant (e.g., M_s).

Rock scour is a highly complicated mechanism, and its evaluation should start by identifying the relevant rock mass parameters to assess this mechanism. For this purpose, in 2019, Boumaiza et al. developed a method on the basis of real data and previous empirical methods [35]. They examined a set of rock mass parameters to determine those that are considered related parameters to evaluate the rock mass erosion. In the proposed approach, various parameters are assessed, such as E_{doa} , $NPES$, J_o , J_s , K_d , K_b , V_b , and UCS . Finally, K_d , V_b , J_o , E_{doa} , and $NPES$ were chosen as the relevant parameters by sensitivity analysis.

2.4.2 Semi-Theoretical Methods for Computing Scour of the Plunge Pools

Several semi-theoretical equations can be used for computing the final scour depth in the plunge pool bottom in alluvial and weathered rock. Some semi-theoretical equations are identified in Table 2-4 [40–50]. The reduced models of the Froude scale are used to produce most semi-theoretical equations based on the real data analysis and experiments. Some of these equations are proposed on the basis of the prototypes for ski-jump conditions. Several equations are also considered (Table 2-5). In 1985, Mason and Arumugam proposed Equation (2-8) for the intermediate outlet conditions of the free surface reservoir and dam structures on the basis of the several prototype cases and the models of numerous erodible beds [5].

Table 2-4. General scour formulae.

Authors	Formulae
Jaeger (1939) [40]	$D_s = 0.6 q^{1/2} H_n^{1/4} \left(\frac{h}{d_m} \right)^{1/3}$
Yu (1963) [41]	$D_s = 0.617 q^{0.75} H_n^{0.125}$
Damle et al. (1966) [42]	$D_s = 0.362 q^{0.5} H_n^{0.5}$
Mirtskhulava (1967) [43]	$D_s = \left(\frac{0.97}{d_{90}^{1/2}} - \frac{1.35}{H_n^{1/2}} \right) \frac{q \cdot \sin \theta_T}{1 - 0.175 \cot \theta_T} + 0.25h$
Martins (1975) [44]	$D_s = 1.5 q^{0.6} H_n^{0.1}$
Taraimovich (1978) [45]	$D_s = 0.663 q^{0.67} H_n^{0.25}$
Mason (1989) [46]	$D_s = 3.39 \frac{q^{0.6}(1 + \beta)^{0.3} h^{0.16}}{g^{1/3} d^{0.06}}$
Liu (1994) [47]	$D_s = 0.74 \cdot (0.41 + 0.082 \cdot d) \frac{q^{0.67} H_n^{0.33}}{d^{0.33}}$
Chen et al. (2001) [48]	$D_s = 1.1 q^{0.5} H_n^{0.25}$
Bombardelli and Gioia (2006) [49]	$D_s = \Gamma \cdot \frac{q^{0.4} H_n^{0.4}}{g^{0.2} d^{0.4}} \left[\frac{\rho}{\rho_s - \rho} \right]^{-0.6}$
Castillo and Carrillo (2016) [50]	$D_s = h + 0.19 \left(\frac{H_n + h}{d_{90}} \right)^{0.75} \left(\frac{q^{6/5}}{H_n^{23/49} h^{1/3}} \right)$

Table 2-5. Coefficients of five simplified scour formulae.

Analysts	Γ	v	w	x	y	z	d
Hartung (1959) [51]	1.4	0	0	0.64	0.36	0.32	d_{85}
Chee and Padiyar (1969) [52]	2.126	0	0	0.67	0.18	0.063	d_m
Bisaz and Tschopp (1972) [53]	2.76	0	0	0.5	0.25	1	d_{90}
Martins (1975) [44]	1.5	0	0	0.6	0.1	0	—
Machado (1982) [54]	1.35	0	0	0.5	0.3145	0.0645	d_{90}

$$D_s = Y_0 + Y_s = \Gamma \cdot \frac{q^x H_n^y Y_0^w}{g^v d^z} \quad (2-8)$$

The different parameters of Equation (2-8) are illustrated in Fig. 2-6, where Y_s represents the scouring depth below the bedrock, H_n is the net energy head, g is the gravitational acceleration, Γ is the experimental coefficient, D_s stands for the sum of the scour depth and tailwater depth, q represents the specific flow rate, Y_0 is the tailwater depth, and d stands for the block and bed material size [50].

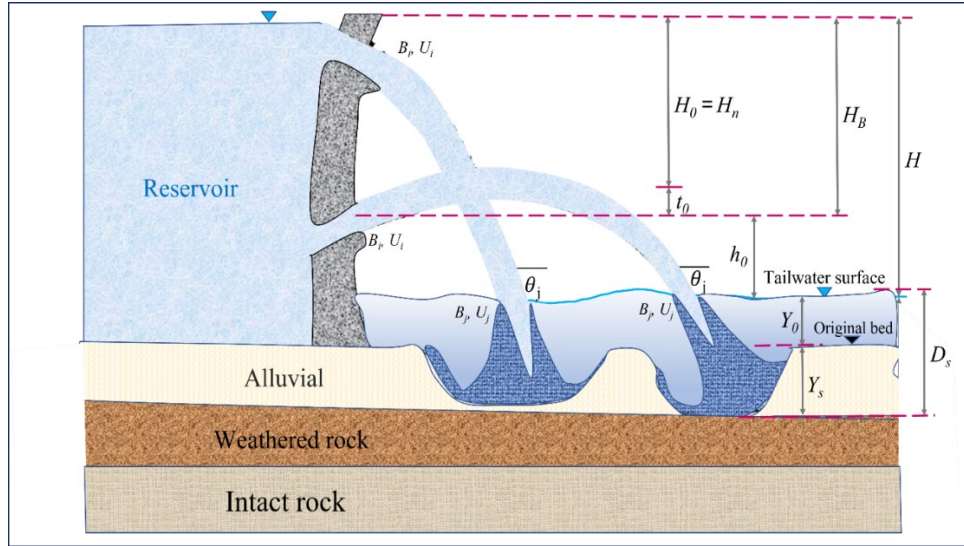


Fig. 2-6. Scheme of scour in semi-theoretical methods [50].

In Equation (2-8) and Fig. 2-6, x , y , z , v , and w are experimental and empirical constants settled in Table 2-4 by different authors. Various coefficients of Table 2-4 contrasted with general equations. H represents the vertical interval between the tailwater level and the reservoir, and t_0 stands for the energy loss in the chute; h_0 is the vertical distance between the outlet exit and the tailwater level, and $H_n = H_0 = H_B - t_0$ stands for the net energy head at the outlet exit. U_i , B_i , and θ_i are the jet velocity, thickness, and angle in the initial point, respectively. U_j , B_j , and θ_j are the total jet velocity, thickness, and angle in the impact point, respectively. Table 2-6 shows the abbreviation list of the plunge pool semi-theoretical approaches.

Table 2-6. Symbol notation list of the plunge pool semi-theoretical method.

Abb.	Definition	Unit	Abb.	Definition	Unit
d_m	Average particle size of the bed material	m	H_n	Net energy head	m
d_{90}	Bed material size, 90% is smaller in weight	-	h	Energy head at the crest weir	m
θ_T	Impingement jet angle	degree	Y_0	Tailwater depth	m
g	Gravitational acceleration	m/s ²	Y_s	Scour depth below the original bed	m
β	Air-water relationship	-	q	Specific flow	m ² /s
ρ	Water density	kg/m ³	t_0	Energy loss in the duct	m
ρ_s	Density of sediment	kg/m ³	H_0	Vertical distance between outlet and tailwater level	m
Γ^+	Experimental coefficient	-	H	Fall height	m
D_s	Scour depth below tailwater level	m	H_n	Net energy head;	m

2.5 SEMI-ANALYTICAL METHODS

Semi-analytical methods are derived by calibration of at least one parameter using experiments, or empirical calibration of coefficients using data. A jet plunging into a pool leads to the development of average

and fluctuating dynamic pressures that can cause the breakup and removal of rock. When a jet plunges into a pool, it creates dynamic pressures below the point of jet impact. These pressures consist of average and fluctuating dynamic pressures. If free air is introduced into a plunge pool by the jet, then the average dynamic pressure decreases with the increase in the air concentration [3,55–57]. In 2019, Maleki and Fiorotto analysed the block stability and potential rock scour in the plunge pool bottom on the basis of new experimental study by focusing on the mean dynamic pressure and fluctuating pressure coefficients produced by rectangular water jets [58]. In the fluvial erosion case, the comprehensive scour model (*CSM*) of Bollaert is one of the adopted semi-analytical methods [59]. This model was proposed in 2002 for plunge pools with circular jets and later in 2010 developed for riverbed by Bollaert.

Plunging jets occur in different types of hydraulic structures, including the characteristic location of the spillways, overtopping dams, valves, and dam structural gates [59]. In such a manner, the *CSM* could be used for plunging jets. The *CSM* of Bollaert comprises three unique techniques, for example, comprehensive fracture mechanics (*CFM*), quasi-steady impulsion (*QSI*), and dynamic impulsion (*DI*) (Fig. 2-7). In the main strategy, the *CSM* explains the fracture propagation by utilising linear elastic fracture mechanics. In the subsequent technique, the second law of Newton (impulsion) and net uplift pressure are used to determine the single block uplift. Bollaert proposed the *QSI* technique to assess the eroded area in walls of plunge pools and determine the scour depth. The *QSI* technique is developed for protruding rock blocks on the basis of the different flow conditions and relative flow direction. The hydraulic parameters are determined along the critical area in the pool bottom and rock mass surface for every fracture mechanism. Fig. 2-7 illustrates the *CSM*.

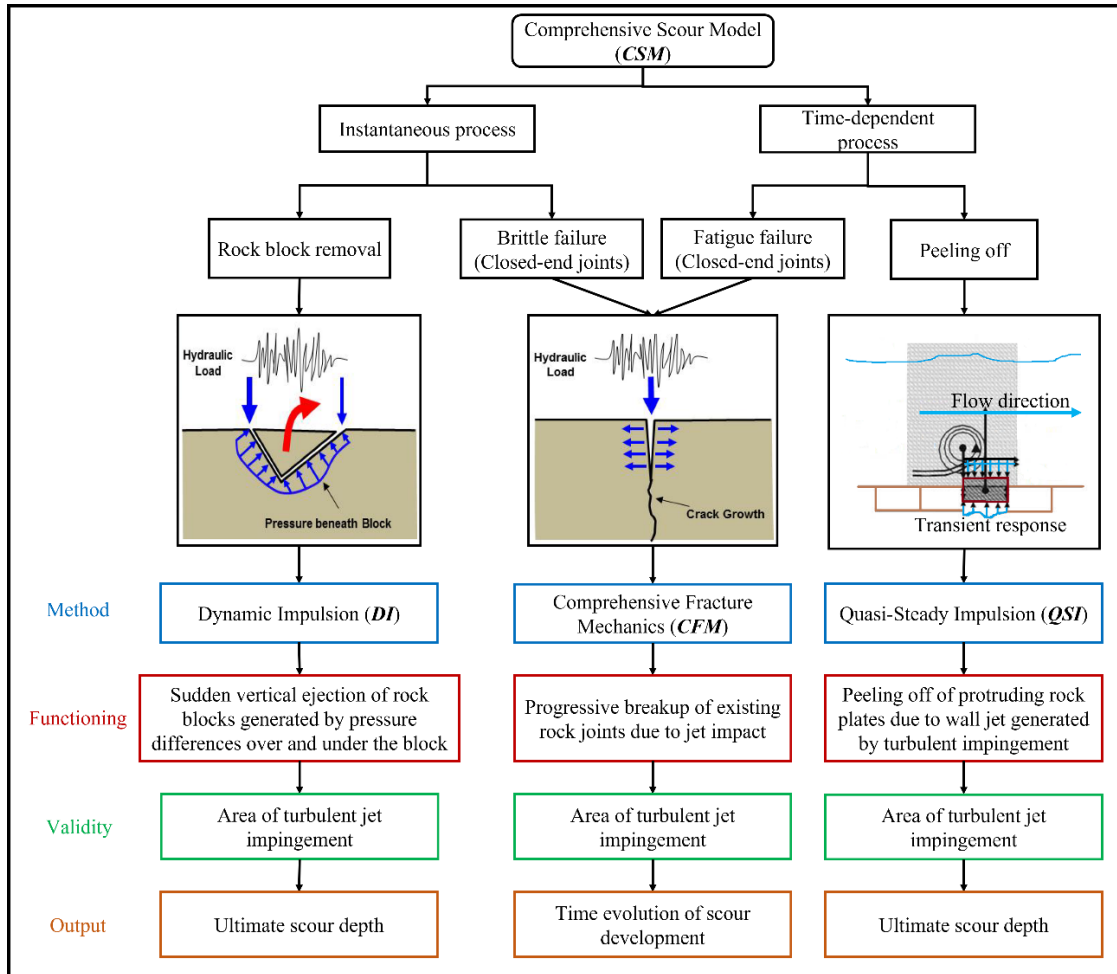


Fig. 2-7. Description of CSM.

Fig. 2-7 illustrates the main physical and mechanical processes used for determination of rock scouring (CSM). CFM comprises three modules: falling jet module, plunge pool module, and rock mass module. The latter executes the fracture mechanism.

The falling jet module (Fig. 2-8) clarifies how the geometrical and hydraulic parameters of the plunging jets are changed from outlet exit to impact point of plunge pool surface. Issuance jet velocity (V_i), initial turbulence intensity (T_u), and issuance jet diameter (D_i) identify the jet characteristics at the outlet exit. T_u represents the extent of the root-mean-square (RMS) estimation of the fluctuating velocity of the plunging jet to the mean axial velocity of the plunging jet. The plunging jet pathway relies upon air drag and ballistics. The falling jet module can determine the jet pathway length L from issuance to the impact point, the longitudinal distance of the plunging jet from issuance to the impact point, the jet velocity (V_j), and the jet diameter (D_j) at the impact point (Equations (2-9) and (2-10)) [60,61].

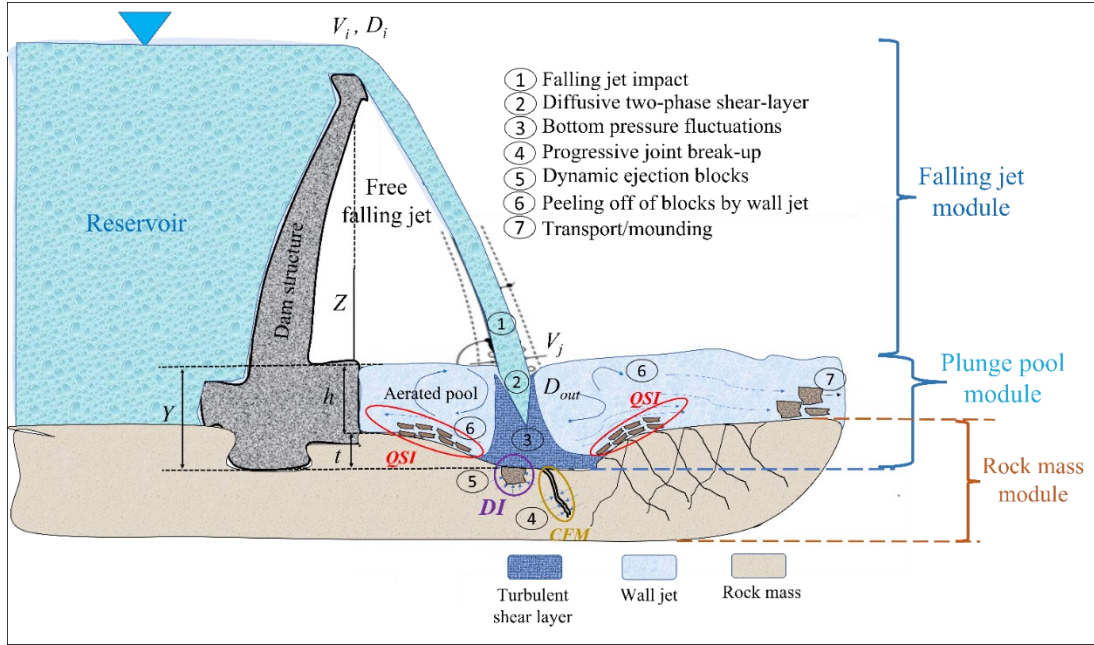


Fig. 2-8. Main physical processes used for computation of rock scour (CSM) [59,60].

The plunge pool module depicts the plunging jet whilst crossing the plunge pool. This module characterises and computes the pressures of water at the plunge pool bottom on the rock surface. The Y/D_j ratio plays an important role in defining coefficients, which is straightforwardly identified with jet diffusion. Y is fundamental and represents the plunge pool water depth. The fluctuating dynamic pressures C'_{pa} and the mean dynamic pressure coefficient C_{pa} , which are determined by using Equations (2-11)–(2-13), are the important pressures straightforwardly estimated under the centreline of the jet impact point. These pressure coefficients were defined on the basis of the experimental data analysis of [55].

$$D_j = D_i \sqrt{\frac{V_i}{V_j}} \quad (2-9)$$

$$V_j = \sqrt{V_i^2 + 2gZ} \quad (2-10)$$

$$C'_{pa} = a_1 \cdot \left(\frac{Y}{D_j}\right)^3 + a_2 \cdot \left(\frac{Y}{D_j}\right)^2 + a_3 \cdot \left(\frac{Y}{D_j}\right)^1 + a_4 \cdot \left(\frac{Y}{D_j}\right)^0 \quad (2-11)$$

$$C_{pa} = 38.4 \cdot (1 - \alpha_i) \cdot \left(\frac{D_j}{Y}\right)^2, \quad \text{for } \frac{Y}{D_j} > 4 - 6 \quad (2-12)$$

$$C_{pa} = 0.85 \quad \text{for } \frac{Y}{D_j} < 4 - 6 \quad (2-13)$$

$$\alpha_i = \frac{\beta}{1 + \beta} \quad (2-14)$$

where α_i is the air concentration in % and β is the volumetric air-to-water ratio. Table 2-7 illustrates T_u for various outlet structural types, and the polynomial coefficients for various turbulence intensities. The input and output parameters of the plunge falling jet and pool modules are noted in Table 2-8. Fig. 2-9a,b demonstrate the C_{pa} and C'_{pa} as functions of the pool water depth to jet diameter (Y/D_j) on the basis of the curve fitting of Ervine results [55].

Table 2-7. The range of T_u due to the type of outlet structure (left side) [61]; polynomial and regression coefficients for various T_u (right side) [62].

Outlet Structure	T_u	Type of jet	T_u (%)	α_1	α_2	α_3	α_4
Free overfall	0–3%	Compact	<1	0.0022	–0.0079	0.0716	0
Ski-jump outlet	3–5%	Low turbulence	1–3	0.00215	–0.0079	0.0716	0.050
Bottom, intermediate, and valve	3–8%	Moderate turbulence	3–5	0.00215	–0.0079	0.0716	0.100
		High turbulence	>5	0.00215	–0.0079	0.0716	0.150

Table 2-8. Input and output parameters of the falling jet and plunge pool modules [59].

Falling Jet Module		Plunge Pool Module	
Plunge Pool Module	Output (Falling Jet)	Input (Plunge Pool)	Output
1. Structure of outlet	1. Location of jet impact (X_{ult}) 2. Length of jet trajectory (L) 3. Diameters of jet impact (D_j , D_{out}) 4. Velocity of jet impact (V_j) 5. Turbulence intensity T_u	1. Location of jet impact (X_{ult})	1. Y/D_j 2. Centreline mean pressure C_{pa} 3. Centreline pressure fluctuations C'_{pa}
2. Velocity of jet at issuance point (V_i)		2. Length of jet trajectory (L)	
3. Diameter of jet at issuance point (D_i)		3. Diameters of jet impact (D_j , D_{out})	
4. Initial jet turbulence intensity (T_u)		4. Velocity of jet impact (V_j)	
5. Energy head (Z)		5. Turbulence intensity T_u	

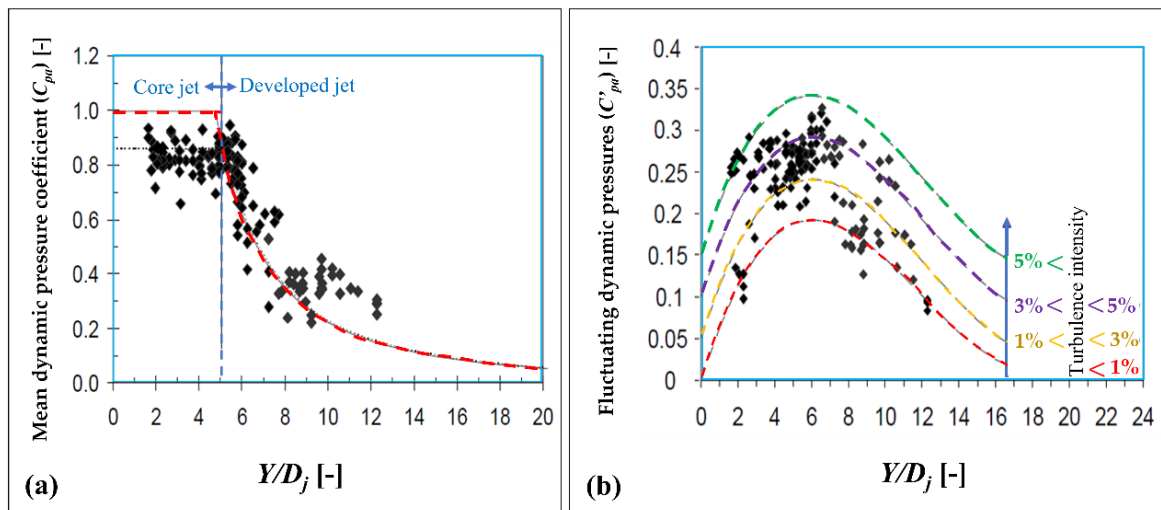


Fig. 2-9. (a) Diversity of the mean dynamic pressure coefficient (along the jet centre line) as a performance of the dimensionless ratio of $\frac{Y}{D_j}$ [55]; (b) nondimensional root-mean-square dynamic pressure coefficient for jet velocities higher than 20 m/s [62].

In the rock mass module (third module), the water pressures at the plunge pool bottom on the rock surface (water–rock interface) are utilised to determine the pressures inside the rock mass discontinuities. Several

pressure fluctuations can be observed in the open- and close-ended discontinuities. The fluctuating pressures introduced into the close-ended fissures and open-ended joints in the rock or concrete masses by the average and dynamic fluctuating pressures originate from the interaction between the plunging jets and the surrounding water in the plunge pools. The major parameters follow: coefficient of maximum dynamic pressure (C_p^{max}) used for the closed-end rock joints and brittle failure mechanism, the characteristic amplitude (ΔP_c) and pressure cycle frequency (f_c) used for closed-end rock joints, brittle failure and fatigue failure mechanism, and the coefficient of maximum DI (C_I^{max}) used for the open-ended rock joints and single blocks [59].

2.5.1 CFM

The *CFM* method recognises the final scour depth in the pool bottom around the area of the turbulent jet impingement for the close-ended joints. This method presents two different approaches for brittle failure and fatigue failure mechanism.

For this purpose, the maximum dynamic pressure in the close-ended fissures P_{max} is determined by using Equation (2-15) [59]:

$$P_{max} [Pa] = \gamma \cdot C_p^{max} \cdot \frac{V_j^2}{2g} = \gamma \cdot (C_p + \Gamma^+ \cdot C'_p) \cdot \frac{V_j^2}{2g} \quad (2-15)$$

where C_p^{max} represents the dynamic pressure coefficient and is provided from multiplication of the amplification factor Γ^+ with C'_{pa} , which is determined by using Table 2-9 and by superposition by C_{pa} .

Table 2-9. Conditions for computing the amplification factor (Γ^+) [63].

Curve of Maximum Values		Curve of Minimum Values	
Γ^+	Condition of Y/D_j	Γ^+	Condition of Y/D_j
$4 + 2 \cdot \left(\frac{Y}{D_j}\right)$	for $Y/D_j < 8$	$-8 + 2 \cdot \left(\frac{Y}{D_j}\right)$	for $Y/D_j < 8$
20	for $8 \leq Y/D_j \leq 10$	8	for $8 \leq Y/D_j \leq 10$
$40 - 2 \cdot \left(\frac{Y}{D_j}\right)$	for $10 < Y/D_j$	$28 - 2 \cdot \left(\frac{Y}{D_j}\right)$	for $10 < Y/D_j$

In 2016, Bollaert modified and simplified the P_{max} and defined the new equation for P_{max} (MPa) (Equation (2-16)) [64].

$$P_{max} [MPa] = 10^{-6} \cdot \rho \cdot (C_{pa} + \Gamma^+ \cdot C'_{pa}) \cdot \frac{V_j^2}{2} \quad (2-16)$$

where ρ is the density of water with a dimension of kg/m^3 .

As noted in the past area, the minimum and maximum pressures of the cycles are used to determine ΔP_c . The f_c follows the supposition of an ideal resonator framework and relies upon the air concentration (Equation

(2-14)) in the joint α_i and on the joint length L_f that appeared in Fig. 2-10 [59]. Fig. 2-10a shows the L_f in the closed-end rock joints, and Fig. 2-10b presents the L_f in the open-ended rock joints.

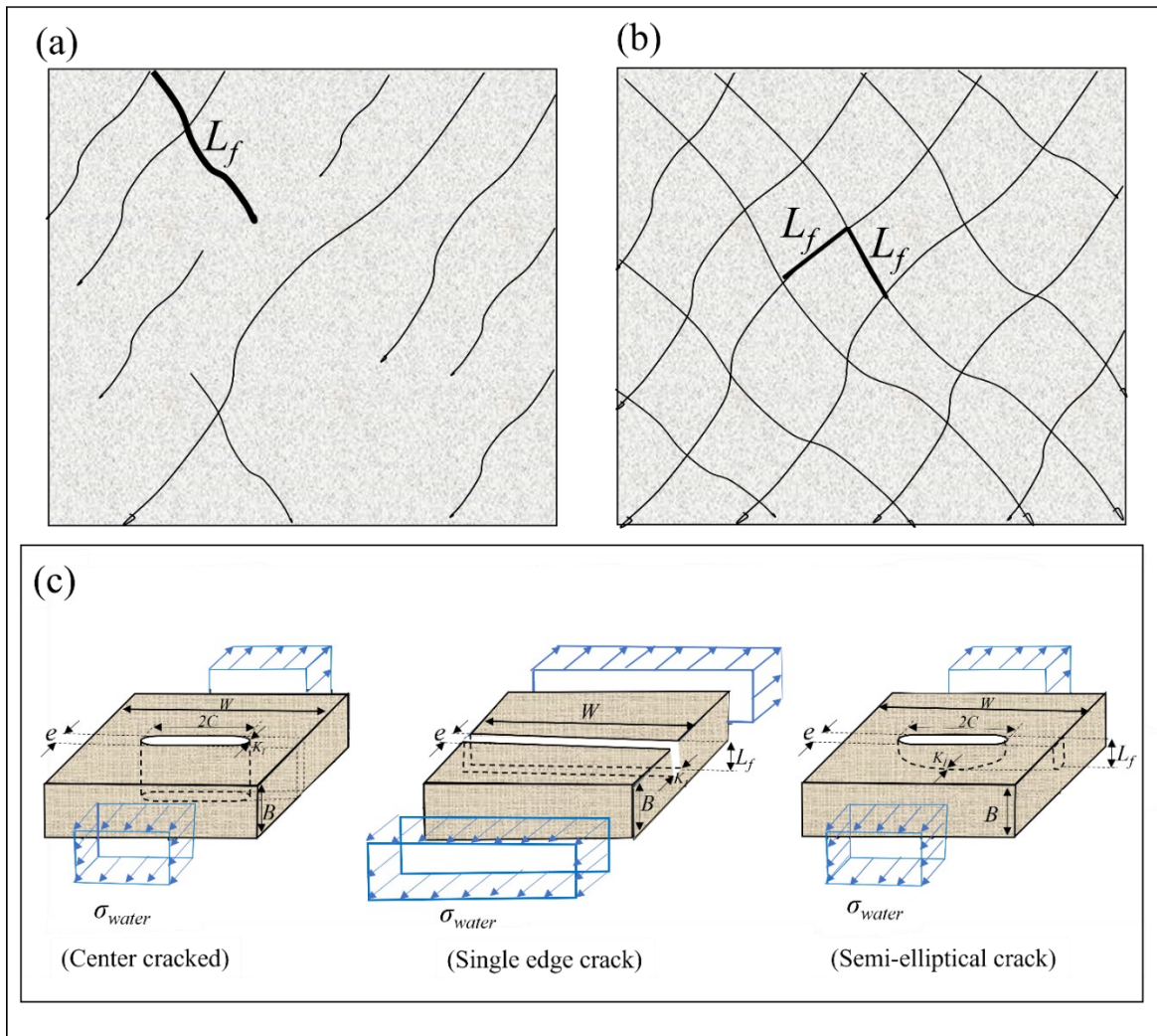


Fig. 2-10. Encountered rock mass layer circumstances for (a) irregularly and (b) totally jointed rocks; (c) proposed structure for the essential geometrical designs of the discontinuously jointed rock [59].

Crack propagation represents the stresses occurring at the joint tip because of the fatigue mechanism owing to the cyclic nature of pressures inside the rock joints. This concept is depicted by linear elastic fracture mechanics. The propagation of cracks can be fragile or time subordinate diffusion. The fragile or brittle failure occurs when an applied stress intensity (K_I) surpasses the fracture toughness (K_{Ic}). Fatigue failure occurs in the contrary case. Stresses are described by K_I (Equation (2-17)) [65]:

$$K_I = \sigma_{water} \cdot f \cdot \sqrt{\pi L_f} \quad (2-17)$$

where K_I is the stress intensity (MPa/m^{1/2}), which is produced by dynamic pressures in the pool bottom and applied to the crack tip that may cause joint propagation; σ_{water} is water stress (MPa) and determined as 80% of P_{max} because of the varying values of P_{max} inside the fracture; f represents the boundary correction factor and relies on the joint type and persistency. Three relevant joint geometries are presented in Fig. 2-10. These geometries are a semi-elliptical crack (*EL*), single edge crack (*SE*), and centre cracked (*CC*). In each of these configurations, the boundary correction factors (f) are defined by Equations (2-18)–(2-20).

$$f\left(\frac{a}{B}, \frac{a}{c}, \phi\right) = C \cdot \frac{\left(\sin^2 \phi + \frac{a^2}{c^2} \cdot \cos^2 \phi\right)^{\frac{1}{4}}}{\frac{3\pi}{8} + \frac{\pi}{8} \cdot \frac{a^2}{c^2}} \quad (2-18)$$

$$f\left(\frac{a}{B}\right) = \left[1.12 - 0.231\left(\frac{a}{B}\right) + 10.55\left(\frac{a}{B}\right)^2 - 21.72\left(\frac{a}{B}\right)^3 + 30.39\left(\frac{a}{B}\right)^4\right] \quad (2-19)$$

$$f\left(\frac{c}{W}\right) = \left[1 + 0.256\left(\frac{c}{W}\right) - 1.152\left(\frac{c}{W}\right)^2 + 12.2\left(\frac{c}{W}\right)^3\right] \quad (2-20)$$

where C is coefficient in Equation (2-18) graphically determined on the basis of the $\frac{a}{B}, \frac{a}{c}, \frac{c}{W}$ ratios and ϕ . Bollaert (2016) simplified Equation (2-17) and proposed Equation (2-21) for determining the stress intensity [64].

$$K_I = 0.8 \cdot P_{max} \cdot f \cdot \sqrt{\pi L_f} \quad (2-21)$$

As previously mentioned, stress intensity (K_I) is produced by dynamic pressures in the pool bottom and applied to the joint tip that may cause joint propagation. If the stress intensity (K_I) is higher than the fracture toughness K_{Ic} , then crack propagation may occur.

The K_{Ic} relies on the mineralogical type of rock, tensile strength (T), and UCS . The changes are conducted to illustrate the rate of loading and in situ stress. Along these lines, the in situ fracture toughness $K_{I,ins}$ is developed on the basis of data analysis and constrained by using Equations (2-22) and (2-23) and Table 2-10 [3].

Table 2-10. Parameters of Equations (2-22) and (2-23) for the in situ fracture toughness value $K_{I,ins}$ [59].

Type of Rock	A	B	C	D
Silicate	0.0648	0.8693	0.0023	1.3257
Carbonate	0.3230	-0.0405	0.0145	-0.0190
Quartz	0.1283	0.2747	0.0088	0.1429

$$K_{I,ins,T} = A \cdot (1.2 \text{ to } 1.5) \cdot T + (0.054 \sigma_c) + B \quad (2-22)$$

$$K_{I,ins,UCS} = C \cdot (1.2 \text{ to } 1.5) \cdot UCS + (0.054 \sigma_c) + D \quad (2-23)$$

where σ_c indicates the confinement horizontal in situ stress and is determined by using vertical stress and K_0 (σ_h/σ_v). UCS , σ_c , and T are in MPa. If the applied stress intensity surpasses the in situ fracture toughness ($K_I \geq K_{I,ins}$), then brittle failure will occur; otherwise, failure mechanics and crack propagation are communicated as Equation (2-24) [66]:

$$\frac{da}{dN} = C. (\Delta K_I)^m \quad (2-24)$$

where C and m rely on the rock characteristics that are recognised on the basis of fatigue tests; dN represents the number of pressure cycles; and ΔK_I defines the most and the least stress intensity differences. Variables m and C must be determined to handle time-dependent crack propagation into the model [67].

In 2016, Bollaert et al. modified Equation (2-24) and proposed Equation (2-25) as the new equation for the fatigue process. Fracture toughness (K_{Ic}) was considered in the new equation [68]:

$$\frac{dL_f}{dN} = C. (\Delta K_I / K_{Ic})^m \quad (2-25)$$

The flowchart of *CFM* is presented in Fig. 2-11. The ultimate scour depth and time of scouring could be computed on the basis of the maximum dynamic pressure in the pool bottom (P_{max}), stress intensity (K_I), in situ fracture toughness ($K_{I,ins}$), and fatigue failure mechanism owing to this method.

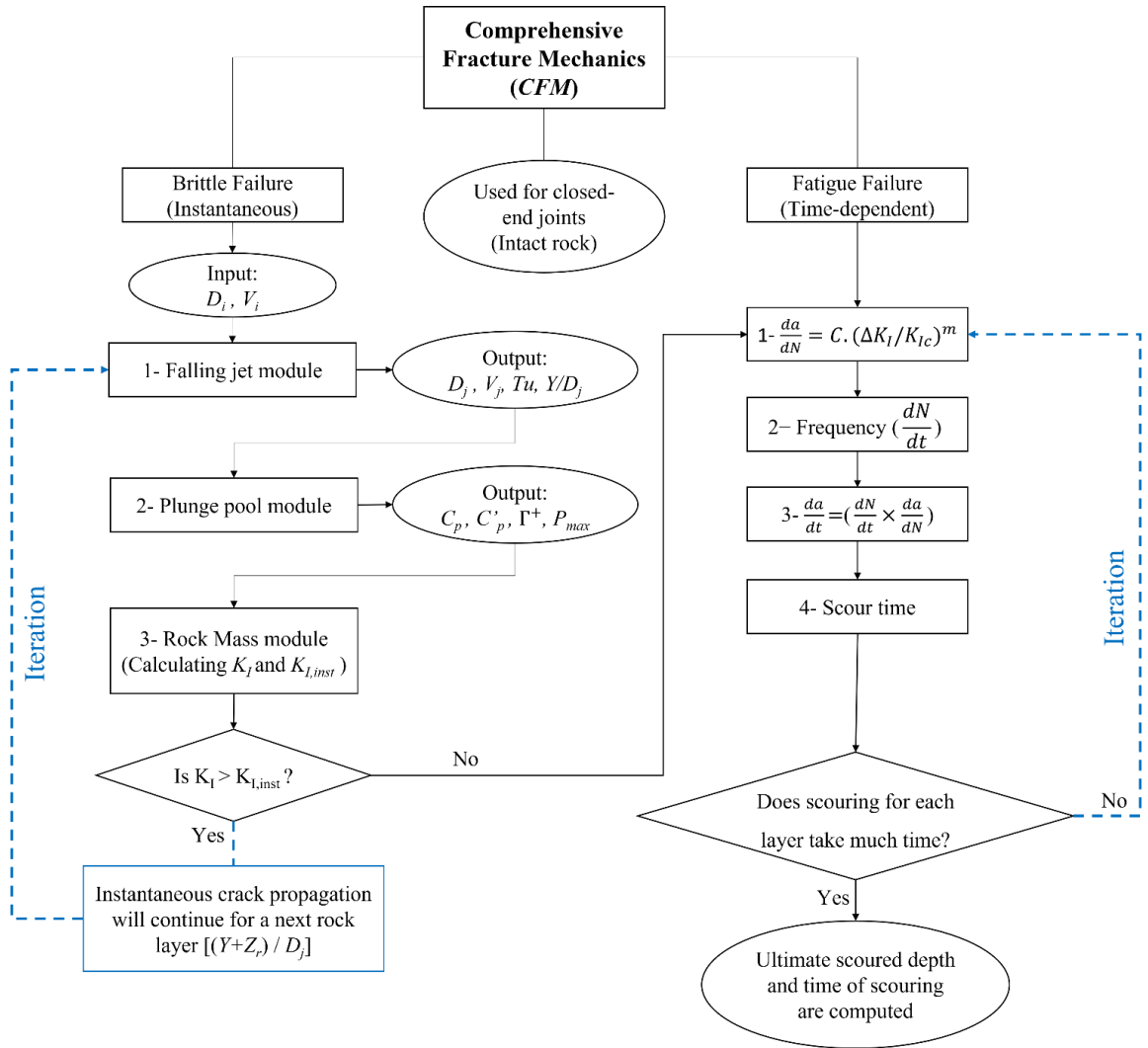


Fig. 2-11. CFM flowchart.

2.5.2 DI Method

Bollaert proposed the *DI* method for the first time, which is used for predicting the ultimate scour depth in the plunge pools for open-ended joints and single rock blocks [59]. This method explains the movement of rock blocks by their mass on the basis of the uplift pressures. *DI* is based on the maximum impulse (I_{max}) in an open-ended rock mass fracture (single rock block) that is provided by the time integral of net forces. Net forces consist of the submerged weight of the block, shear and interlocking forces, and forces produced by pressures under and over the block [59,62]. The final purpose in the *DI* method is to determine the uplift height (h_{up}) by using net uplift velocity ($V_{\Delta tpulse}$), which is determined by net impulsion (I_{net}) (kN/s), and the block mass (m_s) (kg). The *DI* method is explained stepwise in the following paragraphs. The flowchart of *DI* is presented in Fig. 2-12; Fig. 2-13 shows the impulse dynamics on a block.

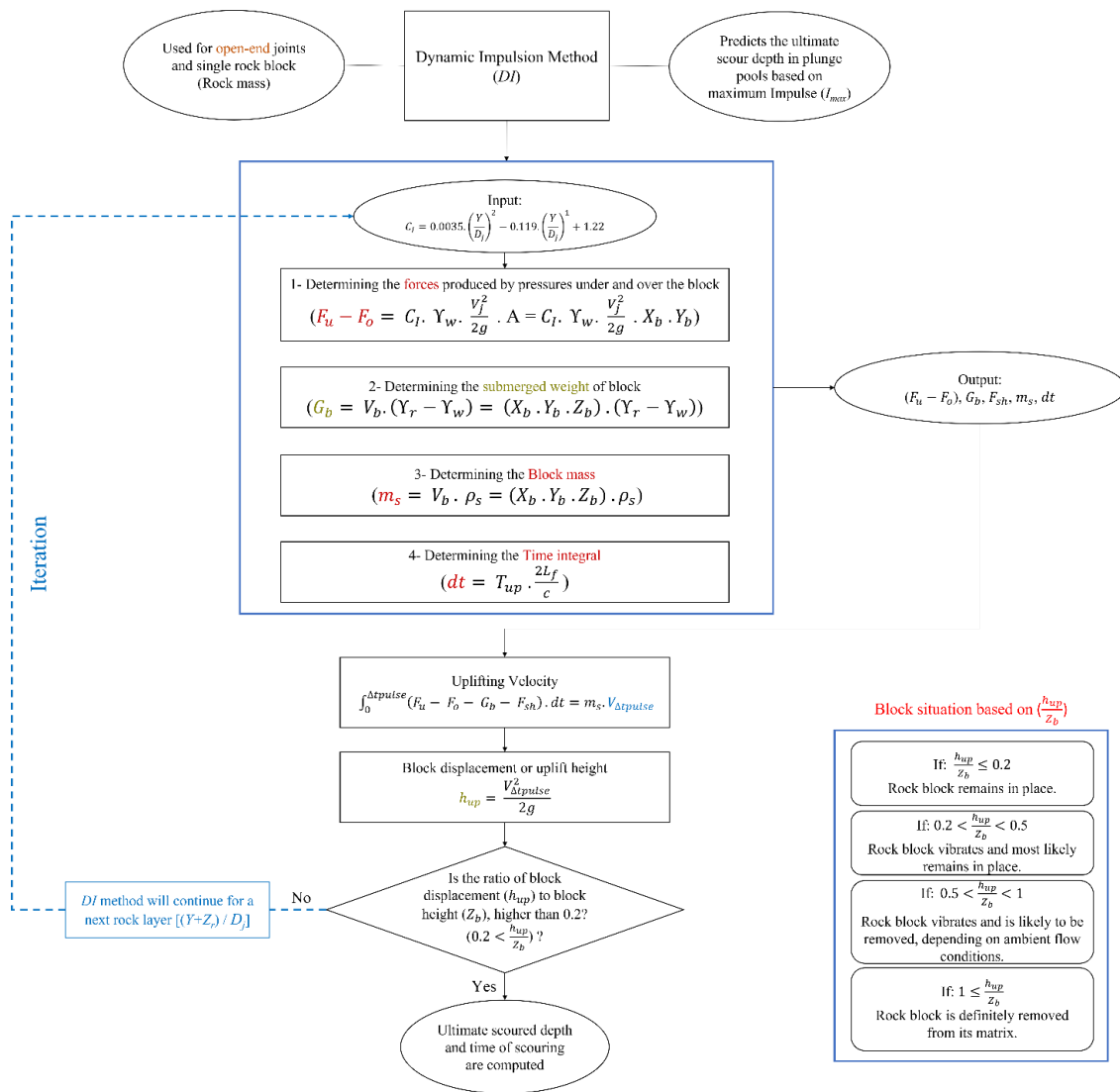


Fig. 2-12. DI flowchart.

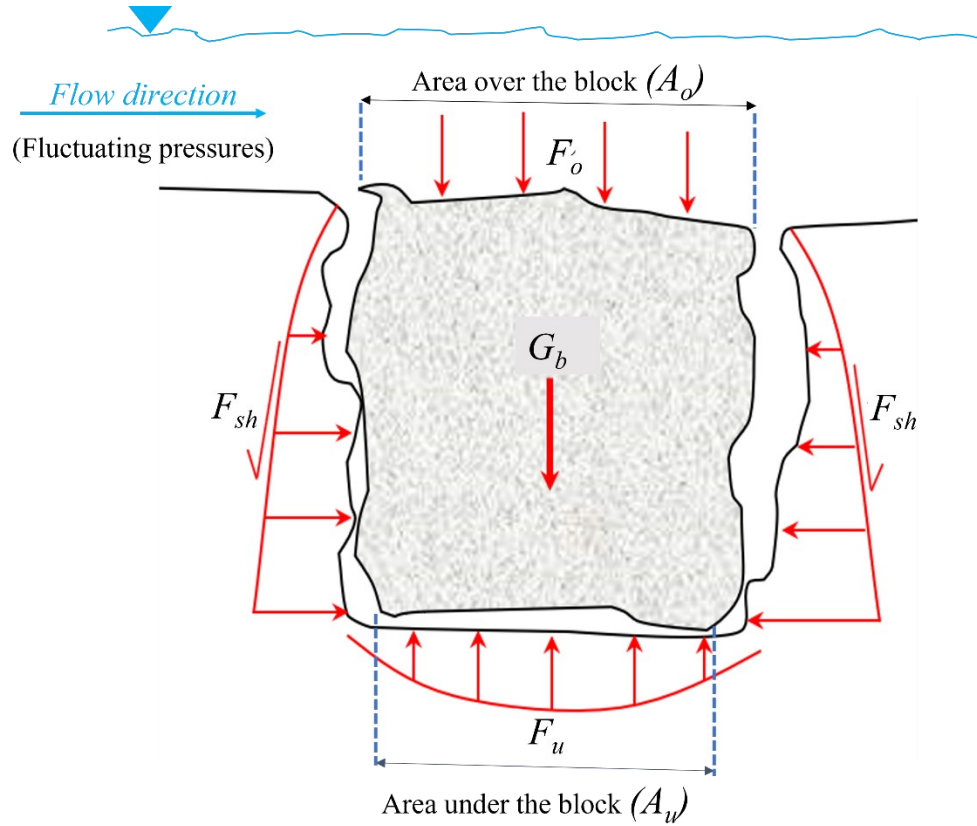


Fig. 2-13. Conceptualisation of impulse dynamics on a block, based on the Bollaert DI method [59].

Kinetic and potential energies have been used in Equation (2-26) for determining the uplift height (h_{up}) (m) from Equation (2-27) and comparing with block height (Z_b) (m).

$$mgh_{up} = \frac{1}{2} mV_{\Delta tpulse}^2 \quad (2-26)$$

$$h_{up} = \frac{V_{\Delta tpulse}^2}{2g} \quad (2-27)$$

where $V_{\Delta tpulse}$ is the uplifting velocity (m/s), which is also named ‘launch velocity’ computed from Equation (2-36) and net impulsion (I_{net}) shown in Equation (2-28).

$$I_{net} = \int_0^{\Delta tpulse} (F_u - F_o - G_b - F_{sh}) \cdot dt = m_s \cdot V_{\Delta tpulse} \quad (2-28)$$

where F_u and F_o are considered the forces produced by pressures under and over the block (kN), and are produced because of the dynamic pressure in the pool bottom; G_b is the submerged weight of block (kN), which is determined by using Equation (2-29); and F_{sh} is the shear force (kN). Shear force (F_{sh}) is considered zero because it acts in a direction parallel to a surface. This variable is zero for a cubic block. Time integral (dt) is

in seconds, taken over the Δt period (Δt is the period in which positive differences exist in forces produced by pressures over and under the block), and is determined by Equation (2-34). The block mass m_s is in kilograms and determined by Equation (2-35).

$$G_b = V_b \cdot (Y_r - Y_w) = (X_b \cdot Y_b \cdot Z_b) \cdot (Y_r - Y_w) \quad (2-29)$$

where V_b is the block volume (m^3); Y_r is the unit weight of rock (kN/m^3); Y_w is the unit weight of water (kN/m^3); and X_b , Y_b , and Z_b are the block width, length, and height, respectively.

The shear force F_{sh} was dismissed in these relations. The nature of the rock joints is rough in real situations. The roughness of the rock joints plays an important role in determining the shear strength. The shear strength of rock must be determined when designing rock-engineering structures. In this regard, the shear resistance must be determined in the block uplift process. The block uplift velocity relies upon the lateral pressure differences and frictional resistance of the sidelong discontinuities. For this reason, in 2014, Pan et al. developed several analytical equations for computing shear resistance force (F_{sh}) for two unique modes [69]. The first mode (Equation (2-30)) is used when the pressure fluctuations are equal in the opposite surface (top and bottom) of the block. The second mode (Equation (2-31)) is used when the pressure fluctuations at the top of a rock block are more prominent than that at the bottom of a rock block.

$$F_{sh} = \mu \cdot K_0 \cdot Y' \cdot Z_b^2 (X_b + Y_b), \text{ For } P_{bottom} = P_{top} \quad (2-30)$$

$$F_{sh} = \mu \cdot K_0 \cdot (Y' + Y_w \cdot \frac{\Delta h}{Z_b}) \cdot Z_b^2 (X_b + Y_b), \text{ For } P_{bottom} < P_{top} \quad (2-31)$$

where μ stands for the frictional coefficient, Y' is the submerged unit weight (kg/m^3), and Δh is the pressure head difference.

Bollaert determined the difference between the forces under and over the block by using a nondimensional (C_I) coefficient (Equation (2-32)), which is produced by curve fitting on the basis of some experiments [59]. Variable C_I is the coefficient for determining the difference between pressures under and over the block. Thus, Equation (2-33) should be used for computing net uplift force ($F_u - F_o$).

$$C_I = 0.0035 \cdot \left(\frac{Y}{D_j}\right)^2 - 0.119 \cdot \left(\frac{Y}{D_j}\right) + 1.22 \quad (2-32)$$

where Y is the water depth in the plunge pool and D_j is the jet diameter at the impact. Both variables are in meters.

$$F_u - F_o = C_I \cdot Y_w \cdot \frac{V_j^2}{2g} \cdot A = C_I \cdot Y_w \cdot \frac{V_j^2}{2g} \cdot X_b \cdot Y_b \quad (2-33)$$

where $\frac{V_j^2}{2g}$ is the incoming kinetic energy (m), V_j is the jet speed at impact (m/s), and A is the area of the block surface over or under the block (m).

$$dt = T_{up} \cdot \frac{2L_f}{c} \quad (2-34)$$

where T_{up} is a nondimensional time coefficient and assumed by large-scale laboratory experiments, L_f is the total length of the joint (m), and c is the mean wave celerity (m/s). If X_b , Y_b , and Z_b are considered as block width, length, and height, respectively, then the total length of the joint is $L_f = 2Z_b + X_b$.

$$m_s = V_b \cdot \rho_s = (X_b \cdot Y_b \cdot Z_b) \cdot \rho_s \quad (2-35)$$

where V_b stands for the block volume (m^3), and ρ_s is the density of rock (kg/m^3). Considering Equations (2-26)–(2-29) and (2-32)–(2-35), uplifting velocity ($V_{\Delta tpulse}$) is computed similar to Equation (2-36):

$$V_{\Delta tpulse} = \frac{(F_u - F_o - G_b - F_{sh}) \cdot dt}{m_s} = \left[\frac{[C_I \cdot \gamma_w \cdot \frac{V_j^2}{2g} \cdot X_b \cdot Y_b - (X_b \cdot Y_b \cdot Z_b) \cdot (\gamma_r - \gamma_w) - F_{sh}] \cdot (T_{up} \cdot \frac{2L_f}{c})}{(X_b \cdot Y_b \cdot Z_b) \cdot \rho_s} \right] \quad (2-36)$$

Finally, the uplift height is directly computed by using Equation (2-37).

$$h_{up} = \frac{\left[[C_I \cdot \gamma_w \cdot \frac{V_j^2}{2g} \cdot X_b \cdot Y_b - (X_b \cdot Y_b \cdot Z_b) \cdot (\gamma_r - \gamma_w) - F_{sh}] \cdot (T_{up} \cdot \frac{2L_f}{c}) \right]^2}{2g \cdot [(X_b \cdot Y_b \cdot Z_b) \cdot \rho_s]^2} \quad (2-37)$$

After h_{up} is determined, the ratio of uplift height to block height (h_{up}/Z_b) must be characterised. The capability of rock scour must be evaluated by utilising Fig. 2-14, which depends on field data analysis. In 2005, Bollaert and Schleiss determined that the block might be separated from the rock mass when h_{up}/Z_b is greater than 20% ($h_{up}/Z_b > 0.20$) [61].

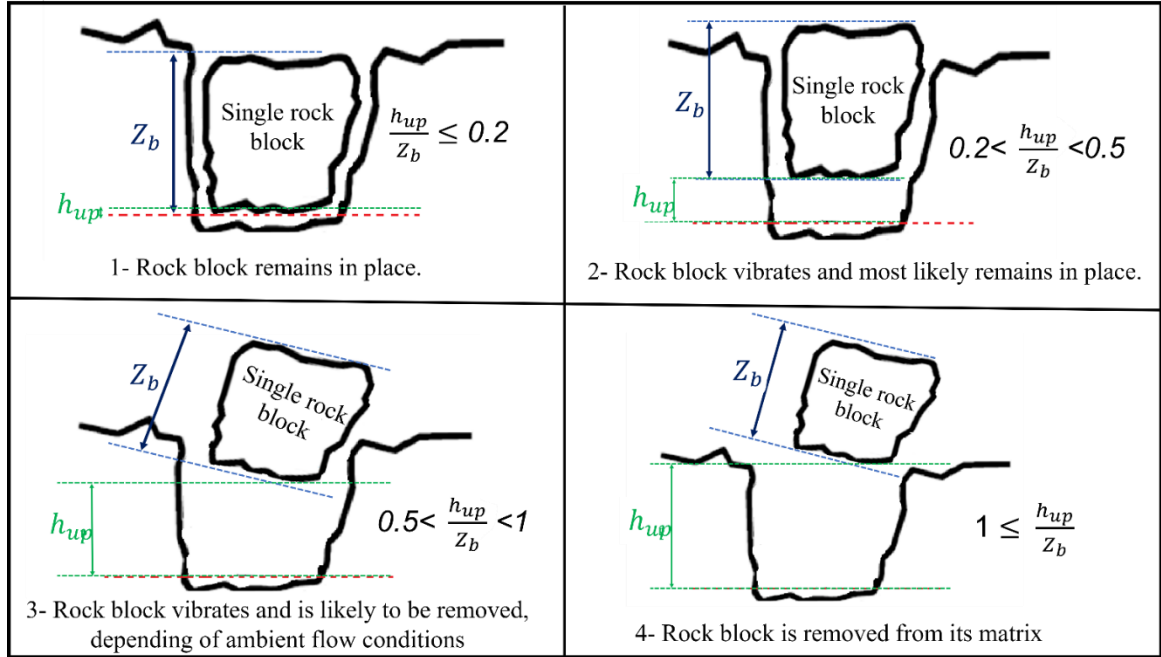


Fig. 2-14. Proposed criteria to evaluate the rock scour potential by DI [63,70].

The Bollaert portrayal for the DI method has two ambiguities, especially in enlisting $(F_u - F_o)$. A comparable delineation was determined for DI and portraying C_l coefficient in several articles of Bollaert [59,61–63].

The C_l , $(F_u - F_o)$, and uplift height (h_{up}) are difficult to determine considering this description. The final dimension of $(F_u - F_o)$ is in m instead of kN by considering this description. The unit weight of water (γ_w) and area of block surface (A) are not intended for converting the DI coefficient (C_l) to force.

In 2004, Annandale corrected Bollaert's problem in converting C_l to force and proposed a modified equation for determining (h_{up}) [71]. However, Annandale did not consider the nondimensional time coefficient (T_{up}) in Equation (2-37).

Bollaert published a new article and proposed the simplified CSM ($SCSM$) because of the difficulty in understanding the CSM [64]. In $SCSM$, the DI method is explained stepwise. Bollaert corrected the problem in previous publications. This time, he converted C_l to pressure instead of force and did not consider the block surface area (A). We present Equation (2-38) for computing the h_{up} by considering its explanation about the DI method and block surface area (A).

$$h_{up} = \frac{\left[C_l \cdot \gamma_w \cdot \frac{V_j^2}{2g} \cdot A - (X_b \cdot Y_b \cdot Z_b) \cdot (\gamma_r - \gamma_w) - F_{sh} \right] \cdot \left(T_{up} \cdot \frac{2L_f}{c} \right)^2}{2g \cdot [(X_b \cdot Y_b \cdot Z_b) \cdot \rho_s]^2} \quad (2-38)$$

where the block surface area (A) is in m^2 .

In 2006, Manso developed the *CSM* of Bollaert and studied the effects of the plunge pool geometry on the rock scour with a high velocity jet. Manso performed different experiments by considering the various plunge pool geometries (12 geometries) [72]. This work was conducted to determine the effect of the plunge pool geometry on pressure produced by circular jets. In 2014 and 2016, Duarte developed the *CSM* focused on the jet aeration and considered various types of fluid on the basis of air content (β) to propose a new equation for determining block displacement (uplift height h_{up}) [73,74].

In 2009, Asadollahi proposed a semi-analytical methodology for assessing the single block stability in the plunge pools by using three-dimensional block stability (*BS3D*) [75]. Asadollahi developed this methodology by numerical *BS3D* code. *BS3D* is used to compute the block uplift acceleration by using Federspiels' experimental studies [76–78]. In this methodology, the uplift height can be determined on the basis of Newton's second law after the aforementioned acceleration is computed. Asadollahi assessed the erosion in the plunge pools on the basis of Bollaert *DI* technique. Moreover, Asadollahi modified Bollaert's criteria for deciding the occurrence of block removal and proposed the $h_{up}/Zb > 0.25$ ratio based on data analysis of several case studies and using Martins' experimental data [79]. For this reason, Asadollahi actualised a Fortran code dependent on the calculation presented by Tonon (2007) [80]. *BS3D* considers all expansive displacement techniques for rock blocks subject to conventional powers. This methodology had admissible results compared with the observed block uplift.

2.5.3 QSI Method

In 2010, Bollaert proposed the *QSI* technique to assess the scour in walls of the plunge pools for parallel flow condition relative to the rock surface [81]. Bollaert developed this methodology on the basis of Reinius' study, which was for identification of the effect of the pressure fluctuations on the rectangular rock block uplift and protruding block cases [82]. The effective forces that are applied to the block and cause the rock block uplift or ejection follow: rock block submerged weight, quasi-steady uplift force produced because of the pressures underneath the rock block, and the turbulent uplift forces produced because of the pressure fluctuations (Fig. 2-15b) [81]. The uplift forces produced because of the pressure fluctuations are significant to cause the block uplift in protruding rock block cases. In 2015, George studied various flow condition analyses and concluded that the quasi-steady system is more effective than the other lifting forces when considering the parallel flow condition. George also found that the forces produced by pressure fluctuations could be neglected from calculations. The flowchart of *QSI* is presented in Fig. 2-16 [83].

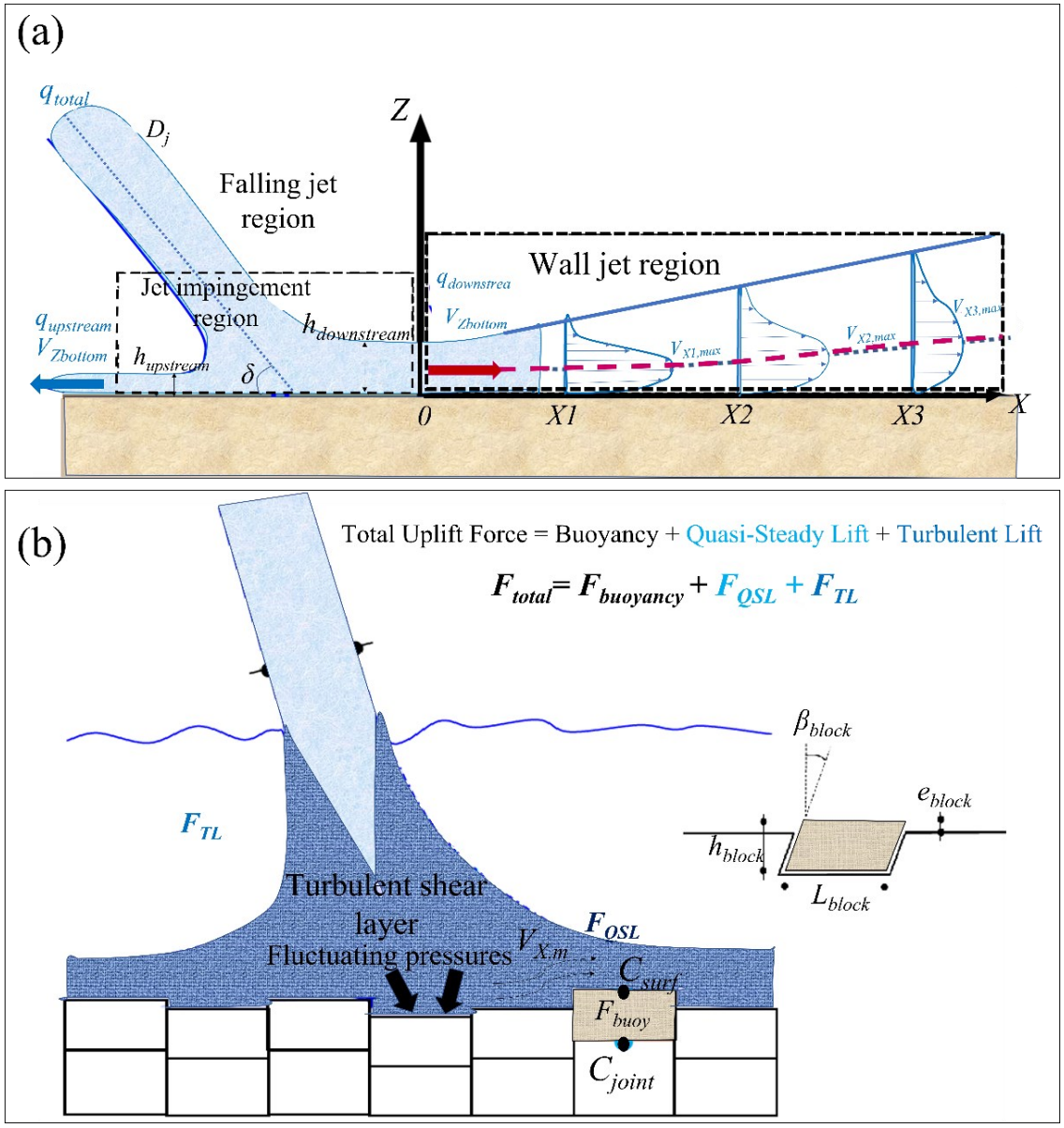


Fig. 2-15. (a) Plane jet deflection on a flat bottom and wall jet velocity profiles; (b) effective forces on block uplift [81]

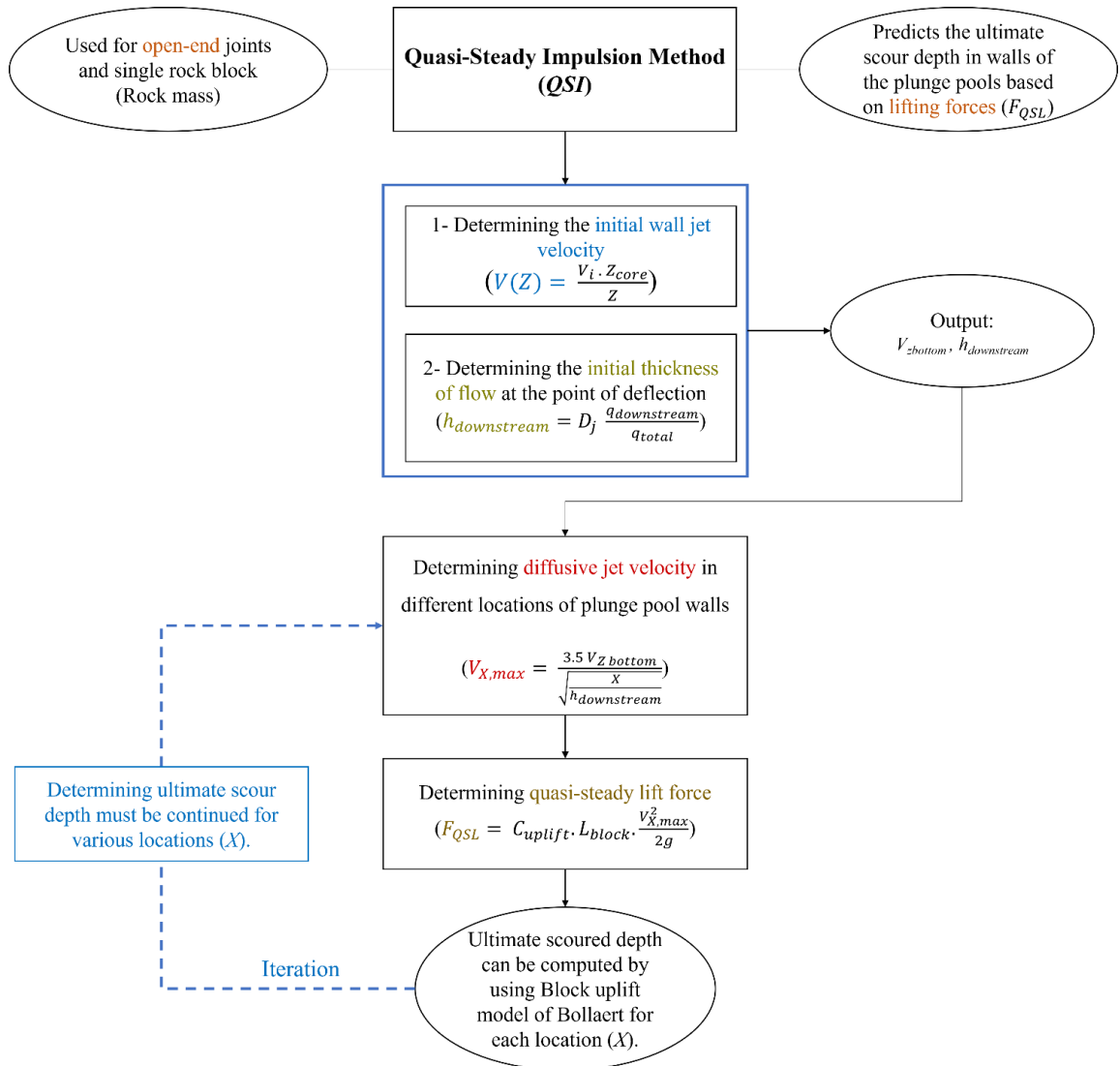


Fig. 2-16. QSI flowchart.

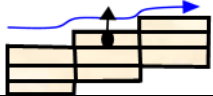



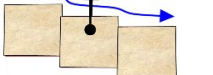
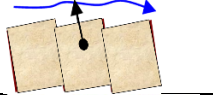
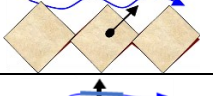

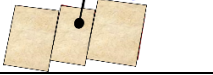
Fig. 2-15a shows the various areas that developed as a result of the falling jet in the plunge pools. Fig. 2-15b illustrates the effective lifting forces that cause the rock block uplift, where e_{block} represents the block protrusion, h_{block} is the block height, L_{block} denotes the block length, and β_{block} is the angle between the block edges.

In the QSI, only quasi-steady lift force is considered in the calculations. The quasi-steady lift force is determined by using Equation (2-39) [81]:

$$F_{QSL} = C_{uplift} \cdot L_{block} \cdot \frac{V_{x,max}^2}{2g} \quad (2-39)$$

where C_{uplift} denotes the net uplift pressure coefficients and computed by deducting the surface pressure coefficient (C_{surf}) from the pressure coefficient inside the joints (C_{joint}) ($C_{joint} - C_{surf}$). Table 2-11 shows the potential net static uplift pressures for various arrangements of rock blocks [82].

Table 2-11. Net uplift stagnation pressures for the various setups of block projection and joint points [82].

Test No.	Block Configuration	Block Protrusion (β_{block})	h_{block}/e_{block}	C_{joint}	C_{surf}	C_{uplift}
1		0°	17–29	0.250	0.030	0.220
2		9°	2–4	0.36–0.55	–0.10 to 0.17	0.37–0.47
3		0°	17–29	0.250	0.030	0.220
4		0°	17–29	0.105	0.020	0.085
5		0°	4–9	–0.110	0.075	–0.070
6		–3°	4.2–87	–0.105	0.02 to 0.13	–0.070
7		18°	1–2.5	0.23–0.40	–0.15 to 0.00	0.25–0.45
8		0°	17–34	0.145	0.010	0.155
9		3°	4–10	0.350	0.030	0.310

As referenced, L_{block} is the block length (m) that appeared in Fig. 2-15b, and $V_{x,max}$ represents the diffusive jet velocity in different locations. The different distances from wall jet issuance points and are computed by using Equation (2-40) [84]. The jet velocity profile and jet thickness have an inverse relationship where the wall jet velocity decreased, and the wall jet velocity profile smoothed when the jet thickness is increased (Fig. 2-15a).

$$V_{x,max} = \frac{3.5 V_{Z\ bottom}}{\sqrt{\frac{X}{h_{downstream}}}} \quad (2-40)$$

where $h_{downstream}$ is the initial thickness of flow (Fig. 2-15a) at the point of deflection and determined by using Equation (2-41), where $q_{downstream}$ is the discharge rate in the downstream side and q_{total} is the total discharge rate of the falling jet.

$$h_{downstream} = D_j \frac{q_{downstream}}{q_{total}} \quad (2-41)$$

The $V_{Z_{bottom}}$ is the initial wall jet velocity (m/s). $V_{Z_{bottom}}$ relies upon the angles that the jet makes with the water surface at the impacting point and water depth Z , and computed by utilising the model of Hartung and Häusler, which is presented in Equation (2-42) [85].

$$V(Z) = \frac{V_i \cdot Z_{core}}{Z} \quad (2-42)$$

where Z_{core} (m) represents the vertical distance that the core jet needs to be deflected inside plunge pools and commonly considered as 4–5 times the D_j . The V_i represents the initial plunging jet velocity with a dimension of m/s, and Z is the water depth.

Table 2-12 illustrates the downstream and upstream digressed pieces of the absolute stream rate for various impingement angles δ , which are introduced by Reich [86].

Table 2-12. Upstream and downstream strayed pieces of the absolute discharge rate for various points of impingement δ [86].

Jet Angles (δ) (degree)	10	20	30	40	90
qupstream	1.5%	6%	7%	12%	50%
qdownstream	98.5%	94%	93%	88%	50%

Block shape is one of the important parameters in rock block removal. For this purpose, the common blocks shape was identified on the basis of the existing rock mass geomechanical data and field observations. In that capacity, a plate-like formed block will be ejected just by jet impact. Finally, the ultimate scour depth can be determined by utilising Bollaert's *DI* technique after the lifting forces are determined.

On the basis of Lesleighter's study on Paradise Dam in Australia, the *DI* method overestimates the scour depth, where the prediction of *CFM* is close to the actual case [87].

The basis of the semi-analytical methods is experimental. For this purpose, Table 2-13 illustrates some information about the setup of these experiments.

Table 2-13. Hydraulic geometrical characteristics of the experiments.

Method Name	Type of Model	Configuration	Flow	Inclination	Method of Analysis
Manso and Schleiss (2006) [72]	Vertical jet in plunge pool	Variable: Pool bottom type, Flow characteristics Fix: Joint characteristic	Medium 120 L/s	Vertical 90°	Quantitative: Pressure measured in the joint and on the pool surface
Lesleighter and Bollaert (2016) [87]	Scale of 1:70 of Paradise Dam	-	Very High 1200 L/s	At Scale	Quantitative: Pressure and speed
Reinius (1986) [82]	Open channel flow, set of blocks	Variable: Dip of blocks Fix: Joint opening, Block volume	High 311 L/s	Horizontal	Quantitative: Pressure measured on one block's faces
Annandale (1995) [21]	Plunging jet in a plunge pool, two layers of blocks	Fix: Block disposition, Jet characteristics	Very high 3400 L/s	15° Jet flow	Quantitative: Pressure measured on the basin surface and between blocks layers
Bollaert and Schleiss (2002) [59]	Vertical jet in a basin, various steel joints	Variable: Flow characteristics, Types of joints Fix: Orientation of joints	Medium 120 L/s	Vertical	Quantitative: Pressure measured in the joints and on the pool surface
George (2015) [83]	Open channel flow, one tetrahedral block	Variable: Block orientation Fix: Channel slope, Block volume	High 300 L/s	Realistic 21°	Quantitative: Speed at block displacement

Numerous parameters affect the plunge pool scour. These parameters can be studied in two different aspects: hydraulic and rock mass.

The most critical parameter in the hydraulic aspect is uplift pressure, which depends on many other geometrical and hydraulic parameters; for example, tailwater depth, initial jet velocity, jet diameter, and plunging jet height affect pool bottom and total uplift pressures. Increasing the tailwater depth will decrease the uplift pressure; conversely, the uplift pressure will increase by raising the initial jet velocity, jet diameter, and plunging jet height.

Numerous geometrical and geomechanical parameters in the rock mass aspect affect the ultimate scour depth. These parameters include joint opening, block volume, block shape, joint roughness, and fracture toughness. This selection of parameters can be comprehensively studied as future challenges.

2.6 SCOURING AT THE MULTIBLOCK SYSTEM WITH NUMERICAL METHODS

Most previous methods used for computing the scour depth or to assess the hydraulic erodibility were developed for the analysis of a single rock block related to the geomechanical, geometrical, and hydraulic parameters. In most plunge pool cases, the stability of a single rock block is assessed as a representative block

of a characteristic blocky layer in various hydraulic conditions. This assessment is continued for nether layers because the representative block started to be stable for removal. Limited methods have been proposed to assess the scouring for multiblock systems, which are presented in section 4. Fig. 2-17 presents the numerical approach.

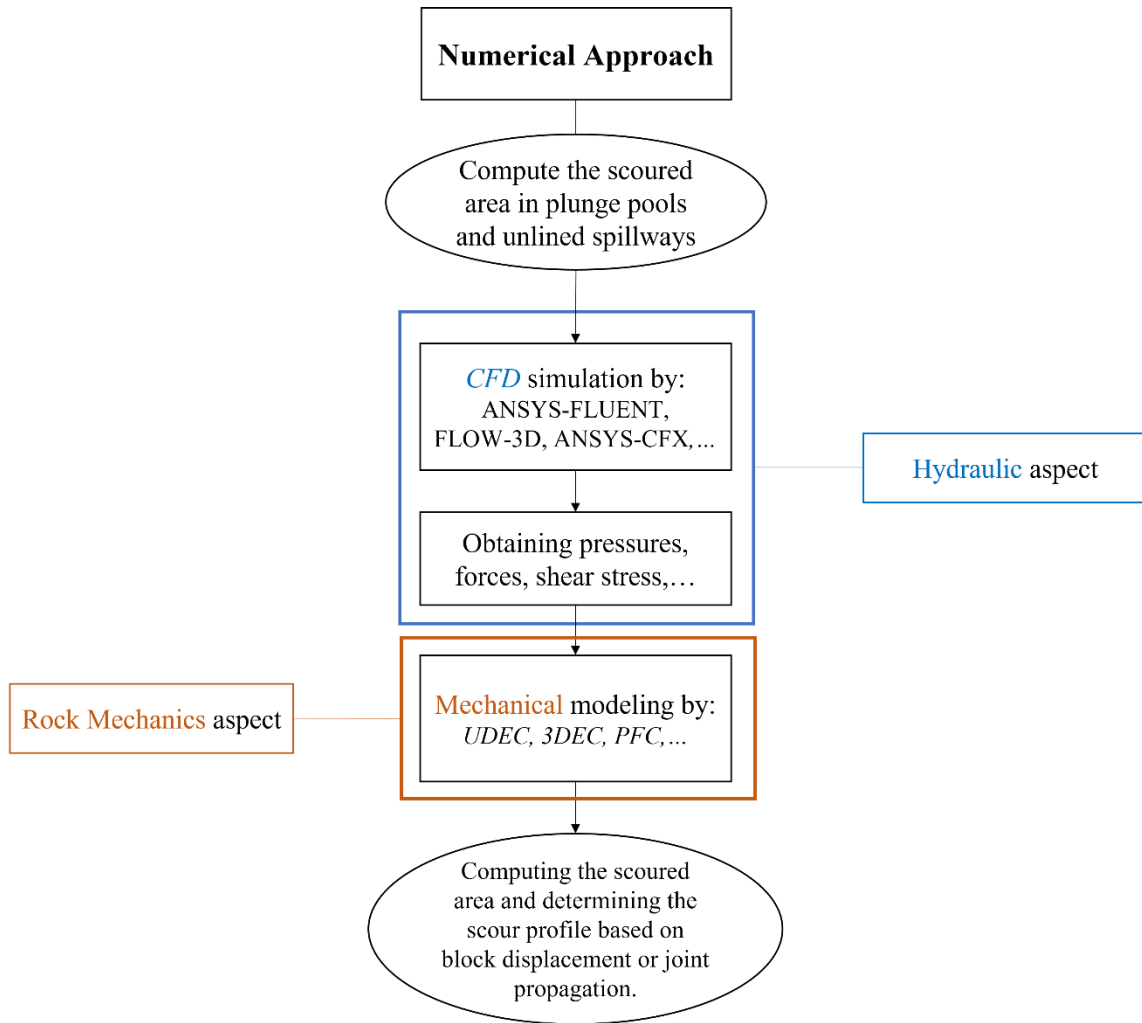


Fig. 2-17. Flowchart of the numerical approach.

Multi-block assessments are more important than single-block assessments because of the location dependent assessment of this system. This system can assess the scouring for various rock block shape and geometrical conditions. In 2009, Wibowo evaluated rock erosion by modelling in universal distinct element code (*UDEC*) software for dam spillways, based on the block theory of Goodman [88,89]. Fig. 2-18 shows the *UDEC* model. The red blocks in this model are more vulnerable to removal than those shown in blue.

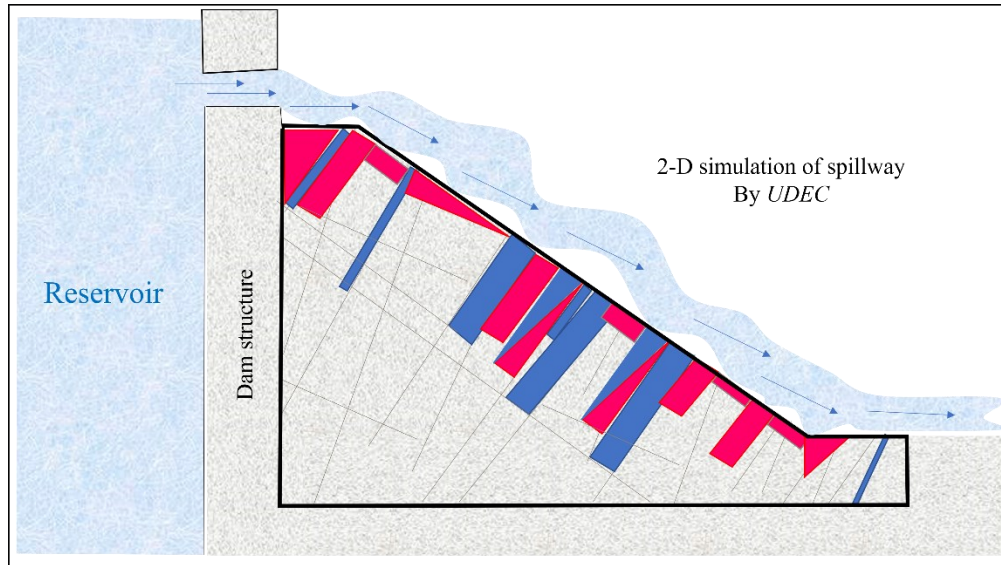


Fig. 2-18. Two-dimensional ejectable blocks in an unlined spillway [88].

In 2016, Castillo and Carrillo proposed a numerical simulation by using computational fluid dynamics (CFD) in FLOW-3D software to help in determining the bed erosion in plunge pools [50]. Their methodology solves the Navier–Stokes equations and combines various turbulence models, a block transport model, a semi-theoretical model of the rock mass erosion, and a methodology for computing the free surface of the fluid. This methodology evaluates the hydraulic erodibility of the bed rock by using the combination of the aforementioned models by accurate characterization. In the final step of their study, they conducted a comparison between the pressures and the mean dynamic pressure coefficients obtained exactly at the stagnation area with the parametric approach and studied the local effects of the block’s movement.

Li and Liu, in 2010, proposed another numerical method on the basis of the discrete fracture network (DFN) for evaluating scouring in the plunge pools. The DFN is developed based on a numerical analysis of the hydraulic erodibility in the downstream of dams and the Monte Carlo technique. Ejectable 2D rock blocks were determined by considering the geometry of the plunge pools and discontinuity behaviour. Li and Liu simulated the fluctuating pressures inside the joint and the distribution pressure fluctuating inside the fractured media. Li also analysed the rock block stability on the basis of the empirical equations as a function of rock joint hydraulic pressures [90].

In 2011, Dasgupta, proposed a methodology for evaluating the plunge pool scouring on the basis of three-dimensional computational fluid dynamic (CFD) programming for computing the representative erosive agent of water that is applied to the rock surface [91]. Dasgupta used 2D UDEC to simulate the rock mass. The results of ANSYS FLUENT (plunge pool bottom pressures) were applied to the UDEC to assess the rock block ejection and brittle failure. Fig. 2-19a highlights the 3D flow pattern of the plunging jet of a single valve. Fig. 2-19b shows the primary results of the surface erosion. Fig. 2-19b(1), Fig. 2-19b(2), and Fig. 2-19b(3) show the results

of the block removal simulation, brittle failure of the rock block simulation, and combination of the two latter simulations, respectively. The fluctuation of the transient pressure is applied to the rock surface as the dynamic pressure and the time-dependent pressures inside cracks and fractures. The rock block removal at the water–rock interface explains the scouring mechanism.

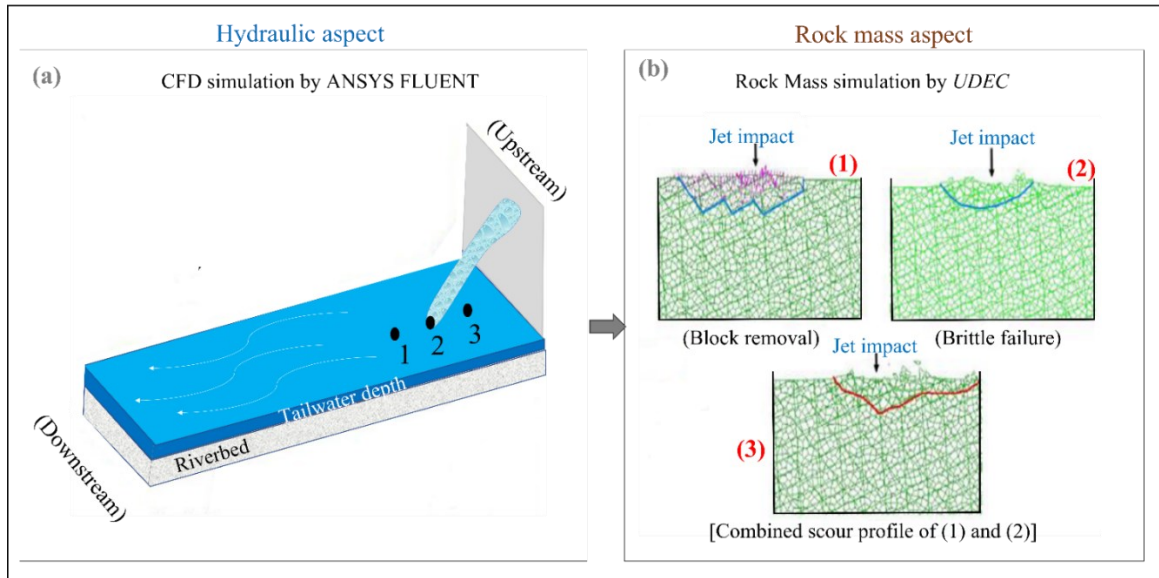


Fig. 2-19. Numerical simulation of plunge pool scour [91].

The methodology of Dasgupta demonstrates promise to utilise numerical techniques for combining the three-dimensional rock mass geometry alongside complicated stream cases.

George presented a non-numerical (experimental–analytical) methodology by using block theory to evaluate the stability of the 3D rock blocks and potential hydraulic erodibility in dam spillways [83]. The methodology of George and Sitar proposed to evaluate the hydraulic erodibility on the basis of multiblock systems [92,93]. Scaled physical model testing and a prototype field experiment (the first of its kind) were performed to examine the role of the 3D geologic structure on the block erodibility. They assessed the possibility of ultimate block failure and the most probable failure mechanism by using Monte Carlo simulations and a first-order reliability method [93]. This study was the first to consider noncubic/nonrectangular block geometries and showed how the geometry influenced a block response. The block theory method was shown to reasonably predict block stability under channel flow conditions. Fig. 2-20 shows the spillway geometry and situation of the removable block inside a rock mass.

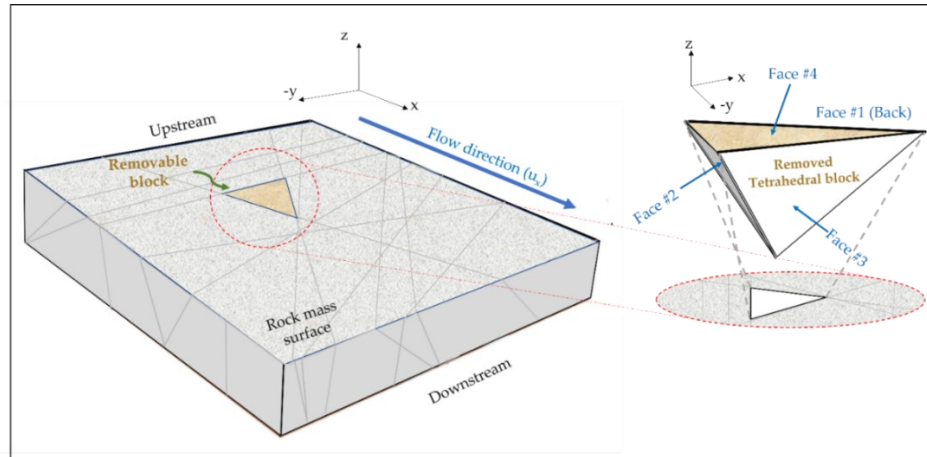


Fig. 2-20. Schematic of the spillway and removable block geometry for reliability analysis [83].

In 2018, Gardner developed the experimental–analytical methodology of George and proposed a new numerical methodology to evaluate rock scour in the jointed rock mass [83,94]. Gardner performed the coupled fluid–solid simulations to assess the water–rock interaction behaviour and potential of the 3D polyhedral rock block erosion. This methodology was developed on the basis of the coupled discrete element method (DEM)–lattice Boltzmann method (LBM) programme. In the first step, Gardner developed a new open-source DEM code, which is written using C++ language, to evaluate the mechanical behaviour and the kinematic response of the jointed rock mass. Then, Gardner developed a DEM code and coupled it with LBM to analyse the ejection and movement of 3D polyhedral rock blocks in water. In this methodology, various block shapes and geometries were analysed, and a comparison between its coupled solid-CFD approach with real dataset was performed.

2.7 CRITICAL ANALYSIS AND APPLICATION OF DIFFERENT APPROACHES ON REAL CASES

To compare various approaches of hydraulic erodibility assessment, we applied the existing methods to real data and presented their results in the present section. Accurately comparing semi-theoretical approaches with semi-analytical and numerical methods is challenging due to the distinct nature of these methodologies. The foundations of these approaches differ, necessitating comparisons within the same category of approaches.

More detailed data and in situ tests are required to analyse and compare the semi-analytical methods, such as the *CSM* method and the existing dataset, making it difficult to compare this approach with other approaches.

There are no clear methodology and or software for the application of numerical methods for rock erosion prediction. The flow parameter should be determined by hydraulic software and implemented to geomechanical software. The principal question is, which flow parameter should be deduced from hydraulic software and how should it be implemented in the geomechanical software because of their existing limitations. The application

and comparison have been performed on the methods used most often, such as Kirsten, Annandale, Van Schalkwyk, *RMEI*, and *eGSI*. For comparison purposes, the field data collected from various case studies conducted by Pells on unlined rocky spillways are used in this comparative critical analysis. Table A1 illustrates the result of the application of various semi-theoretical approaches on several case studies. These results are obtained by using the threshold lines proposed by these five approaches.

The efficiency of the five comparative scour thresholds is determined herein according to the number of case studies with poorly evaluated scour conditions. According to the results shown in Table A1 and Fig. 2-21a, it can be seen that the minimum committed error is related to *RMEI* with 41%, and the maximum error is associated with Kirsten and Annandale methods with 81% error. This error is 81%, 78%, 81%, 51%, and 41%, respectively, for the Annandale, Van Schalkwyk, Kirsten, *eGSI*, and *RMEI* approaches.

According to Fig. 2-21b, it can be seen that the committed error for 'Negligible to Moderate' for all methods except *eGSI* is almost below 50%, and this shows that the performance of these methods for lesser erosions has less error. Conversely, for the 'Large to Extensive' classification, the performance of the *eGSI* has less error, but for the other approaches, it is extremely high.

According to Fig. 2-21c, it can be deduced that all the compared methods, except the *RMEI* method, underestimate the degree of rock mass erosion. The underestimation percentage for Kirsten, Van Schalkwyk, Annandale, *RMEI*, and *eGSI* approaches are, respectively, 100%, 96.5%, 90%, 73%, and 33%. Underestimation can have hazardous consequences for hydraulic structures, and overestimation can increase costs.

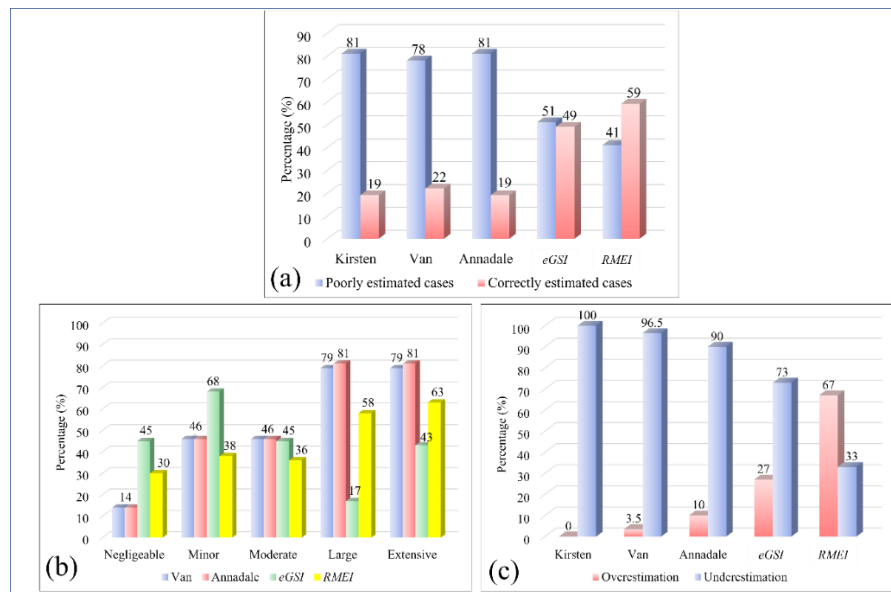


Fig. 2-21. (a) The percentage of poorly estimated cases for each approach. (b) Committed errors of various methods according to different erosion classes. (c) Over- and underestimation rates of various semi-theoretical approaches.

2.8 SUMMARY AND DISCUSSION

Since 1930, several methods have been proposed to predict the hydraulic erodibility of materials. Several theoretical, semi-theoretical, numerical, and semi-analytical approaches have been developed for assessing the hydraulic erodibility of rocks. Most of these methods are developed for soils, granular materials, and diving jet cases. Some approaches have been proposed for computing and assessing the hydraulic erodibility of rocks in unlined spillways (open channels). Studies on erodibility in spillways and scour in plunge pools have two important aspects, namely, geomechanical and hydraulic aspects. Most semi-theoretical studies use the erodibility index (i.e., Kirsten index), except for Pells' method, in which *RMEI* and *eGSI* indices are used, to assess the geomechanical aspect of erodibility.

In semi-analytical methods, specifically, in the *CSM* of Bollaert, several factors, such as dynamic pressure, fatigue, fracture toughness, and stress intensity in the *CFM* method (for close-ended joints) and net impulsion in the *DI* method (for open-ended joints), are employed to compute the ultimate scour depth and time in such scouring. The *QSI* method of Bollaert's *CSM* computes scour depth in the plunge pool walls. The channel bottoms based on the total lift (quasi-steady lift (*QSL*) force) are applied to a protruding block, where the *QSL* force depends on the flow velocity and uplift pressure. Dasgupta proposed a numerical technique in 2011. They utilised 2D *UDEC* for modelling the rock mass to freely assess the block evacuation and fragile crack alongside the 3D *CFD* programming (ANSYS FLUENT) to decide the erosive limits. The erodibility file (for example, Kirsten index) is first created to survey excavatability, and the heaviness of the erodibility list boundaries is inapplicable for evaluating erodibility in hydraulic structures. In most cases, contradictions are observed between the erodibility predictions of existing methods and the observations made after dams are used for operation. An example is the erosion observed in the drainage channel of the Mokolo Dam in South Africa, where the erosion process generated a 30 m deep gully. In most semi-theoretical methods, limited data are used to assess erodibility. Results are limited and do not cover every type of geomechanical situation, and the hydraulic conditions are observed at the dam spillways around the world. In the aforementioned methods [18,21,24], the effects of spillway geometry, especially spillway surface roughness, are not comprehensively studied. The relationship between the geomechanical and hydraulic parameters is not elucidated.

Regarding the consideration of erosive force of water, the velocity of flowing water (V), shear stress applied to a rock surface (τ_b), unit stream power dissipation of water (Π_{UD}), stress intensity (K_I) and lifting force (F_L) have been used in several studies as the hazard parameters during erosion. A unique method for determining the erosive force of water for rock mass erodibility evaluation is lacking. The existing methods also have several limitations and can be used only in specific cases. For example, various equations exist to determine the unit stream power dissipation of water (Π_{UD}), which was developed as a parameter on the basis of the internal flow conditions. Stress intensity (K_I) was initially developed for metallurgical cases and used only to determine the

possibility of crack propagation in intact rocks but not in rock masses. In addition, stress intensity (K_I), which is used in Bollaert's method, is based on the maximum pressure in pool bottoms, in which Bollaert's *CFM* method can compute pressure heads just under the centreline of jets but not the exact pressure of water applied to joint tips. Developments for unlined spillway structures are also lacking. In Bollaert's *DI* approach, which is on the basis of impulsion and Newton's second law, the geomechanical and geometrical parameters of rock masses are not comprehensively considered, and only block size is used. Shear force (F_{sh}) is deemed zero owing to the vertical fracture consideration. The single rock block models and Bollaert's *CSM* are restricted when the fractures directions are not symmetrical and vertical. This situation is common in volcanic and heterogeneous rock types. Two-dimensional nonrectangular obstructs are as yet prohibitive in their capacity to have contact to a rock mass, and the procedure is intrinsically 3D. Table 2-14 illustrates the advantages and disadvantages of various approaches. Table 2-15 shows the detailed information references about erodibility phenomena.

Table 2-14. Advantages and disadvantages of the various approaches.

Approaches		Advantages	Disadvantages
Semi-theoretical	Kirsten	Easy to use Quick	The committed error of these methods is high Lack of consideration of effective geomechanical parameters Lack of estimation of the scour depth and the approximate location of erosion
	Annandale		
	Van Schalkwyk		
	<i>RMEI</i>	Easy to use Quick Consideration of various geometries Consideration of representative hydraulic erosive parameter	The committed error of these methods is high Lack of consideration of effective geomechanical parameters Lack of estimation of the scour depth and the approximate location of erosion
<i>eGSI</i>			
Semi-analytical	<i>CSM</i>	Estimation of the ultimate scour depth and the approximate location of erosion Has a physical, experimental, and mechanical background Consideration of various geometries Consideration of some geomechanical parameters	Confusing and ambiguous Requires in situ tests Practical for plunge pools Consideration of various hydraulic erosive parameters
Numerical		Estimation of the ultimate scour depth and the approximate location of erosion Good accuracy Easy to extract the results of various parameters	Estimation of the ultimate scour depth and the approximate location of erosion Lack of unit software to consider hydraulic and geomechanical aspects at the same time Requires a highly skilled workforce Long processing time

Table 2-15. Detailed information references about erosion or scour in spillways, plunge pools, rivers, and gullies.

Methods/Systems	Main Idea	<i>P, R and S</i> *
Franke (1960) [95]	–	–
Mih (1989) [96]	Axisymmetric and two-dimensional turbulent jets	<i>P</i>
Annandale and Kirsten (1994) [17]	Erodibility of rocks and other rock materials	<i>R</i>
Van Schalkwyk et al. (1994a) [24]	Erosion of rock in spillways	<i>S</i>
Van Schalkwyk et al. (1994b) [29]	Computing erosion in unlined spillways	<i>S</i>
Annandale (1995) [21]	Erodibility	<i>P, S and R</i>
Aderibigbe and Rajaratnam (1996) [8]	Erosion of loose beds	<i>P</i>
Annandale et al. (1998) [16]	Evaluation of erodibility in fractured zone	<i>P and S</i>
Hoffmans (1998) [97]	Jet scour in equilibrium phase	<i>P</i>
Kirsten et al. (2000) [18]	Erodibility criterion auxiliary spillways	<i>P and S</i>
Bollaert and Schleiss (2002) [59]	Formation of rock scour due to high velocity jet impact	<i>P</i>
Bollaert and Schleiss (2003) [62]	Discussion about the Castillo method around rock scour	<i>P</i>
Bollaert (2004) [63]	<i>CSM</i>	<i>P</i>
Arnaboldi et al. (2005) [98]	–	–
Bollaert and Schleiss (2005) [61]	Assessment of the final depth of rock scour	<i>P</i>
Pagliara et al. (2008) [99]	Temporal evolution of plunge pool scour	<i>P</i>
Pagliara et al. (2008) [100]	Hydraulics of 3D plunge pool scour	<i>P</i>
Asadollahi (2009) [75]	Assessment of single 3D rock block stability by developed <i>BS3D</i> code	<i>P</i>
Hoffmans (2009) [101]	Closure problem to jet scour	<i>P</i>
Bollaert (2010) [3]	Discusses about physics of failure	<i>P</i>
Federspiel (2011)	Block response regarding high-velocity jet impact	<i>P</i>
Bollaert (2011) [102]	3D scour assessment downstream of the penstocks	<i>P</i>
Bollaert (2012) [56]	Evaluation of the rock erosion at the plunge pool walls	<i>P</i>
Bollaert et al. (2013) [57]	Quasi-3D numerical predictions	<i>P</i>
Pan et al. (2013) [103]	Estimation of final scour depth	<i>S and R</i>
Huang et al. (2013) [104]	Modifications of the <i>EIM</i> soft bedrock erosion	<i>P</i>
Bollaert and Lesleighter (2014) [60]	Spillway rock scour	<i>S</i>
George (2015) [83]	Influence of a 3D geological structure on the erosion of blocks	<i>P</i>
Tanaka and Sato (2015) [105]	Relationship between damage and hydraulic parameters	–
Pells et al. (2015) [15]	Assessment of the erosion for unlined spillways case	<i>S</i>
Pells (2016) [1]	Spillways erosion evaluation	<i>S</i>
Castillo and Carrillo (2016) [50]	Evaluation of velocities, pressures, and scour for spillway cases	<i>P and S</i>
George and Sitar (2016) [93]	Evaluation of rock erosion on the basis of system reliability	<i>S</i>
Bollaert et al. (2016) [68]	Scour potential	<i>P</i>
Bollaert (2016) [64]	<i>SCSM</i> compared to <i>EIM</i>	<i>P</i>
Lai et al. (2017) [106]	Erodibility in rivers downstream of dams	<i>R</i>
Wüthrich et al. (2018) [107]	Hybrid modelling for evaluate scouring on the basis of <i>CSM</i>	<i>P and S</i>
Wu et al. (2019) [108]	A field investigation on erodibility	<i>S</i>
Bi et al. (2019) [109]	Channel scouring	<i>R</i>
Boumaiza et al. (2019) [35]	Relevant geomechanical parameters and non-orthogonal joint sets	–
Dong et al. (2019) [110]	Effect of rock mass failure on erodibility	<i>P</i>
Rong et al. (2020) [111]	Effect of fracture geometry on flowing	–
Saeidi et al. (2020) [38]	Rock erosion analysis using developed vulnerability and fragility functions	<i>S</i>
Palermo et al. (2020) [112]	Shear-stress estimation at 2D equilibrium scour holes	<i>P</i>
Palermo et al. (2021) [113]	Scour processes on granular beds	<i>P</i>
Gioia and Bombardelli (2005) [114]	Turbulent flows on scouring granular beds	–
Boumaiza et al. (2019) [115]	Relevant geomechanical parameters to assess the erodibility	<i>S and P</i>
Boumaiza et al. (2021) [116]	Relative importance of geological parameters in hydraulic erodibility assessment	<i>S and P</i>
Koulibaly et al. (2021) [117]	A review of hydraulic erosive parameters	<i>S and P</i>

* *P, R, and S* describe plunge pool, river, and spillway, respectively.

2.9 CONCLUSIONS AND POTENTIAL FUTURE RESEARCH DIRECTION

Several theoretical, semi-theoretical, semi-analytical, and numerical methods have been developed for evaluating rock mass erosion in hydraulic structures. Semi-theoretical methods should develop an erodibility index based on the geomechanical and hydraulic aspects of rock mass erosion.

In the case of semi-analytical methods, a detailed evaluation of the effect of each geomechanical parameter is not yet conducted. A unique method for determining the erosive parameter of water is not yet available. The existing semi-analytical methods developed in the case of the plunge pool could not be used for the spillway case. Applying these methods to each site is necessary to identify some constants that are difficult to determine.

The results from the application of existing approaches for the evaluation of the potential risk of rock mass erosion in dam spillways show that:

- 1) Between semi-theoretical approaches, the Pells' *RMEI* approach has less error than other semi-theoretical approaches in the same category, despite its significant committed error.
- 2) Regarding semi-analytical methods, the *CSM* approach of Bollaert can be used as a representative method to analyse and evaluate the hydraulic erodibility phenomena in plunge pool cases despite existing difficulties in the preparation of its input data for each dam site. Because of the channel flow nature of this methodology, the principles of this method could be used to develop a new analytical approach in the case of unlined spillways, which could consider the spillway geometrical parameters and rock mass geomechanical parameters.

Moreover, the utilisation of computational fluid–structure interaction systems is highly recommended to perform a numerical evaluation of rock mass erodibility in future works by considering various geometrical parameters of the rock mass and hydraulic structures. Development of a new or modification of existing methods for erosion prediction is crucial for dam spillway design. For this, the following topics should be addressed:

- 1) Defining the unique hydraulic erosive parameter;
- 2) Determining the effect of dam spillway geometrical parameters on a hydraulic erosive parameter (different flow channel profiles);
- 3) Determining the effect of rock mass geometrical parameters on a hydraulic erosive parameters (block volume, joint opening, dip, and dip direction);
- 4) Determining the effect of geomechanical parameters on a hydraulic erosive parameter;
- 5) Consideration of the shear force within the joints.

CHAPTER 3

Article 2: Evaluation of the effect of surface irregularities on the hydraulic parameters within unlined dam spillways

Yavar Jalili Kashtiban ^{a *}, Ali Saeidi ^a, Marie-Isabelle Farinas ^a, Javier Patarroyo ^b

^a Department of Applied Sciences, University of Quebec at Chicoutimi, Saguenay, G7H 2B1, QC, Canada

^b Hydro-Québec Production Unité Expertise en barrages, 75 Boulevard René-Lévesque Ouest, Montréal, QC H2Z 1A4, Canada

Published in Water 2023, 15(16), 3004; <https://doi.org/10.3390/w15163004>

Submitted: 19 June 2023 / Revised: 9 August 2023 / Accepted: 19 August 2023 / Published: 20 August 2023

AUTHOR CONTRIBUTIONS: Conceptualization, Y.J.K.; methodology, Y.J.K. and A.S.; software, Y.J.K.; validation, Y.J.K., A.S., M.-I.F. and J.P.; formal analysis, Y.J.K.; investigation, Y.J.K.; resources, Y.J.K. and A.S.; writing original draft preparation, Y.J.K.; writing, review and editing, Y.J.K., A.S., M.-I.F. and J.P.; visualization, Y.J.K., A.S., M.-I.F. and J.P.; supervision, A.S., M.-I.F.; industrial advising, J.P.; project administration, A.S.; funding acquisition, A.S.

FUNDING: This research was funded by: Natural Sciences and Engineering Research Council of Canada and Hydro-Québec (NSERC, Hydro-Quebec) [CRDPJ 537350-18]. Natural Sciences and Engineering Research Council of Canada (NSERC) [RGPIN-2019-06693].

ACKNOWLEDGEMENT: The authors would like to thank the Natural Sciences and Engineering Research Council of Canada (NSERC) and Hydro-Quebec for funding this project (CRDPJ 537350 - 18, NSERC-RGPIN-2019-06693) and all those who helped us to improve the quality of this paper.

CONFLICTS OF INTEREST: The authors declare that they have no conflict of interest regarding the content of this document.

*Email: Yavar.jalilikashtiban1@uqac.ca

3.1 ABSTRACT

Erosional incidents have heightened the necessity of studies regarding rock mass erosion in unlined dam spillways. Enhanced comprehension of hydraulic erodibility necessitates an investigation into the geomechanical and hydraulic aspects of erosional phenomena. Controlled blasting is commonly employed to establish unlined spillways in rock masses, and this process results in irregularities along the spillway surface profile. Recent research has identified key geometric parameters of rock masses that impact erosion in unlined spillways, such as joint opening, dip and dip direction, and joint spacing. However, the effect of spillway surface irregularities on hydraulic parameters remains uncertain. Numerous studies have examined the surface roughness of rock at the millimeter scale within the domain of hydraulic engineering. Despite these efforts, a noticeable gap persists in our understanding of how surface irregularities specifically exert influence over hydraulic parameters. Currently, there is a lack of a clear equation or methodology to incorporate irregularities into hydraulic erosive parameters. The main aim of this study is to show how such irregularities affect the hydraulic parameters. This study is dedicated to emphasizing the importance of considering these irregularities. Building upon the findings obtained, the core aim of this research is to facilitate the formulation of an equation in future investigations that effectively accounts for these irregularities when calculating hydraulic erosive parameters. To assess the significance of surface irregularities in unlined spillways, computational fluid dynamics (CFD) with ANSYS-Fluent software was employed to analyze 25 configurations of spillway surface irregularities and their effects on various factors including pressure (total, dynamic, and static pressures), shear stress, flow velocity, and energy. The findings indicated that irregularities significantly influenced the hydraulic parameters. Specifically, an increased irregularity height led to a decrease in maximum velocity, total pressure, and shear stress. Conversely, total energy loss increased, amplifying the rock mass's vulnerability to erosion due to these irregularities.

Keywords: dam, hydraulic structures, unlined spillways, erodibility, CFD.

3.2 HIGHLIGHTS

- Investigation of geomechanical and hydraulic aspects of erosional phenomena is important for improving understanding of hydraulic erodibility in unlined dam spillways.
- Computational fluid dynamics (CFD) with ANSYS-Fluent software model was used to analyze 25 configurations of spillway 2D surface irregularities and their effect on hydraulic parameters.
- Irregularities on the surface 2D profile of the spillways discharge channel were found to affect each hydraulic parameter, including maximum velocity, static pressure, dynamic pressure, total pressure, shear stress, and energy.

- Total energy loss increased as well as the rock mass's vulnerability to erosion due to increased irregularity height.
- The study suggests incorporating the effect of surface irregularities into hydraulic erosive parameter equations to accurately evaluate the influence of irregularities on hydraulic erosion in unlined spillways.
- Future directions for assessing the hydraulic erodibility of rock in hydraulic structures (dams) are discussed.

3.3 INTRODUCTION

Unlined dam spillways and other hydraulic safety structures, such as sluice gates, stilling basins, and plunge pools, protect dam infrastructure during high water events. Dam safety can be improved by studying the hydraulic erodibility of these structures and the hydraulic characteristics of flowing water over these constructions. Erodibility, scour, and hydraulic erosion are technical terms related to the erosion that occurs when the hydraulic erosive intensity—erosive capacity of flowing water—exceeds the rock mass resistance [1, 2].

Rock mass erosion due to flowing water is a complex phenomenon that can occur instantaneously or over time. Hydraulic erosion mechanisms include brittle failure, fatigue failure, rock block removal, peeling off, and rock block abrasion (Fig. 3-1).

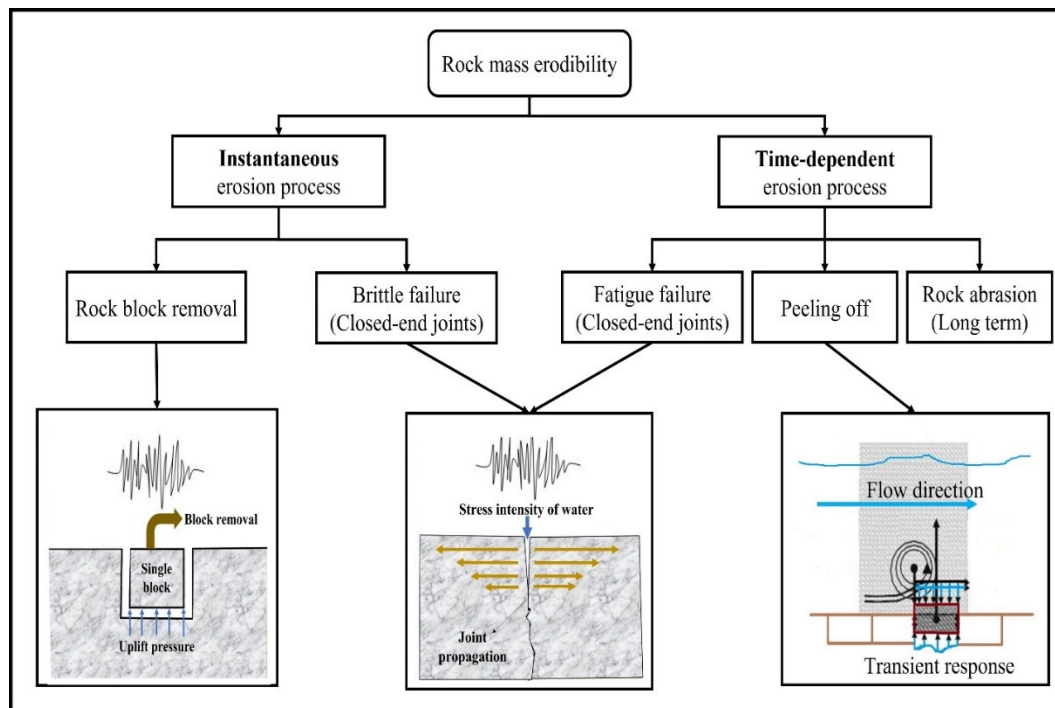


Fig. 3-1. Mechanisms of rock mass erosion [118, 119]

Both the hydraulic and rock mass aspects of erosion must be considered. Studying the effect of various geometries of hydraulic constructions on the hydraulic characteristics of flowing water and the effect of geomechanical parameters of the rock mass can improve the analysis of hydraulic erosive parameters [38]. Several investigations have identified the unit stream power dissipation of water (Π_{UD}), water velocity (V), shear stress (τ_b) applied to a rock surface, stress intensity (K_I), and lifting force (F_L) as important hydraulic erosive parameters (Table 3-1).

Most hydraulic erodibility assessments use an energy dissipation index to reflect the erosive capacity of water because of a lack of an accurate index and the difficulty in determining a specific erosive parameter [18, 20, 21, 24, 31]. An energy dissipation index is selected for simplicity, not for accurately representing the hydraulic erosive agent (Table 3-1). Pells' (2016) analytical methodology appears to be the most reliable among the approaches that use energy dissipation as a hydraulic erosive agent. However, a measure of energy dissipation may not consider all the complexities involved with erosion; for example, spillway geometry (surface profile) and flow modes potentially influence the energy dissipation of water and erosion potential.

Average water velocity is not a representative index of the hydraulic erosive parameter because it depends on the flow channel surface profile, fluid viscosity, and flow nature. Average shear stress along the channel bottom can also be considered a hazard parameter [118]. Nonetheless, it is extremely difficult to resolve all erosion problems within dam spillways by solely considering shear stress, including explaining hydraulic erosion caused by dynamic block removal, brittle failure, or fatigue failure.

Bollaert [3, 59] proposed a comprehensive scour model (CSM) using three methods: a comprehensive fracture mechanics (CFM) approach for analyzing erosion in close-ended joints; a dynamic impulsion (DI) approach for analyzing erosion in open-ended joints (single block); and the quasi-steady impulsion (QSI) approach for computing the scoured depth along plunge pool walls. In the CFM, stress intensity (K_I) is considered a hydraulic erosive parameter and is calculated based on the maximum pressure at the plunge pool bottom. Bollaert's DI considers uplift force to be a hydraulic erosive parameter on the basis of impulsion and Newton's second law of thermodynamics. This method ignores the geomechanical and geometric characteristics of the rock mass. In the DI approach, it is assumed that the shear force (F_{sh}) is zero. Bollaert's QSI method determines the forces applied to channel bottoms through the quasi-steady lift force (F_{QSL}) on a protruding block, where the F_{QSL} is dependent on uplift pressure and flow velocity. Existing methods of assessing and predicting hydraulic erodibility are limited by several elements, and these approaches can be used only in specific situations and conditions. Moreover, a unique parameter is lacking to measure the erosive agent of water when assessing rock mass erodibility. For example, numerous equations exist for determining the unit stream power dissipation of water (Π_{UD})—initially developed using internal flow conditions. The concept of stress intensity (K_I) was originally developed for metallurgical analysis [59] and is only used to estimate the probability of joint propagation in intact rocks, not rock masses. When the existing methods are compared

(Table 3-1), the stream power dissipation parameter is the most commonly used ; however, spillway geometry is not considered.

Here we investigate various spillway surface geometries to determine how unlined spillways surface irregularities affect hydraulic parameters. After selecting a series of geometries found in unlined spillways, we apply computational fluid dynamics (CFD) with ANSYS-Fluent software to perform flow simulations. These simulations are two-dimensional (2D) and are solved as steady-state flows. We then determine how spillway discharge channel surface geometry, i.e., irregularity height (h) and irregularity angle (α_i), alters hydraulic parameters, including pressure (total pressure), shear stress, flow velocity, and energy.

Table 3-1. Existing hydraulic erosive indices

Hydraulic erosive parameter		Equation
Parameter	Approach	
Stream power dissipation (Π_{UD})	(Van Schalkwyk 1994) [24]	$\Pi_D = \rho \cdot g \cdot q \cdot S_f$
	(Annandale 1995) [21]	$\Pi_D = \gamma \cdot q \cdot \Delta E$
	(Pells 2016) [1]	$\Pi_{UD} = \rho \cdot g \cdot q \cdot \frac{dE}{dx}$
Velocity (V)	Chézy (1769)	$V = C \sqrt{R_H \cdot S_f}$
	(Weisbach 1845, Darcy 1857) [120, 121]	$V = \sqrt{\frac{8g}{f(\frac{\epsilon}{D}, h_e)}} \sqrt{R_H \cdot S_f \cos \theta}$
	(Manning et al. 1890) [122]	$V = \frac{1}{n} R_H^{2/3} \cdot S_f^{1/2}$
Shear stress (τ_b)	(Yunus 2010) [19]	$\bar{\tau}_b = \rho \cdot g \cdot R_H \cdot S_f \cos \beta$ $\bar{\tau}_b = \rho \cdot g \cdot R_H \cdot S_f \cos \beta$
	MPM (Khodashenas and Paquier 1999) [123]	$\tau_i = \rho \cdot g \cdot h \cdot S_f$
	(Prasad and Russell 2000) [124]	$\frac{\bar{\tau}_{(b)}}{\rho g h S_f} = (1 - 0.01\%SFw) \left(1 + \frac{P_{(w)}}{P_{(b)}}\right)$
	(Yang and Lim 2005) [125]	$\frac{\bar{\tau}_{(b)}}{\rho g h S_f} = 1 + \frac{h}{b} \frac{1}{\tan \beta} - \psi \frac{h}{b} \frac{1}{\sin \theta}$
	(Guo and Julien 2005) [126]	$\frac{\bar{\tau}_{(b)}}{\rho g h S_f} = \frac{4}{\pi} \text{Arctg} \left[\exp \left(\frac{-\pi h}{b} \right) \right] + \frac{4}{\pi} \frac{h}{b} \exp \left(\frac{-h}{b} \right)$
	(Seekin et al. 2006) [127]	$\frac{\bar{\tau}_{(b)}}{\rho g R S_f} = \frac{a + b(B/H)}{1 + c(B/H) + d(B/H)^2}$
	(Severy and Felder 2017) [128]	$\tau_o = \frac{1}{8} f \rho V^2$
Stress intensity (K_I)	CFM (Bollaert and Schleiss 2002) [59]	$K_I = 0.8 \cdot P_{max} \cdot F \cdot \sqrt{\pi \cdot L_f}$
Lifting force (F_L)	DI (Bollaert and Schleiss 2002) [59]	$I = \int_0^{\Delta tpulse} (F_u - F_o - G_b - F_{sh}) \cdot dt$ $= m \cdot V_{\Delta tpulse}$
	QSI (Bollaert 2010) [3]	$F_{QSL} = C_{uplift} \cdot L_{block} \cdot \frac{V_{x,max}^2}{2g}$

After extensive analysis and investigation of dam construction projects, with a specific focus on hydraulic erosion within unlined spillways and its pivotal role in dam construction, the decision was taken to

deeply explore this matter. Previous research concerning methodologies for assessing hydraulic erosion in dam spillways has shed light on the strengths and limitations of various approaches:

- (1) Semi-Theoretical Approaches: Notably, Pells' RMEI method among semi-theoretical approaches showcased relatively lower errors compared to counterparts within the same category, despite inherent margins of error.
- (2) Semi-Analytical Methods: Among the array of semi-analytical methods, Bollaert's CSM approach emerged as a representative choice for evaluating hydraulic erodibility, particularly in scenarios involving plunge pool dynamics. The challenges associated with obtaining site-specific data were balanced by its applicability to channel flow situations, thereby suggesting its potential as a novel analytical technique tailored for unlined spillways.
- (3) Advancing Erosion Prediction Methods: The significance of developing new or refining existing erosion prediction methods was underscored as crucial for dam spillway design. This endeavor addressed the following pivotal aspects:
 - Distinct Hydraulic Erosive Parameter: A foundational step involved defining a distinctive hydraulic parameter.
 - Dam Spillway Geometry Influence: The influence of dam spillway geometry on the hydraulic erosive parameter.
 - Impact of Rock Mass Geometry: Delving into the implications of rock mass geometry, including factors like block volume, joint characteristics, dip, and dip direction, on the hydraulic erosive parameter.
 - Geomechanical Scrutiny: Definition of the effects of geomechanical factors on the hydraulic erosive parameter.

With the recognition that hydraulic erodibility within unlined spillways encompasses both hydraulic and geomechanical aspects, this phenomenon is studied to encompass both aspects. Given the industry's reliance on established approaches like the Annandale methodology, the initial focus was directed toward the hydraulic aspect. This article stands as an important part of a comprehensive study on introducing a holistic framework for assessing hydraulic erosion. This phase concentrated on examining the influence of geometric parameters on hydraulic parameters, setting the stage for future exploration into the interplay of geomechanical parameters with hydraulic properties. This study specifically undertook a meticulous examination of the effects of geometric parameters, with a specific emphasis on rock surface irregularities, on hydraulic parameters. The new findings provided the basis for introducing the comprehensive methodology for assessing hydraulic erodibility. Future research phases will delve into the influence of geomechanical parameters on hydraulic parameters. Combining the knowledge accumulated from these phases will result in the development of a distinctive equation for the hydraulic erosive parameter. The ultimate objective is to present a comprehensive and coherent methodology for evaluating hydraulic erosion within unlined dam spillways.

In the article, various unlined spillway surface geometries were investigated to determine how hydraulic parameters are affected by irregularities on unlined spillway surfaces. A series of geometries found in unlined spillways were selected, and flow simulations were performed using computational fluid dynamics (CFD) with ANSYS-Fluent software. ANSYS-Fluent was chosen based on its industry-standard recognition, versatility in handling complex simulations, user-friendly interface, and robust solver options, all of which were aligned with the research requirements. These simulations were two-dimensional (2D) and were solved as steady-state flows. Within turbulent model simulations, the intricacies of irregular rock surfaces were explored—a pursuit characterized by challenges and significance. The chosen approach encompassed the utilization of the k-epsilon turbulence model with Explicit Enhanced Wall Treatment, which proficiently managed the complexities arising from surface roughness. Beyond being a necessity, the drive for accuracy assumed the role of a conduit for informed decision-making. Central to the methodology was the reliance on y^+ values, serving as evaluative measures. Their impact extended to the refinement of the model and the adaptation of mesh sizes by the computed y^+ values. The alterations in hydraulic parameters, including pressure (total pressure), shear stress, flow velocity, and energy, were then determined based on spillway surface geometry, i.e., irregularity height (h) and irregularity angle (α_I).

3.4 MATERIALS AND METHODS

The flowchart of the methodology (Figure 3.2) presented the steps in subsections. The most effective geometric parameters of spillways and irregularities were first identified and selected by analyzing the available data from Pells [1]. Pells' data involves more than 100 case studies from dams in Australia, Africa, and the United States [1].

These selected parameters combined with observed controlled-blasting patterns and available data, resulted in a specific model geometry. We then simulated water flow over this rock geometry using ANSYS-Fluent software and extracted the results using CFD-Post.

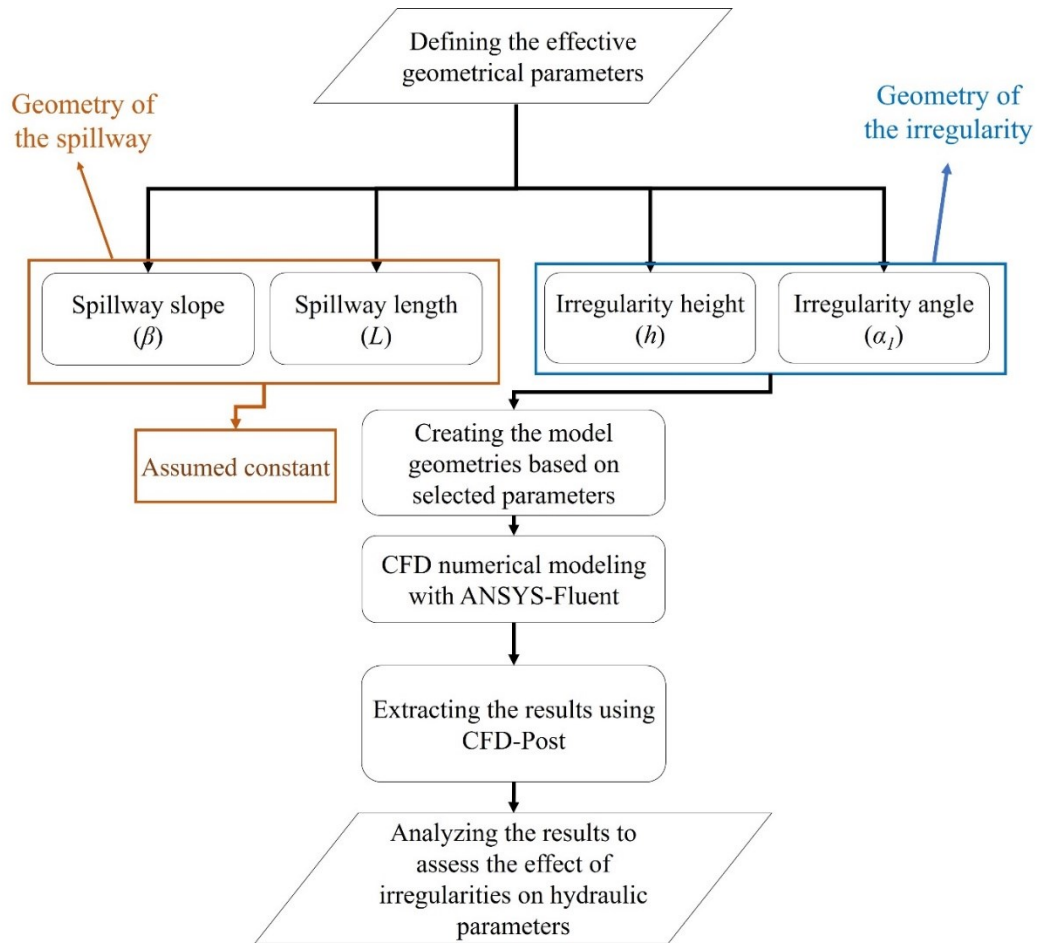


Fig. 3-2. Flowchart presenting the steps of modeling spillway for assessing the effect of irregularity geometry on hydraulic parameters

The spillway geometric parameters, including spillway length and constant spillway slope, and the geometric parameters of the irregularities, including their length, height, and angle, will be explained in Section 3.4.1.

The purpose of this study is to provide a foundational understanding of hydraulic erosion science. This phenomenon was characterized by the synergy of hydraulic and geomechanical principles. Parameters in this science were categorized into three main groups: hydraulic, geomechanical, and geometric.

- Hydraulic parameters included total pressure, shear stress, flow velocity, force, stream power, and energy.
- Geomechanical parameters encompassed block volume, joint aperture, dip angle, and dip direction.
- Geometric parameters involved the shape of the rock surface, slope, and channel structure.

Given the complexity, these parameters will be analyzed separately. The focus was directed towards examining how geometric attributes, specifically the length (l), height (h), and angle (α_1) of rock surface irregularities, impacted hydraulic parameters. With the value of l held constant (given its direct relationship

with other geometrical parameters), the focus was exclusively directed towards h and α_l . The investigation primarily centered on hydraulic parameters such as velocity, pressure, force, and energy. These parameters played a pivotal role, as they affected a range of other factors. By exploring the influence of h and α_l on these hydraulic parameters, insights were gained into broader interactions.

Subsequent research delved into the impact of the remaining geometric and geomechanical factors on hydraulic parameters. Ultimately, the aspiration is to develop a comprehensive equation that integrated all attributes, offering a unified perspective on the science of hydraulic erodibility.

3.4.1 Determining model geometry

Spillway geometric characteristics in this study include spillway length, spillway slope, and the length, height, and angle of each irregularity. We considered the effects of each parameter separately because of the high number of variables. For this paper, we present only the results of irregularity height (h) and angle (α_l).

3.4.1.1 Step 1: Blasting effect on the profile of surface irregularities

In the context of mining, tunnelling, and dam construction, blasting is a common method of breaking and removing rock mass. In mining and tunneling operations, the high levels of detonation energy are emitted, a portion of which is productively expended on rock fragmentation [129]. Unlined dam spillways are generally built on hard rock, and controlled blasting is usually used to create the surface of the unlined spillways (Fig. 3-3). The applied drilling and blasting produce irregularities along a spillway's surface profile [130]. When designing blasting patterns for unlined dam spillways, burden (B) and spacing (S) are important (Fig. 3-3c). Burden denotes the distance between a blasting-hole row to the excavation face or between blasting-hole rows. Spacing refers to the distance between blasting holes along the same row [130]. According to the blasting theory, the burden for hard rocks is 1–2 m. Based on the blasting patterns and the created post-blasting surfaces, we considered the burden to be equivalent to irregularity length (Fig. 3-3d).

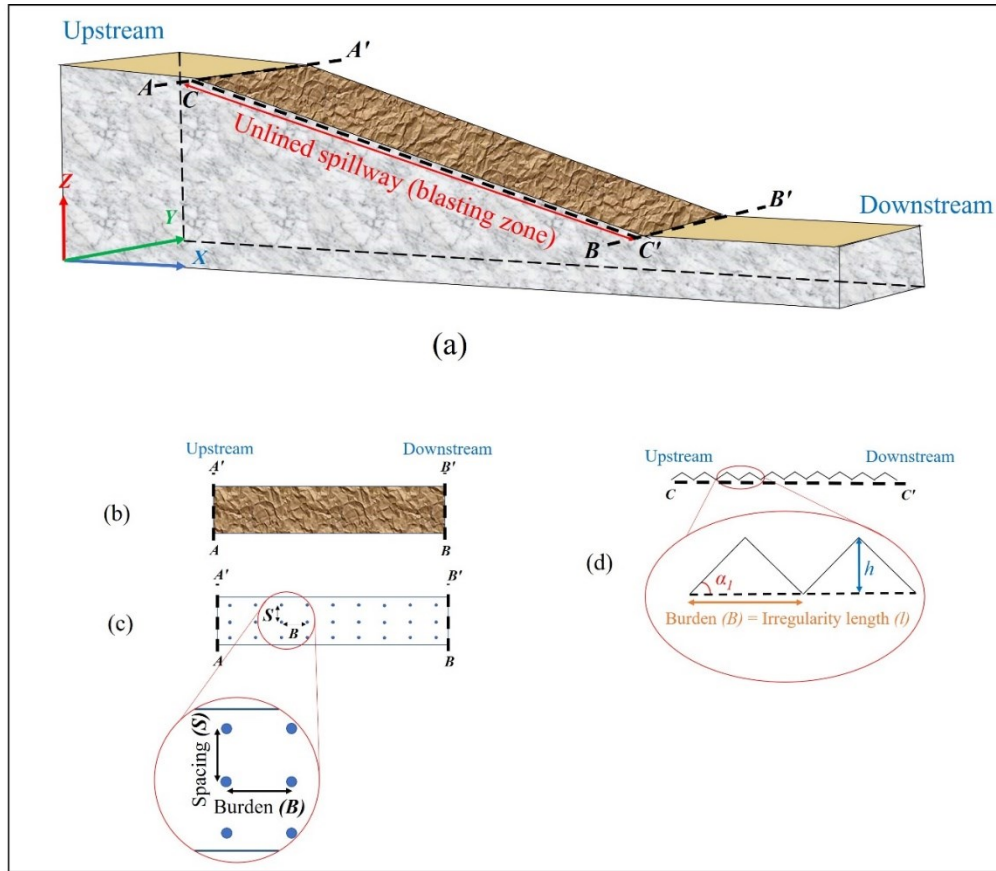


Fig. 3-3. (a) Diagram of an unlined dam spillway; (b) channel view from above; (c) controlled-blasting pattern of the channel showing spacing and burden; and (d) channel surface profile after blasting

3.4.1.2 Step 2: Selection of geometries for unlined surface profiles

In this study, the spillway geometric characteristics of spillway length (L) and spillway slope (β) were considered, and the selected geometric parameters of irregularities comprised the length (l), height (h), and angle (α_i) of the irregularities. It was assumed that the spillways' geometric parameters remained constant. An irregularity angle ranging from 12° to 40° covered most irregularities, and the irregularity height varied between 10 and 30 cm. The irregularity length was proportional to the height and angles and generally fell between 1 and 2 m. A length of 1.5 m was selected for all the models. These parameters were chosen through an analysis of Pells' thesis database, a thorough review of existing methodologies, and consideration of blasting theory.

The geometric characteristics of the spillway (slope and length) were also considered significant, and future studies aimed to evaluate the effects of these parameters. For the models, an unlined spillway slope of 5° and a length of 50 m were selected based on available data from Pells (2016), choosing the average values of these observations (Fig. 3-4). A total of 25 geometric configurations of spillway surface irregularities were produced.

To identify the geometric parameters of the irregularities, equations (3-1) – (3-3) from geometry science were applied. These equations are a function of the input parameters, and the irregularity geometry could be created using these equations and the input parameters α_1 , h , and l . The length of irregularity surfaces with and against water flow was represented by e_b and e_f , respectively (Fig. 3-4). The irregularity angle in the flow direction, along with the spillway slope, was known as α_2 .

In this study, we consider the spillway geometric characteristics of spillway length (L) and spillway slope (β); our selected geometric parameters of irregularities comprise the length (l), height (h), and angle (α_1) of the irregularities. We assume that the spillways' geometric parameters remain constant. An irregularity angle of 12° to 40° covers most irregularities, and irregularity height varies between 10 and 30 cm. Irregularity length is proportional to the height and angles and is generally between 1 and 2 m. We selected a length of 1.5 m for all our models. The geometric characteristics of the spillway (slope and length) are also key, and future studies aim to evaluate the effects of these parameters. For our models, we selected 5° and 50 m for profile angle and length, respectively, on the basis of our observations of unlined spillways—we chose the average values of these observations (Fig. 3-4). We produced 25 geometric configurations of spillway surface irregularities.

To identify the geometric parameters of the irregularities, we apply equations (3-1) – (3-3) from geometry science. These equations are a function of the input parameters, and the irregularity geometry can be created using these equations and the input parameters α_1 , h , and l . The length of irregularity surfaces with and against water flow are represented by e_b and e_f , respectively (Fig. 3-4). The irregularity angle in the flow direction along with the spillway slope is known as α_2 .

$$\alpha_2 = \tan^{-1} \left(\tan \alpha_1 \times \left(\frac{l \tan \alpha_1}{l \tan \alpha_1 - h} - 1 \right) \right) \quad (3-1)$$

$$e_f = \frac{h}{\sin \alpha_1} \quad (3-2)$$

$$e_b = \frac{h}{\sin \alpha_2} \quad (3-3)$$

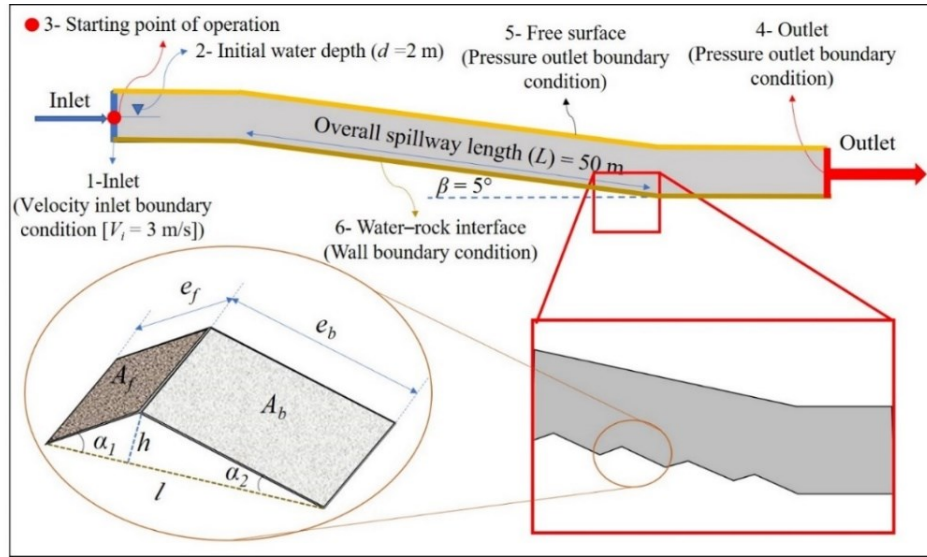


Fig. 3-4. The assumed spillway geometry used in our model of irregularities along an unlined rock spillway

h (m) \ α_1 ($^\circ$)	12	19	26	33	40
0.1	$\alpha_3 = 5.55$	$\alpha_3 = 4.73$	$\alpha_3 = 4.42$	$\alpha_3 = 4.25$	$\alpha_3 = 4.14$
	$e_f = 0.48$	$e_f = 0.31$	$e_f = 0.23$	$e_f = 0.18$	$e_f = 0.16$
	$e_2 = 1.03$	$e_2 = 1.21$	$e_2 = 1.3$	$e_2 = 1.35$	$e_2 = 1.38$
0.15	$\alpha_3 = 10.7$	$\alpha_3 = 8.02$	$\alpha_3 = 7.17$	$\alpha_3 = 6.74$	$\alpha_3 = 6.48$
	$e_f = 0.72$	$e_f = 0.46$	$e_f = 0.34$	$e_f = 0.28$	$e_f = 0.23$
	$e_2 = 0.81$	$e_2 = 1.07$	$e_2 = 1.2$	$e_2 = 1.28$	$e_2 = 1.33$
0.2	$\alpha_3 = 19.7$	$\alpha_3 = 12.28$	$\alpha_3 = 10.4$	$\alpha_3 = 9.52$	$\alpha_3 = 9.01$
	$e_f = 0.96$	$e_f = 0.61$	$e_f = 0.46$	$e_f = 0.37$	$e_f = 0.31$
	$e_2 = 0.59$	$e_2 = 0.94$	$e_2 = 1.11$	$e_2 = 1.21$	$e_2 = 1.28$
0.25	$\alpha_3 = 37.7$	$\alpha_3 = 17.9$	$\alpha_3 = 14.21$	$\alpha_3 = 12.64$	$\alpha_3 = 11.75$
	$e_f = 1.2$	$e_f = 0.77$	$e_f = 0.57$	$e_f = 0.46$	$e_f = 0.39$
	$e_2 = 0.41$	$e_2 = 0.81$	$e_2 = 1.02$	$e_2 = 1.14$	$e_2 = 1.23$
0.3	$\alpha_3 = 73.54$	$\alpha_3 = 25.5$	$\alpha_3 = 18.73$	$\alpha_3 = 16.12$	$\alpha_3 = 14.71$
	$e_f = 1.44$	$e_f = 0.92$	$e_f = 0.68$	$e_f = 0.55$	$e_f = 0.47$
	$e_2 = 0.31$	$e_2 = 0.7$	$e_2 = 0.93$	$e_2 = 1.08$	$e_2 = 1.18$

Fig. 3-5. Configurations of the various modeled spillway surface irregularities

3.4.2 Numerical modeling

To simplify the computation of wall parameters on irregular surfaces, we used ANSYS-Fluent Version 2020 R2. ANSYS-Fluent converts scalar transport equations into algebraic equations that can be run numerically on the basis of a controlled volume approach. Functioning within a 2D framework, the CFD model was employed to solve under steady-state conditions. This configuration allowed for a focused examination of essential fluid dynamics aspects. The objective behind these simulations was to capture the sensitivity of hydraulic parameters to irregularities present on the rock surface. The open-channel submodel in ANSYS-Fluent, which is partially based on the volume of fluid (VOF) multiphase model, was used in our analysis [131]. In the original VOF technique, Hirt and Nichols [132] used a specialized methodology to obtain a standard definition of the free surface, whereas ANSYS-Fluent solves the combined air–water flow systems [133]. In the realm of turbulent model simulations, the investigation of irregular rock surfaces emerges as both a challenge and an avenue of significance. The selected path involves employing the k-epsilon turbulence model

with Enhanced Wall Treatment, a strategic choice well-suited for addressing the intricacies arising from surface roughness. This approach, motivated by the pursuit of accuracy as a foundation for informed decision-making, hinges on the pivotal role of y^+ values. Y^+ values, acting as evaluative indicators, play a crucial role in refining the model and adjusting mesh sizes. Serving as a touchstone for near-wall resolution in turbulent simulations, y^+ values enable the calibration of the model's mesh. This calibration, guided by the computed y^+ values, fine-tunes the mesh sizes, ensuring a harmonious fit that mirrors real-world intricacies accurately. Within the framework of k -epsilon turbulence modeling, precise alignment with y^+ values not only rectifies errors arising from improper meshing but also creates a simulation environment faithfully capturing the physics near rough wall interfaces. Incorporating the y^+ value and executing grid convergence analysis on several parameters, endeavors were made to confine them within the range of $1 < y^+ < 30$. Following successive iterations of mesh refinement and subsequent reduction, the y^+ value was progressively brought to an approximate range of 30. The accuracy of the model was subsequently evaluated through rigorous grid convergence analysis, closely associated with the y^+ values. The k - ϵ turbulence model with enhanced wall treatment conditions captured results at the water–rock interface. Solutions to the Navier–Stokes equations were derived using a stable, implicit technique in the simulations. Pressure–velocity coupling was treated for stability using the widely used COUPLED method. To enhance momentum, we applied a second-order upwind.

Table 3-2 presents the model input data for our fluid flow modeling. We applied a 3 m/s velocity–inlet boundary condition. In open channels, upstream velocity–inlet boundary conditions define the flow velocity and relevant scalar characteristics of the flow at the flow inlet. At the outflow zone, a pressure–outlet boundary condition was specified. We assumed a no-slip boundary condition at the water–rock interface (Fig. 3-4). The water depth at the model’s entrance (inlet) was the starting point for the simulation calculations. Atmospheric pressure and a 2 m water depth were also set in the model. Fig. 3-6 shows the produced model in ANSYS-Fluent and the meshing used. To avoid the impact of localized bursts, it was effectively mitigated by the employed mesh refinement strategy, thereby enhancing the fidelity of CFD simulations. The ultimate aim was to attain an optimum simulation model that harmonized accuracy and cost-effectiveness.

Table 3-2. Input parameters used in the computational fluid dynamics (CFD) modeling

Parameters	Value	Description
Initial flow depth	2 m	See point 3 in Fig. 3-4
Initial flow velocity	3 m·s ⁻¹	See point 1 in Fig. 3-4
Inlet boundary condition	–	Velocity inlet (point 1 in Fig. 3-4)
Outlet boundary condition	–	Pressure outlet (point 4 in Fig. 3-4)
Unlined spillway length	50 m	–
No. of irregularities	32	–
Irregularity height (h)	10, 15, 20, 25, 30 cm	
Irregularity angle (α_i)	12°, 19°, 26°, 33°, 40°	
Channel slope	5°	–

3.4.2.1 Step 1: Model geometry and boundary conditions

Designing the geometry is the first step of *CFD* numerical modeling. We therefore used the ANSYS geometry tool to produce various simulation geometries. We identified five irregularity heights (h) and five irregularity angles (α_i) based on the Pells data set. We considered 25 configurations for this study (Fig. 3-5).

3.4.2.2 Step 2: Meshing and convergence analysis

The physical model was mesh-constructed in our research using a triangular structural grid. The inflation layer was applied along the spillway wall. Meshing gradually increased in size from bottom to top to provide a more faithful simulation that captured the boundary layer. At the channel bottom, five inflation layers with a growth rate of 1.2% were considered. To find out whether the precision of our numerical simulations was affected by grid cell size—and to determine the optimal grid size—we meshed the first branch–channel physical model using five distinct techniques (the maximum grid cells were 20, 15, 10, 5, and 1 cm). This analysis was conducted for the final irregularity along the spillway, and the results were evaluated in terms of total pressure, maximum velocity, and water depth for $h = 10$ cm and $\alpha_i = 12^\circ$. A meshing size of 10 cm was deemed optimal on the basis of outcomes of this grid convergence analysis (Table 3-3), considering the criteria of the time calculation and precision of the results. Finally, we analyzed an approximately 48 m long portion of the channel (CC' red line in Fig. 3-3a).

Table 3-3. Grid independence study at the last irregularity

Boundary conditions	Structural schemes				
	20	15	10	5	1
Maximum size of grid cell (cm)	20	15	10	5	1
Maximum velocity ($\text{m}\cdot\text{s}^{-1}$)	9.46	10.31	10.64	10.68	10.67
Water depth (cm)	82.1	73.3	68.9	68.1	68.1
Maximum total pressure (kPa)	52.63	60.16	63.18	63.52	63.6

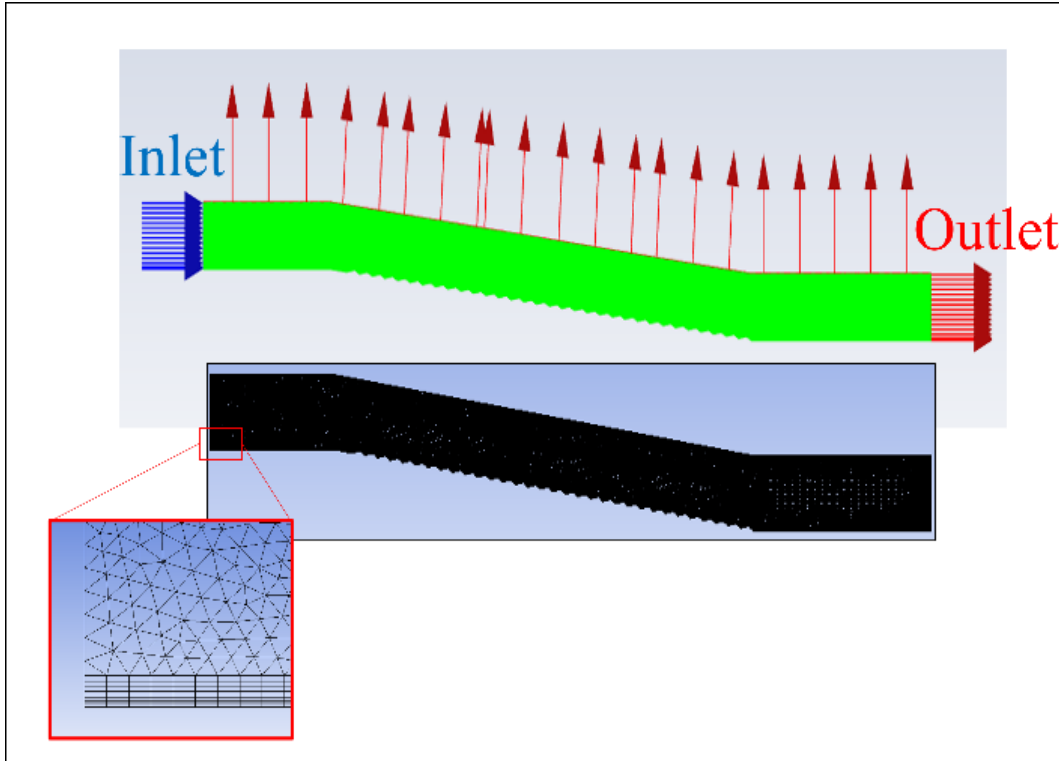


Fig. 3-6. Diagram of the numerical modeling and the applied meshing

3.4.2.3 Step 3: Model setup (VOF method, turbulence model, control equation)

Free surface channel fluctuations impact both the air and water phases and complicate the modeling. By resolving a single momentum equation and storing a record of the volume fraction of each immiscible fluid inside the computational region, the VOF model can simulate two or more immiscible fluids. Moreover, the VOF approach can be applied to a wide range of discontinuous interfaces and flowing water and allows monitoring the water surface in open channels. The sum of all volume fractions of all phases in each control body is one [134].

$$a_w + a_a = 1 \quad (3-4)$$

where a_w and a_a represent the volume fractions of water and air, respectively. When $a_w = 1$, water fills every control unit in the calculation domain, and when $a_a = 1$, it fills with air. Tracking the air–water interaction requires the following continuity equation [135]:

$$\frac{\partial a_w}{\partial t} + u_i \frac{\partial a_w}{\partial x_i} = 0 \quad (3-5)$$

where x_i represents the coordinate and u_i denotes the flow velocity. (For units of the various parameters, please refer to the included symbol notation table)

Both the continuity and momentum equations for a free and incompressible fluid in an open channel can be expressed as

$$\frac{\partial u}{\partial x} + \frac{\partial v}{\partial y} = 0 \quad (3-6)$$

$$\rho \frac{\partial u}{\partial t} + \rho \operatorname{div}(uV) = \mu \operatorname{div}(\operatorname{grad} u) - \frac{\partial P}{\partial x} + F_u, \text{ and} \quad (3-7)$$

$$\rho \frac{\partial v}{\partial t} + \rho \operatorname{div}(vV) = \mu \operatorname{div}(\operatorname{grad} v) - \frac{\partial P}{\partial y} + F_v \quad (3-8)$$

where V is the flow velocity, u and v are the velocity components of fluid particles in the 2D spatial directions x and y , ρ is the density of water, μ is the dynamic viscosity, P is the pressure (P_a), and F_u and F_v are the forces of fluid particles in 2D directions.

The RNG k - ϵ turbulence model eliminates average flow rotation and whirling by modifying turbulent viscosity. The related equation is [136]

$$\frac{\partial(\rho k)}{\partial t} + \frac{\partial(\rho k u_i)}{\partial x_i} = \frac{\partial}{\partial x_i} \left[\alpha_k \mu_{eff} \frac{\partial k}{\partial x_j} \right] + G_k + \rho \epsilon \quad (3-9)$$

$$\frac{\partial(\rho \epsilon)}{\partial t} + \frac{\partial(\rho \epsilon u_i)}{\partial x_i} = \frac{\partial}{\partial x_i} \left[\alpha_\epsilon \mu_{eff} \frac{\partial \epsilon}{\partial x_j} \right] + \frac{C_{1\epsilon}}{k} G_k - C_{2\epsilon} \rho \frac{\epsilon^2}{k}, \text{ and} \quad (3-10)$$

$$G_k = \mu_t \left(\frac{\partial u_i}{\partial x_j} + \frac{\partial u_j}{\partial x_i} \right) \frac{\partial u_i}{\partial x_j} \quad (3-11)$$

where k denotes the turbulent kinetic energy, ϵ represents the turbulent energy dissipation rate, μ expresses the hydrodynamic viscosity coefficient, G_k denotes the turbulent kinetic energy production term, μ_{eff} represents the effective dynamic viscosity coefficient $C_{1\epsilon}$ and $C_{2\epsilon}$ denote the constants 1.42 and 1.68, respectively.

3.5 RESULTS

We evaluated the effect of surface irregularity on pressure, stress, flow velocity, and energy under 25 different irregularity configurations. In the following subsections, the effects of irregularities on the hydraulic parameters are examined independently. Fig. 3-7 shows the software output for the configuration of $\alpha_l = 19^\circ$ and $h = 10$ cm, depicting the volume fraction of water (VF), the contours of dynamic pressure (P_D) and total pressure (P_T) extracted directly from Ansys Fluent.

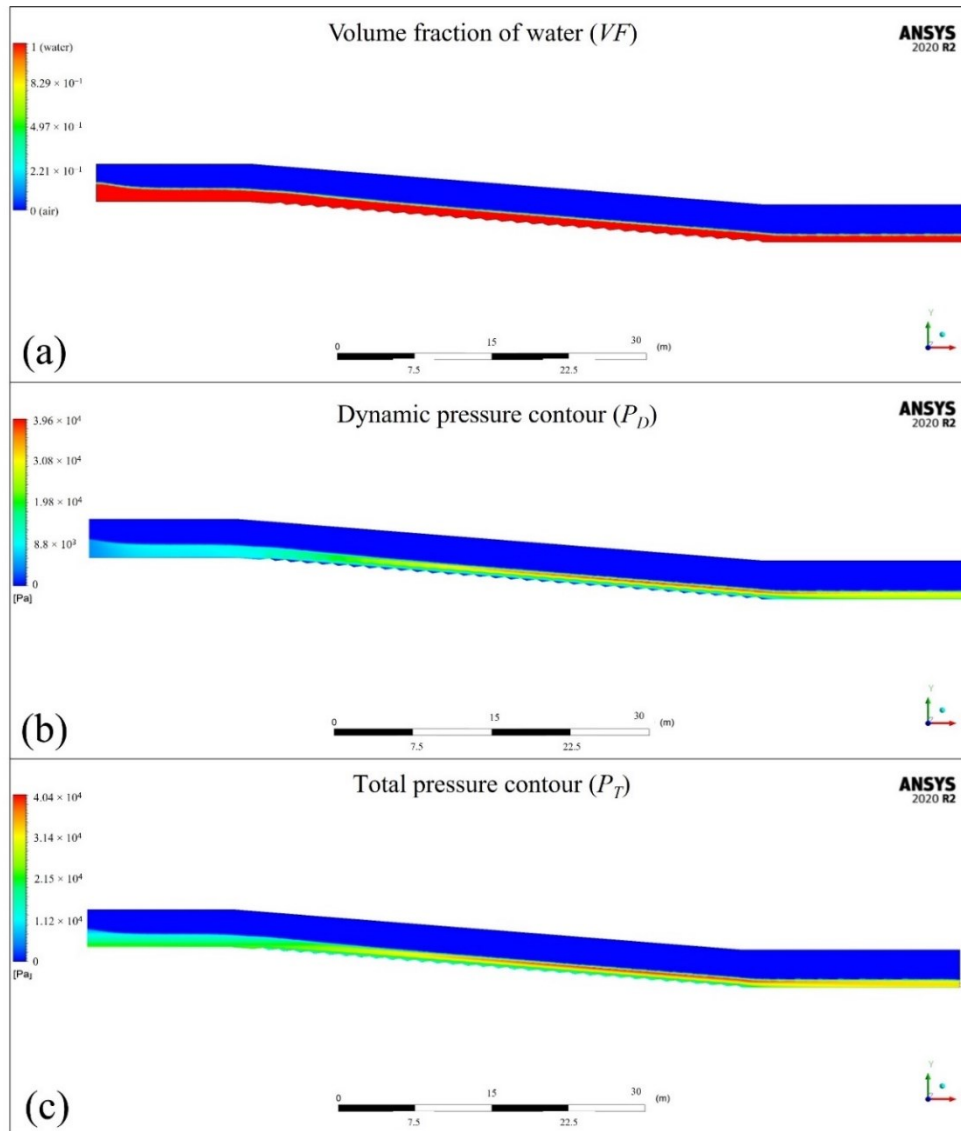


Fig. 3-7. The volume fraction of water, dynamic pressure contour, and total pressure contour.

3.5.1 Effect of irregularities on velocity

Eleven vertical cross-sections were analyzed along the spillway to estimate the maximum velocity profile. Each section covered the channel bottom to the water's surface, allowing us to calculate maximum velocity and water depth. Along the spillway, maximum velocity decreased as α_I and height increased (Fig. 3-8). Moreover, the effect of height on flow velocity was greater than the effect of α_I . For instance, at a constant α_I ($\alpha_I = 12$), maximum velocity decreased from approx. $11.5 \text{ m}\cdot\text{s}^{-1}$ at $h = 10 \text{ cm}$ to approx. $8 \text{ m}\cdot\text{s}^{-1}$ at $h = 40 \text{ cm}$. At a constant height, however, velocity did not necessarily decrease as α_I increased, the change often being minor and could be ignored. For instance, at a constant height ($h = 10 \text{ cm}$), the maximum velocity for $\alpha_I = 12$

was approx. $11.5 \text{ m}\cdot\text{s}^{-1}$ and for $\alpha_l = 40$, it was approx. $9 \text{ m}\cdot\text{s}^{-1}$. Flow velocity did not change significantly at a constant height (i.e, $h = 30 \text{ cm}$) as α_l increased. At greater heights (h), α_l variations did not affect maximum velocity, and the height of the irregularity had a greater impact.

When we evaluated velocity as a function of flow depth at various irregularity heights (for the final irregularity along the channel), we observed that a greater irregularity height, at a constant irregularity angle, caused water depth to increase, and maximum velocity was also higher (Fig. 3-9).

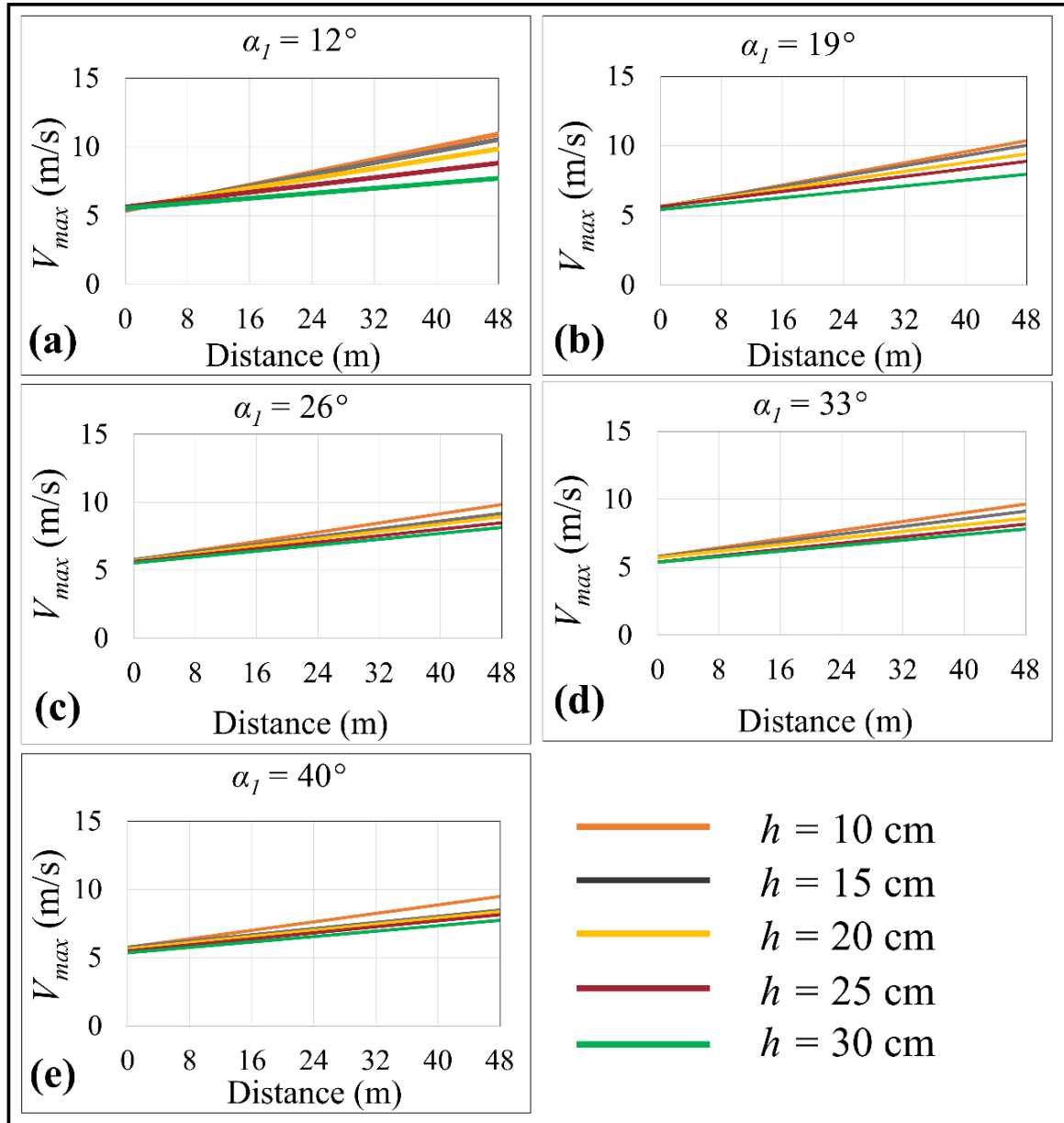


Fig. 3-8. Maximum velocity profiles of the flow along the unlined spillway; (a) $\alpha_l = 12^\circ$; (b) $\alpha_l = 19^\circ$; (c) $\alpha_l = 26^\circ$; (d) $\alpha_l = 33^\circ$; (e) $\alpha_l = 40^\circ$

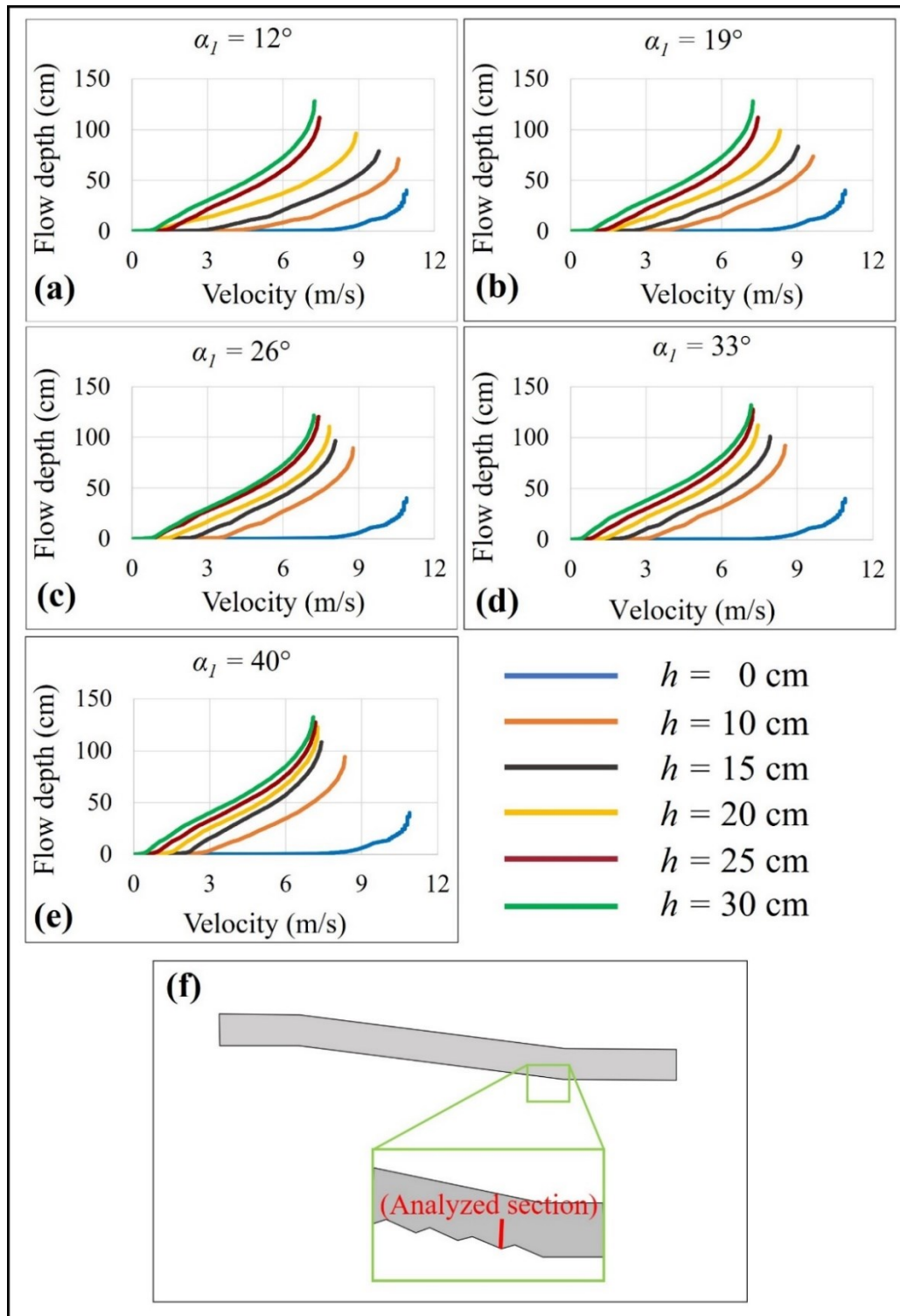


Fig. 3-9. Velocity profiles as a function of flow depth for various irregularity heights; a flow depth of 0 m refers to the channel bottom; (a) $\alpha_l = 12^\circ$; (b) $\alpha_l = 19^\circ$; (c) $\alpha_l = 26^\circ$; (d) $\alpha_l = 33^\circ$; (e) $\alpha_l = 40^\circ$; (f) the analyzed section of the channel profile (red line)

3.5.2 Effect of irregularities on total pressure (P_T)

In hydraulic engineering, *total pressure* is the sum of static and dynamic pressures. The relationship between total, static (P_S), and dynamic (P_D) pressures are described in equations (3-12)–(3-14), respectively.

$$P_T = P_S + P_D \quad (3-12)$$

$$P_S = \rho g d, \text{ and} \quad (3-13)$$

$$P_D = \frac{1}{2} \rho v^2 \quad (3-14)$$

where ρ is the density of water, g is the gravitational acceleration, d is the water depth, and v is the local flow velocity.

We derived total pressure in the first section directly from the ANSYS-Fluent results, which produced a total pressure profile at the water–rock interface (channel bottom). When static pressure is at its maximum, dynamic pressure is at its minimum (equation 3-15).

When we calculated the total pressure, we considered both the maximum static and maximum dynamic pressure (equation 3-16).

$$P_T = P_{S,channel\ bottom} + P_{D,channel\ bottom} \text{ and} \quad (3-15)$$

$$P_{T,max} = P_{S,channel\ bottom} + P_{D,water\ surface} \quad (3-16)$$

where $P_{T, max}$ represents maximum total pressure, $P_{S, channel\ bottom}$ represents the static pressure at the channel bottom, $P_{D,channel\ bottom}$ represents the dynamic pressure at the channel bottom, and $P_{D,water\ surface}$ is the dynamic pressure at the water surface, where it is at its maximum.

At the bottom of the channel, total pressure fluctuated along the spillway length (Fig. 3-10, for $h = 10$ cm and $\alpha_l = 19^\circ$). To analyze these fluctuations, we selected the most representative and appropriate line, that is the upper bound of each graph (e.g., *red line* of Fig. 3-10) of each configuration and grouped them into a single chart (Fig. 3-11).

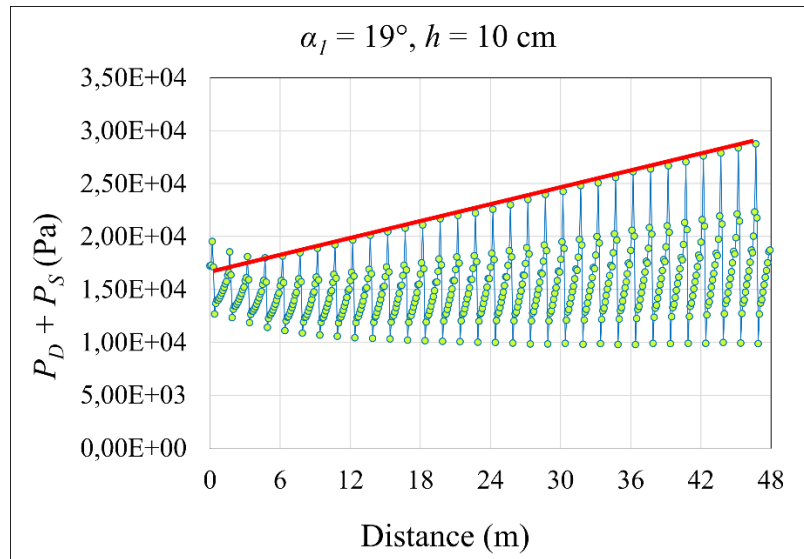


Fig. 3-10. Total pressure (sum of dynamic and static pressures) profile along the water–rock interface for the configuration $\alpha_l=19^\circ$ and $h = 10$ cm; red line describes the upper bound of the graph

Flow velocity increased, and water depth decreased moving downstream; thus, dynamic pressure, which has a direct relationship with flow velocity, trended upward, whereas static pressure, which has a direct relationship with water depth, trended downward along the channel. Overall, total pressure increased toward the downstream end of the profile. According to hydraulic engineering theory, however, flow velocity at the channel bottom is zero; thus, the dynamic pressure should also be zero. Total pressure at the channel bottom should be a function of static pressure, which also trends downward along the profile. The apparent contradiction of an increasing total pressure along the channel bottom and the greater role of dynamic pressure arose as the ANSYS-Fluent software records dynamic pressures at the mesh cell center. The value shown along the wall appears to be an extrapolation that does not necessarily equal zero.

We observed that total pressure decreased as α_l and h increased (Fig. 3-11). For example, at a constant $\alpha_l = 12^\circ$, the total pressure of flowing water at the channel bottom dropped with a higher h , from approx. 25 Pa at $h = 10$ cm to approx. 17 Pa at $h = 40$ cm. At a constant h , however, total pressure did not necessarily decrease as α_l increased; often these changes were negligible and could be ignored. At greater heights (h), altering α_l produced little effect on total pressure, whereas altering the height of the irregularity had a marked effect. The total pressure difference at the zero point occurred because the zero point on the X-axis (distance) did not match the model's zero point (see Fig. 3-11f). We began our analyses 15 m from the model's inlet; thus, the effect of irregularity height could already be observed, causing the initial pressure difference in our graphs.

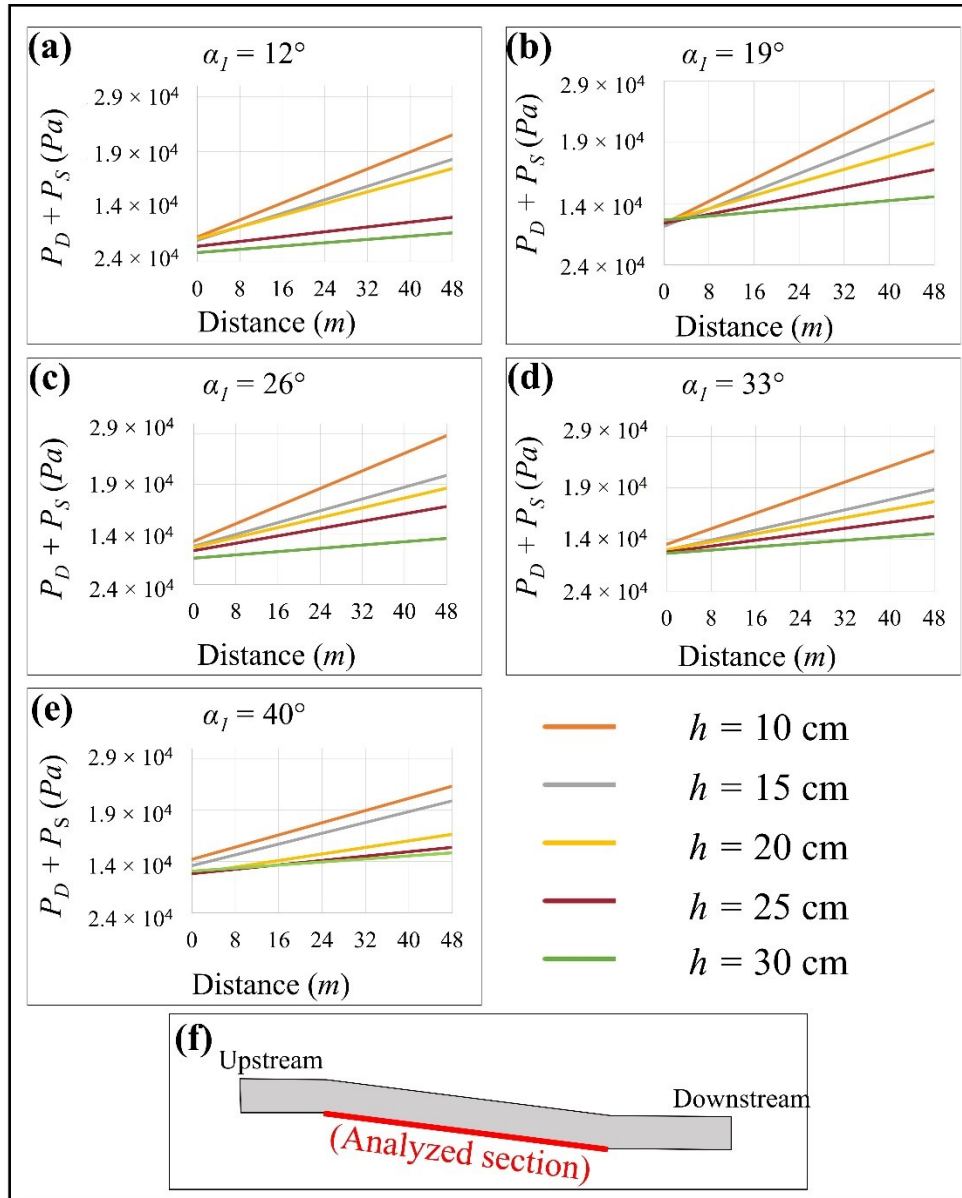


Fig. 3-11. Total pressure (static and dynamic pressure) profiles on water–rock interface as a function of spillway length for various irregularity heights and angles; (a) $\alpha_I = 12^\circ$; (b) $\alpha_I = 19^\circ$; (c) $\alpha_I = 26^\circ$; (d) $\alpha_I = 33^\circ$; and (e) $\alpha_I = 40^\circ$; (f) the analyzed section of the channel profile (red line)

From equation (3-16), we calculated the total pressure. Because dynamic pressure is determined using maximum velocity, the total pressure is at its maximum at the highest velocities (Fig. 3-12), and, consequently, so are dynamic and static pressures along the channel bottom. We also observed that total pressure increased by 2.5–3× compared with pressure along the channel bottom. Total pressure also decreased as α_I and h increased (Fig. 3-12). At greater heights (h), α_I changes had minimal effect on the total pressure, whereas changes to irregularity height did produce a large effect.

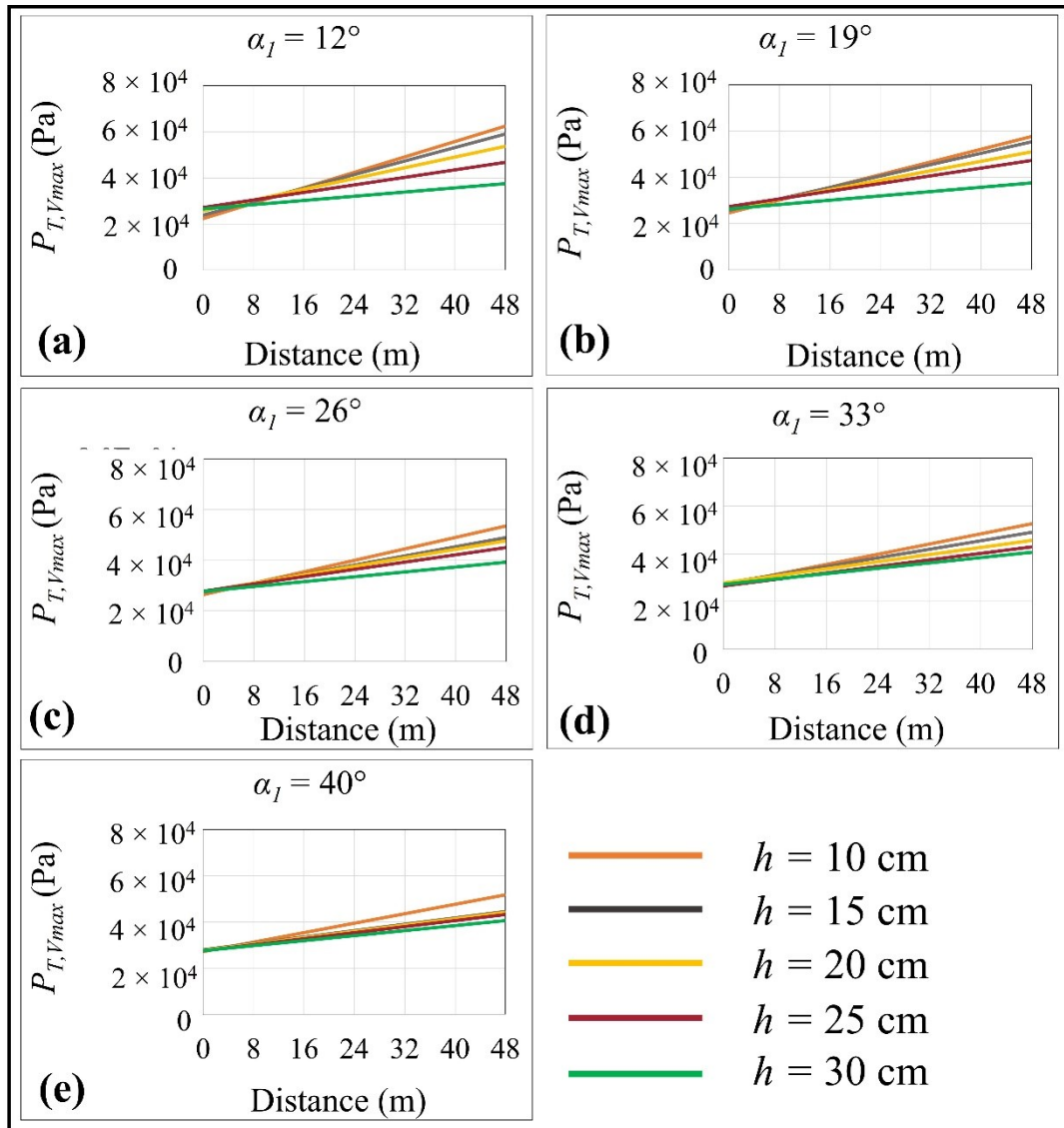


Fig. 3-12. Total pressure profiles on the water surface as a function of spillway length for various irregularity heights; (a) $\alpha_I = 12^\circ$; (b) $\alpha_I = 19^\circ$; (c) $\alpha_I = 26^\circ$; (d) $\alpha_I = 33^\circ$; and (e) $\alpha_I = 40^\circ$

3.5.3 Effect of irregularities on shear stress

We also investigated shear stress at the water–rock interface. Fig. 3-13 shows the surface shear stress on the rock surface for an irregularity angle of $\alpha_I = 12$. Shear stress on the rock surface was negligible relative to the total, static, and dynamic pressures. Nonetheless, as irregularity height (h) increased, shear stress along the wall decreased; however, these values were so small that they could be ignored.

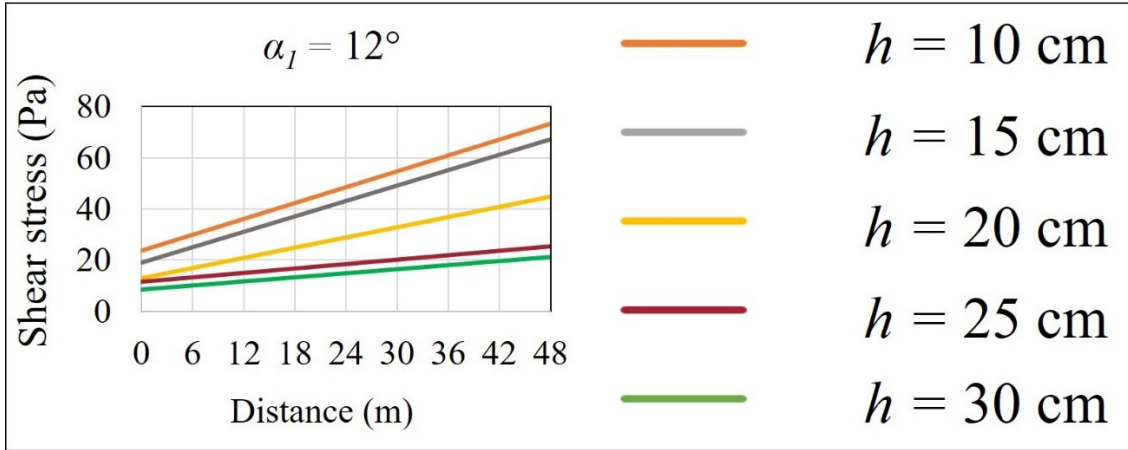


Fig. 3-13. Shear stress along the water–rock interface for an irregularity angle of $\alpha_I = 12^\circ$

3.5.4 Effect of irregularities on the energy gradient

Energy is dependent on the pressure head, velocity head, and elevation. In the preceding section, we described the sum of pressure and velocity heads, i.e., dynamic and static pressure, for two distinct states of dynamic pressure: 1) at the rock mass surface and 2) at the water surface. Here, we analyze the energy at (1) the water surface and (2) the channel bottom.

We computed the relevant energy via equations 3-17 and 3-18 with velocity head determined directly from the flow velocity, and pressure head equals water depth. The elevation of a point was its distance from the datum.

$$E_{\text{water-rock interface}} = H_{P,WRI} + H_{V,WRI} + Z_{WRI}, \text{ and} \quad (3-17)$$

$$E_{\text{water surface}} = H_{P,W.S} + H_{V,W.S} + Z_{W.S} \quad (3-18)$$

where $E_{\text{water-rock interface}}$ represents the energy at the channel bottom, $H_{P,WRI}$ and $H_{V,WRI}$ are the pressure head and velocity head, respectively, at the channel bottom. Z_{WRI} is the elevation of the channel bottom, $E_{\text{water surface}}$ is the energy at the water surface, $H_{P,W.S}$ and $H_{V,W.S}$ represent, respectively, the pressure head and velocity head at the water surface, $Z_{W.S}$ is the elevation of the water surface from the datum, and $Z_{\text{water surface}} = Z_{\text{rock}} + H_{P,WRI}$. These parameters are measured in meters.

For calculating the energy at the rock mass surface, the velocity head was at a minimum and the pressure head at a maximum. In contrast, at the water surface, the velocity head was at a maximum, and the pressure head was zero. The difference between the energy at the water surface and the energy at the channel bottom (water–rock interface) was the velocity head or dynamic pressure. Figure 14 describes the methodology to calculate energy at the water–rock interface and water surface.

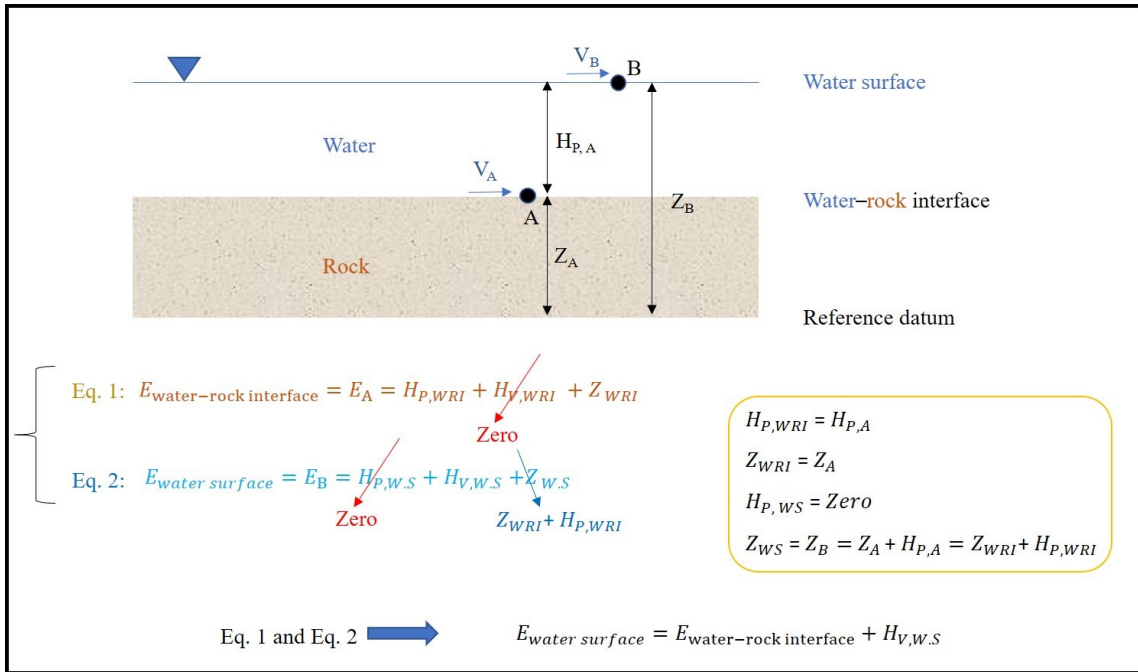


Fig. 3-14. Calculation of energy at the water-rock interface and water surface

We then calculated the energy of water at the water-rock interface and water surface for the entire analyzed area. We also depicted the energy gradients and differences in energy along the profile (Fig. 3-15). Energy decreased upstream to downstream, with 70% of the energy lost along the profile. When the angle was held constant, as h increased, a greater amount of energy was lost. Less energy was lost when h decreased. At a constant h , however, energy loss was not necessarily greater as α_l increased.

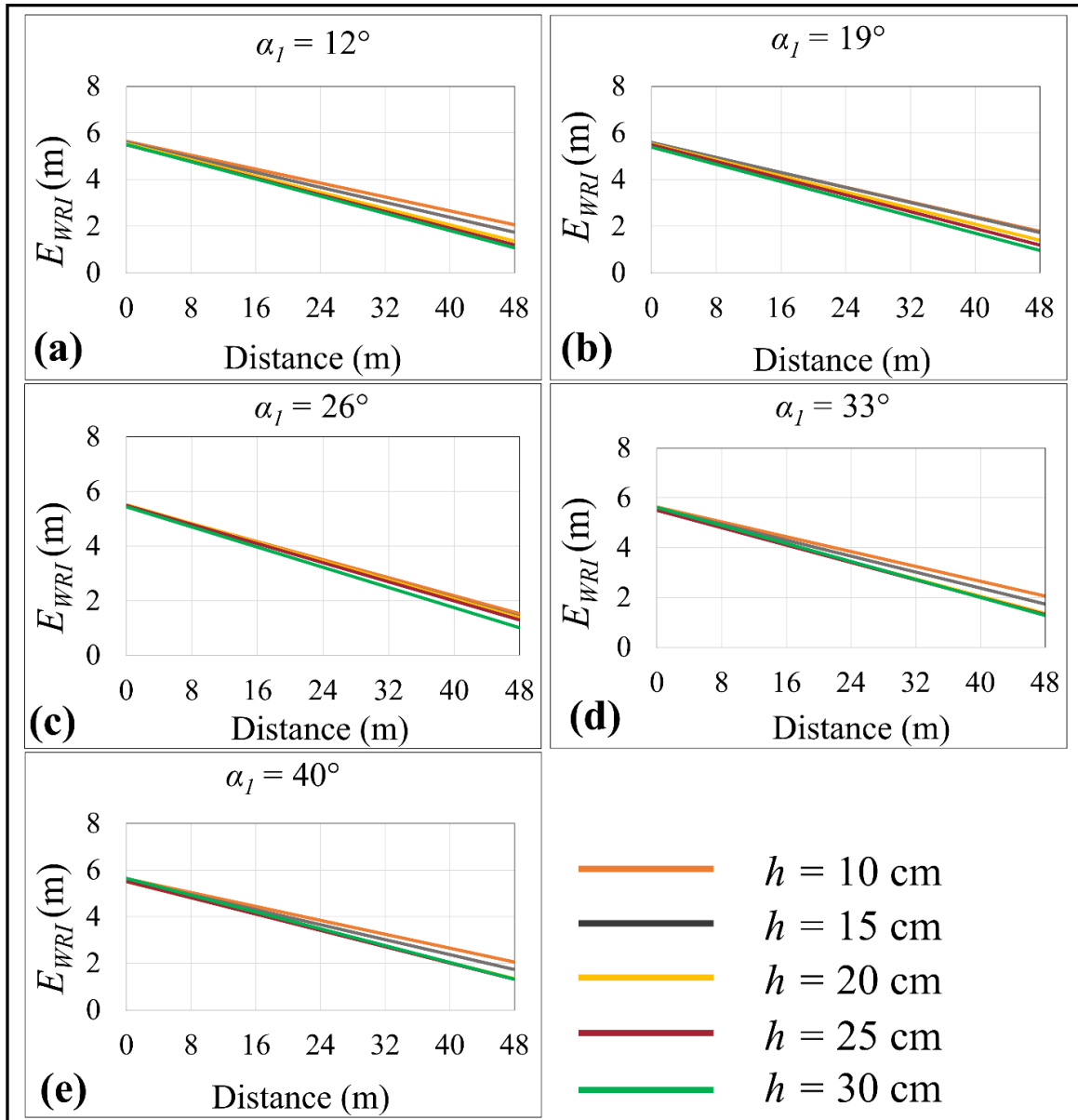


Fig. 3-15. Energy gradient profiles at the water–rock interface; (a) $\alpha_1 = 12^\circ$; (b) $\alpha_1 = 19^\circ$; (c) $\alpha_1 = 26^\circ$; (d) $\alpha_1 = 33^\circ$; and (e) $\alpha_1 = 40^\circ$.

Energy at the water surface (State 1) where energy relates to elevation and velocity head (at their maximum) and the pressure head are at their minimum. Energy increased along the profile relative to the energy at the water–rock interface (State 2). This energy increase was around 30% upstream and 2.5–3.5× times downstream relative to the energy at water–rock interface.

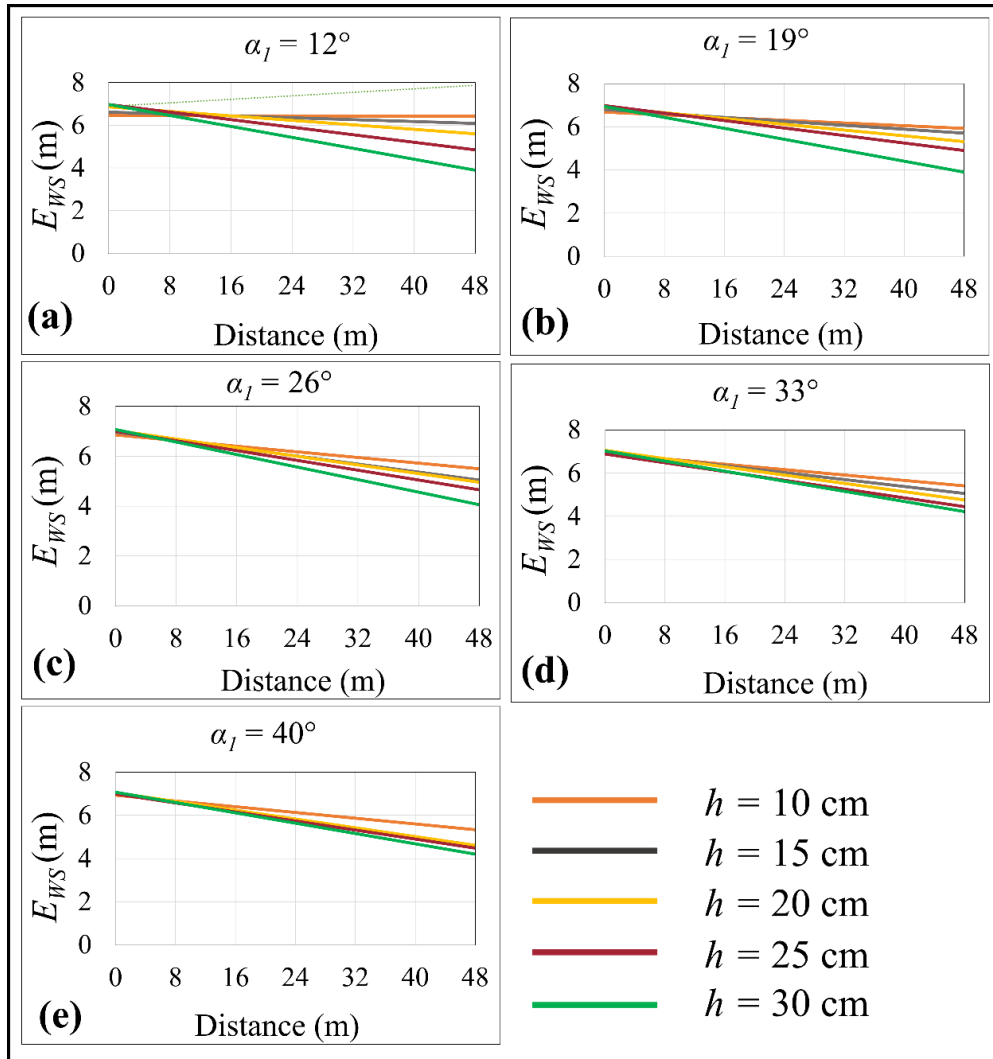


Fig. 3-16. Energy gradient profiles along the water surface; (a) $\alpha_l = 12^\circ$; (b) $\alpha_l = 19^\circ$; (c) $\alpha_l = 26^\circ$; (d) $\alpha_l = 33^\circ$; and (e) $\alpha_l = 40^\circ$.

Differences in the energy state at the water–rock interface (Fig. 3-15) and the water surface (Fig. 3-16) related to the flow velocity and dynamic pressure.

Energy loss at the water–rock interface (State 1) was greater than at the water surface (State 2) because:

- 1) In the first state, the velocity differential between upstream and downstream was close to zero; thus, the slope of the flow–distance relationship was zero;
- 2) In the second state, the difference in velocity between the upstream and downstream was not zero, and flow velocity–distance relationship sloped upward;

Because the sum of Z and H_p was the same for both states, the negative relationship between the energy and distance decreased as the slope of the velocity increased for the second state, i.e., a greater velocity increased the amount of energy and decreased energy loss.

3.6 DISCUSSION

Our study demonstrated the use of ANSYS-Fluent software and 2D steady-state simulations using computational fluid dynamics to determine the effect of unlined spillway surface irregularities (height and angle) on hydraulic parameters. We concentrated on how changes to irregularity height and angle affected flow velocity, dynamic pressure, static pressure, total pressure, shear stress, velocity head, pressure head, elevation, energy, and energy loss. We found that:

- 1) Irregularities affected hydraulic parameters, despite existing approaches for determining hydraulic erosive parameters not considering these irregularities;
- 2) Velocity at a constant height did not continually decrease as α_l increased, and these changes were often negligible;
- 3) Changes in irregularity angle had a minimal effect on maximum flow velocity at greater heights; however, altering irregularity height had a marked effect;
- 4) Holding the irregularity angle constant, total pressure along the channel bottom decreased as h increased. At a constant h , however, total pressure did not consistently decrease as α_l increased; these latter changes were typically negligible. At greater heights, changes in angle had a minimal impact on total pressure; however, altering irregularity height had a marked effect;
- 5) Total pressure, using maximum dynamic pressure to determine the total pressure, increased 2.5–3× relative pressure along the channel bottom;
- 6) Along the water–rock interface, 70% of the energy was lost along the profile;
- 7) Energy at the water–rock interface increased by approx. 30% upstream and 250%–350% downstream;
- 8) Increased flow velocity increased energy and decreased energy loss.

It should be noted that the 2D nature of this research represented a limitation. Additionally, the simulations were steady-state and not time-dependent (transient). Furthermore, the effect of geometric characteristics of the unlined spillway, i.e., overall spillway profile and length, was not considered in this study. Future research should address these limitations to provide a more comprehensive understanding of the subject.

3.7 CONCLUSIONS

In conclusion, this study undertook a comprehensive assessment of the influence exerted by unlined spillway surface irregularities on key hydraulic parameters. The findings unveiled a discernible impact of irregularities on static, dynamic, and total pressures, as well as maximum flow velocity, shear stress, and energy distribution. It is important to acknowledge that while the study successfully examined the effect of surface irregularities, the broader interaction between spillway geometry and hydraulic parameters still requires further exploration. The utilization of a 2D modeling approach proved instrumental in integrating irregularity effects into the evaluation of erosive hydraulic parameters. Nevertheless, it's essential to recognize that the current investigation encountered certain limitations, primarily stemming from its 2D nature and steady-state simulations. The study's focus on irregularities leaves room for subsequent research to encompass the broader influence of geometric characteristics, such as overall spillway profile and length, to provide a more comprehensive and nuanced understanding of the subject matter. This study significantly contributes to the evolving discourse surrounding hydraulic parameters in the context of unlined spillways, paving the way for future investigations to address remaining intricacies and offer practical insights.

CHAPTER 4

Article 3: Modification of the unit stream power dissipation (USPD) equation for unlined spillways considering geometrical parameters and surface irregularities

Yavar Jalili Kashtiban ^{a *}, Ali Saeidi ^a, Marie-Isabelle Farinas ^a, Javier Patarroyo ^b

^a Department of Applied Sciences, University of Quebec at Chicoutimi, Saguenay, G7H 2B1, QC, Canada

^b Hydro-Québec Production Unité Expertise en barrages, 75 Boulevard René-Lévesque Ouest, Montréal, QC H2Z 1A4, Canada

Submitted to Acta Geotechnica journal and currently under review (submitted on October 1, 2023).

AUTHOR CONTRIBUTIONS: Conceptualization, Y.J.K.; methodology, Y.J.K. and A.S.; software, Y.J.K.; validation, Y.J.K., A.S., M.-I.F. and J.P.; formal analysis, Y.J.K.; investigation, Y.J.K.; resources, Y.J.K. and A.S.; writing original draft preparation, Y.J.K.; writing, review and editing, Y.J.K., A.S., M.-I.F. and J.P.; visualization, Y.J.K., A.S., M.-I.F. and J.P.; supervision, A.S., M.-I.F.; industrial advising, J.P.; project administration, A.S.; funding acquisition, A.S.

FUNDING: This research was funded by: Natural Sciences and Engineering Research Council of Canada and Hydro-Québec (NSERC, Hydro-Quebec) [CRDPJ 537350-18]. Natural Sciences and Engineering Research Council of Canada (NSERC) [RGPIN-2019-06693].

ACKNOWLEDGEMENT: The authors would like to thank the Natural Sciences and Engineering Research Council of Canada (NSERC) and Hydro-Quebec for funding this project (CRDPJ 537350 - 18, NSERC-RGPIN-2019-06693) and all those who helped us to improve the quality of this paper.

CONFLICTS OF INTEREST: The authors declare that they have no conflict of interest regarding the content of this document.

*Email: Yavar.jalilikashtiban1@uqac.ca

4.1 ABSTRACT

The unit stream power dissipation (USPD) equation is widely used to predict water flow characteristics over spillways. However, the current formulation of the USPD equation may not provide accurate predictions of the energy dissipation rates of water flowing over unlined spillways, particularly when geometrical parameters and surface irregularities are considered. To address this issue, we modify the USPD equation to improve its accuracy. We determine how geometrical parameters and surface irregularities affect the accuracy of the USPD when applied to unlined spillways. Our modifications to the USPD equation account for these factors and improve predictions of the energy dissipation rate of water flowing over unlined spillways. We demonstrate that incorporating geometrical parameters and surface irregularities into the USPD equation improves the accuracy of estimated energy dissipation rates. Improved prediction accuracy has important implications for spillway design and maintenance, favoring safer and more effective water management systems. Our study highlights the need to consider geometrical parameters and surface irregularities when estimating USPD in unlined spillways.

Keywords: dam, hydraulic structures, unlined spillways, erodibility, computational fluid dynamics, USPD

4.2 HIGHLIGHTS

- Modification of the unit stream power dissipation (USPD) equation for enhanced accuracy in predicting energy dissipation rates over unlined spillways.
- Investigation of how geometrical parameters and surface irregularities impact the precision of the USPD equation in unlined spillway scenarios.
- Modifications lead to improved energy dissipation rate predictions for water flow over unlined spillways.
- Findings hold practical implications, contributing to safer and more effective spillway design and maintenance, thus advancing water management systems.

4.3 INTRODUCTION

In recent years, dam safety concerns have focused on reducing the risk of rock scouring and erosion of hydraulic structures. Erodibility, scour, and hydraulic erosion are synonymous terms to describe the critical centralized erosion produced when the erosive intensity of fluid exceeds the resistive capacity of a rock mass. A major challenge in designing hydraulic structures is creating dam spillways that can discharge a wide range of water quantities without scouring the underlying rock material. The fundamental basis of hydraulic erodibility holds that the erosive power of water is compared with the resistance of a rock mass to erosion, which in turn depends on the flowing water strength (Fig. 4-1). If the erosive power of water is less than the resistance of the rock mass, then the limit of erodibility is not surpassed. However, if the erosive power of water

exceeds the resistance of the rock mass, then values above the erodibility threshold have been exceeded, thereby resulting in the erosion and scouring of the rock mass.

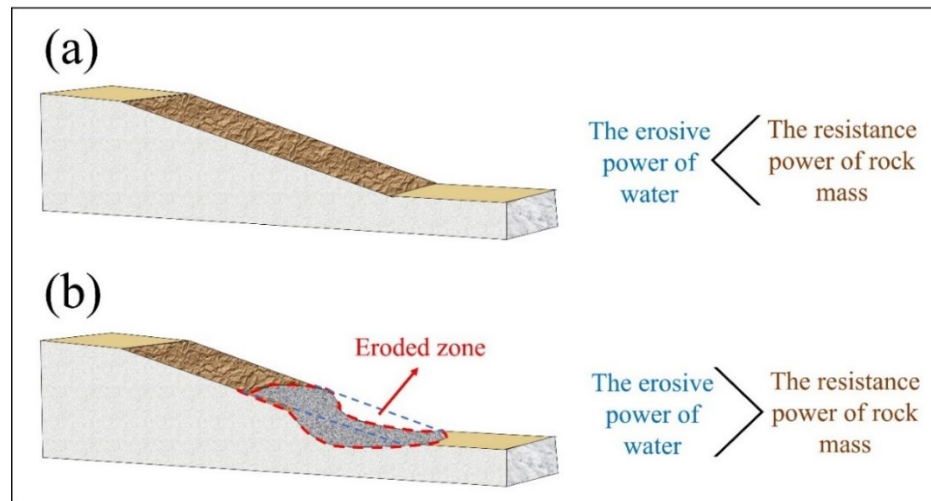


Fig. 4-1. Fundamental basis of hydraulic erodibility

An unlined dam spillway is an essential part of a dam structure and is designed to control water flow during normal and flood conditions. Typically, unlined spillways are constructed using natural materials, such as rocks, and are designed to withstand high velocities and turbulence.

The water that flows through the spillway can erode the natural materials of the discharge channel over time, thereby changing the channel geometry and reducing a spillway's capacity as the eroded material collects within the flow path. The spillway's energy dissipation rate and capacity can also be affected by the turbulence of the flowing water, leading to potential damage to the spillway structure and downstream infrastructure. Erosion can occur through various mechanisms, including hydraulic scour, abrasion, and cavitation. Damage to the spillway structure can also occur because of high-velocity flow and marked turbulence. The water that flows through the unlined spillway can cause pressure fluctuations, producing cracks and other defects in the unlined spillway structure. These defects weaken the structure over time and may eventually lead to catastrophic failure. Thus, it becomes essential to explore the aspects of hydraulic erodibility phenomena, specifically the water's erosive power and the rock mass's resistance. In this study, we focus on the erosive aspects of hydraulic erodibility phenomena.

The unit stream power dissipation (USPD) equation is widely used to predict the energy dissipation rate in spillways (i.e., the erosive power of water). This equation is based on stream power, which refers to the rate at which water transfers energy to the bed and banks of a channel. In the context of spillways, USPD estimates the rate at which the energy of the flowing water is dissipated as it passes over the spillway surface. These

estimates help design spillways that can effectively dissipate energy without suffering erosion or damage. The general definition of USPD is shown by Equation (4-1) [1].

$$\text{USPD} = \rho \cdot g \cdot q \frac{dE}{dx}. \quad (4-1)$$

The unit stream power proposed by Laursen (1958) [137] to predict the energy dissipation rate in natural rivers and channels. Since then, this equation has been widely used in the design and analysis of spillways and in studies related to fluvial geomorphology and river engineering. The USPD equation stems from the principles of conservation of energy and momentum and is derived using dimensional analysis and scaling arguments. Table 4-1 presents the existing hydraulic erosive indices including the USPD. These various equations provide different approaches for calculating the energy dissipation rate in spillways and channels. All listed equations are based on the concept of stream power. However, the equations differ in how they consider surface geometry and roughness.

Table 4-1. Existing hydraulic erosion indices

Hydraulic erosive parameter	Reference	Equation
Unit stream power dissipation (USPD)	(Lacey 1930) [138]	$USPD = \frac{\gamma Q^3}{(2S_f) \left(1 + 1.5 \frac{Q}{Q_c}\right)}$
	(Bakhmeteff 1932) [139]	$USPD = \frac{\gamma Q^3}{2S_f}$
	(Blench 1952) [140]	$USPD = \left(\frac{\rho g}{Q}\right) \left(\frac{H}{d_e}\right)^{\frac{1}{2}}$
	(Laursen and Toch 1956) [141]	$USPD = \frac{k \left(\frac{Qw}{S}\right)^{\frac{2}{3}}}{S_f \left(1 + \alpha \frac{Q}{\beta_f}\right)^{\frac{2}{3}}}$
	(Laursen 1958) [137]	$USPD = \frac{\gamma Q^3}{S_f \left(1 + \alpha \frac{Q}{\beta_f}\right)^{\frac{2}{3}}}$
	(Yalin 1972) [142]	$USPD = \frac{\gamma Q^3}{(\tau_0 S_f) \left(1 + 5.5 \sqrt{\frac{\tau_0}{\gamma D_{50}}} \frac{Q}{B}\right)^2}$
	(Ackers and White 1973) [143]	$USPD = \frac{\gamma Q^3}{\tau_0 S_f}$
	(Chanson 1995) [144]	$USPD = k \left(\frac{Qw}{S}\right)^{\frac{2}{3}} \left(\frac{h_w}{h_f}\right)^{\frac{1}{2}}$
	(Annandale 1995) [21]	$USPD = \gamma \cdot q \cdot \Delta E$
	(Knighton 1998) [145]	$USPD = \frac{\gamma Q^3}{(\tau_0 S_f) \left(1 + k \frac{Q}{Q_c}\right)}$
	(Pells 2016) [1]	$USPD = \rho \cdot g \cdot q \cdot \frac{dE}{dx}$
	(Weisbach 1845, Darcy 1857) [120, 121]	$V = \sqrt{\frac{8g}{f}} \sqrt{R_H \cdot S_f \cos \theta}$
	(Manning et al. 1890) [122]	$V = \frac{1}{n} R_H^{2/3} \cdot S^{1/2}$
Shear stress (τ_b)	(Yunus 2010) [19]	$\bar{\tau}_b = \rho \cdot g \cdot R_H \cdot S_f \cos \beta$
	(Khodashenas and Paquier 1999) [146]	$\tau_b = \rho \cdot g \cdot h \cdot S_f$
	(Prasad and Russell 2000) [124]	$\frac{\bar{\tau}_{(b)}}{\rho g h S_f} = (1 - 0.01\% S F w) \left(1 + \frac{P_{(w)}}{P_{(b)}}\right)$
	(Yang and Lim 2005) [125]	$\frac{\bar{\tau}_{(b)}}{\rho g h S_f} = 1 + \frac{h}{b} \frac{1}{\tan \beta} - \psi \frac{h}{b} \frac{1}{\sin \theta}$
	(Guo and Julien 2005) [126]	$\frac{\bar{\tau}_{(b)}}{\rho g h S_f} = \frac{4}{\pi} \text{Arctg} \left[\exp\left(\frac{-\pi h}{b}\right) \right] + \frac{4h}{\pi b} \exp\left(\frac{-h}{b}\right)$
	(Seckin et al. 2006) [127]	$\frac{\bar{\tau}_{(b)}}{\rho g h S_f} = \frac{a + b(B/H)}{1 + c(B/H) + d(B/H)^2}$
	(Severy and Felder 2017) [128]	$\tau_0 = \frac{1}{8} f \rho V^2$
Stress intensity (K_I)	Comprehensive Fracture Mechanics (CFM) (Bollaert 2002) [59]	$K_I = 0.8 \cdot P_{\max} \cdot F \cdot \sqrt{\pi \cdot L_f}$
Lifting force (F_L)	Dynamic Impulsion (DI) (Bollaert 2002) [59]	$I = \int_0^{\Delta t_{\text{pulse}}} (F_u - F_o - G_b - F_{sh}) \cdot dt$ $= m \cdot V_{\Delta t_{\text{pulse}}}$
	Quasi-Steady Impulsion (QSI) (Bollaert 2010) [3]	$F_{QSL} = C_{\text{uplift}} \cdot L_{\text{block}} \cdot \frac{V_{X,\max}^2}{2g}$

Ackers and White (1973) [143] introduced a sediment transport approach to estimate energy dissipation, whereas Yalin (1972) [142] proposed an equation widely used to estimate sediment transport and energy dissipation in rivers. The Laursen (1958) equation [137] estimates energy dissipation for circular drop shafts, and those of Annandale (2006, 1995) [20, 21] estimate energy dissipation on dam spillways. Chanson (1995) [144] proposed an equation to estimate energy dissipation and air entrainment in free-surface flows on rough surfaces, an equation now widely used in spillway design.

The differences among these equations lie in the factors considered by each equation, such as shear stress, critical velocity, turbulence, boundary layer thickness, and the dimensionless coefficients used to represent these factors. Some equations also incorporate the Froude number, which represents the ratio of inertial forces to gravitational forces and is used to characterize flow conditions. However, the accuracy of these equations depends on the applied assumptions, empirical coefficients, and the specific conditions of the spillway.

The original USPD equation and its modifications assume a smooth, uniform channel surface and do not account for surface irregularities. However, natural rock surfaces in spillways are often irregular, which can affect the energy dissipation rate and the prediction accuracy of the equation. Therefore, the impact of surface irregularities should be considered when using the USPD equation for spillway design and analysis and to ensure the safe and effective operation of spillways in managing water flow and preventing flooding. Various equations have been proposed to calculate the erosive power of water (Kashtiban et al. 2021) [118], although much less attention has been placed on its application to unlined dam spillways. In existing equations, the natural surface of the rock, which has irregularities, has been studied less, or the effects of these irregularities have not been considered in the equations. After evaluating the applicability of the existing equations, we propose an equation that considers the impact of irregularities on the rock surface and spillway slope. We detail the methodology used to obtain this modified equation, including an outline of the desired changes to the existing equation and the assumptions and basis for this equation. We apply the results of 25 simulations conducted in ANSYS-Fluent to modify the USPD equation to account for the irregularities of spillway surfaces. Cross validation of the modified equation using simulation data confirms the equation's effectiveness in accurately predicting energy dissipation. Finally, we summarize the obtained results and discuss the limitations and strengths of this equation and future research avenues.

4.4 METHODOLOGY

We can outline our procedures for determining the impact of spillway surface irregularities on the USPD equation as a flowchart (Fig. 4-2). We first analyzed available data from Pells (2016) [1] to identify and select the most influential geometric parameters of spillways and irregularities to create the model geometry. Next, using the ANSYS-Fluent software, we simulated water flow over the various rock geometries and extracted the results using CFD-Post. Subsequently, we determined the correlations among the velocity head, pressure head, and position head with the rock surface irregularities and spillway slope. We then formulated an equation to

determine the maximum velocity head, average velocity head, maximum velocity, average velocity, pressure head, and position head as functions of distance (x), irregularity angle (α_1), irregularity height (h), and unlined spillway slope (β). Finally, we modified the original USPD equation by relying on the developed equations and determined the error of the equation.

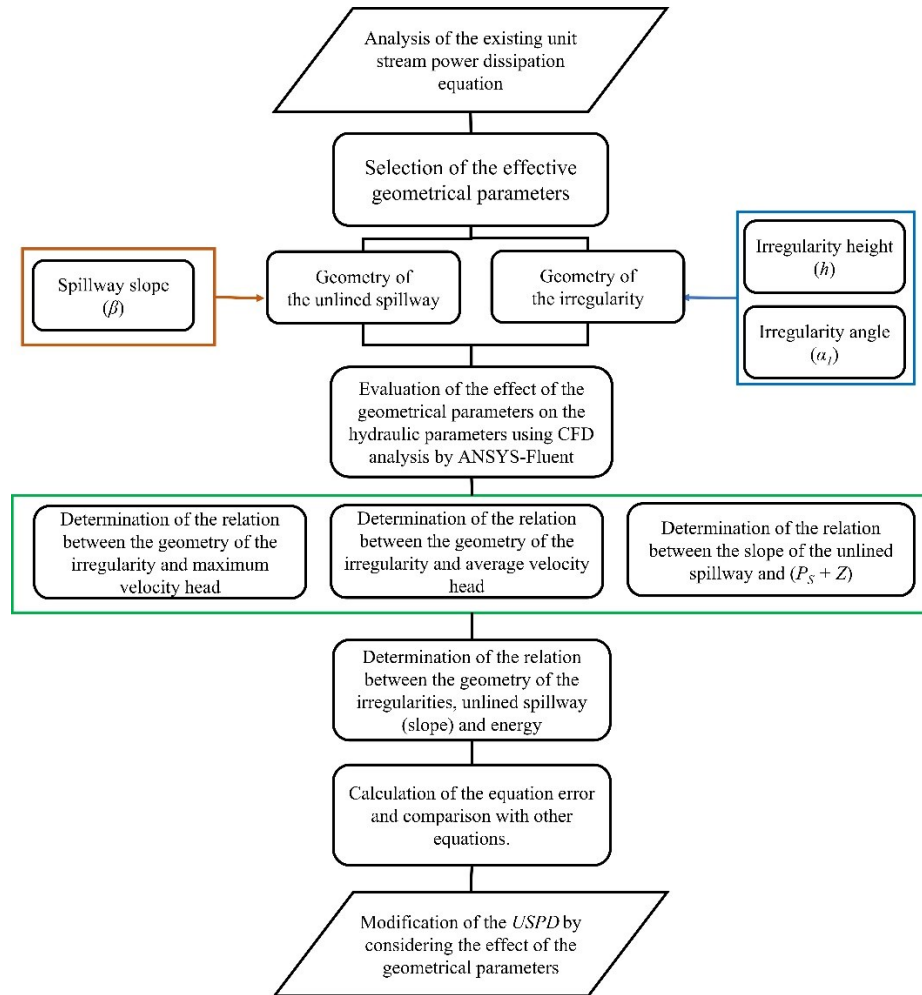


Fig. 4-2. Flowchart of the modification of USPD equation taking into account irregularity geometry

4.4.1 Identification and selection of effective geometric parameters

The first step involved analyzing available data from Pells (2016) collected from more than 100 case studies from dams in Australia, Africa, and the United States—to find the geometrical parameters of the unlined spillway surfaces. We considered spillway geometric parameters, spillway slope, and the geometric parameters of the irregularities, such as the height and angle. We selected these parameters on the basis of their effectiveness in determining the hydraulic performance of unlined spillways and blasting.

Blasting is commonly used to break and remove rock masses in mining, tunneling, and dam construction operations (Kashtiban et al. 2022b). [147] Drilling and blasting produce irregularities along a spillway's surface profile. Burden and spacing are the most important factors to consider when designing blasting patterns for unlined dam spillways, where burden denotes the distance between a blasting-hole row to the excavation face or between blasting-hole rows, and spacing refers to the distance between blasting holes along the same row [148].

4.4.2 Model geometry

In an earlier paper, Kashtiban et al. (2022a) [119] created a specific unlined spillway model geometry by combining selected parameters with observed controlled-blasting patterns. They considered various spillway lengths, spillway slopes (2.5°, 5°, 10°, and 15°), as well as various irregularity lengths (1–2 m; 1.5 m for the simulation), heights (10–30 cm), and angles (12°–40°). To simulate the geometry, Kashtiban et al. (2022a) [119] ran the powerful computational fluid dynamics (CFD) tool DesignModeler in ANSYS-Fluent.

We can apply Equations (4-2) – (4-4) to identify the geometric parameters of the irregularities [119]. These equations correspond to a function of the input parameters, and the irregularity geometry can be created using these equations and the input parameters α_1 , h , and l . The lengths of irregularity surfaces with and against water flow are represented by e_b and e_f , respectively (Fig. 4-3). The irregularity angle in the flow direction and the spillway slope are known as α_2 .

$$\alpha_2 = \tan^{-1} \left(\tan \alpha_1 \times \left(\frac{l \tan \alpha_1}{l \tan \alpha_1 - h} - 1 \right) \right), \quad (4-2)$$

$$e_f = \frac{h}{\sin \alpha_1}, \quad (4-3)$$

$$e_b = \frac{h}{\sin \alpha_2}. \quad (4-4)$$

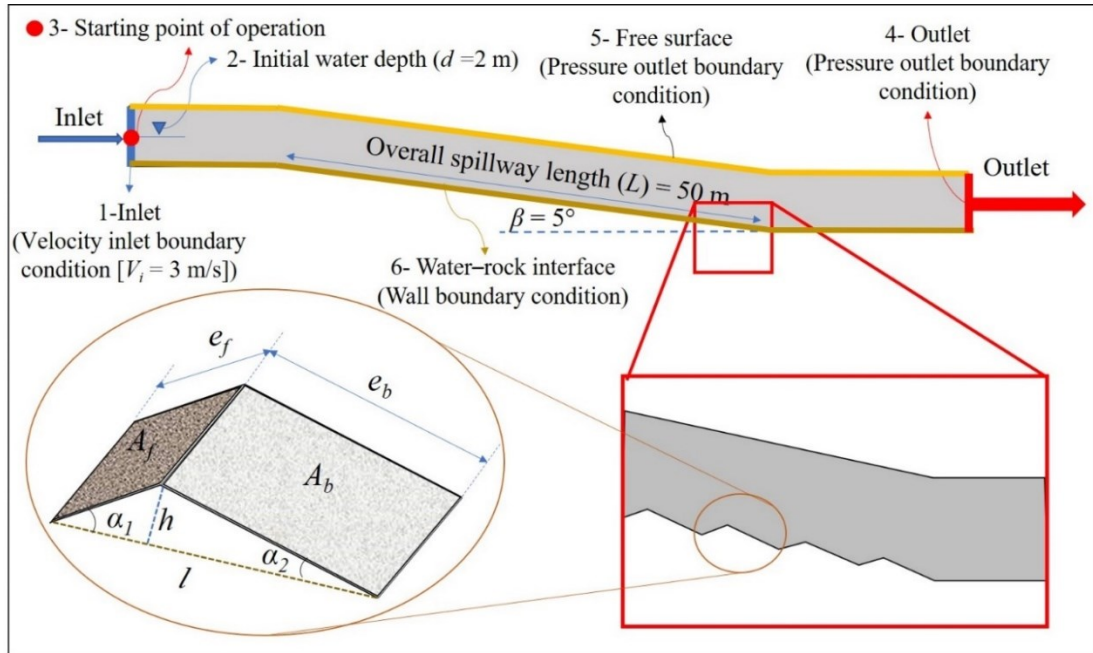


Fig. 4-3. Assumed spillway geometry used in our model of irregularities along an unlined rock spillway, and boundary conditions of the computational fluid dynamics (CFD) modeling

h (m) \ α_j ($^\circ$)	12	19	26	33	40
0.1	$\alpha_2 = 5.55$ $e_f = 0.48$ $e_b = 1.03$	$\alpha_2 = 4.73$ $e_f = 0.31$ $e_b = 1.21$	$\alpha_2 = 4.42$ $e_f = 0.23$ $e_b = 1.3$	$\alpha_2 = 4.25$ $e_f = 0.18$ $e_b = 1.35$	$\alpha_2 = 4.14$ $e_f = 0.16$ $e_b = 1.38$
	$\alpha_2 = 10.7$ $e_f = 0.72$ $e_b = 0.81$	$\alpha_2 = 8.02$ $e_f = 0.46$ $e_b = 1.07$	$\alpha_2 = 7.17$ $e_f = 0.34$ $e_b = 1.2$	$\alpha_2 = 6.74$ $e_f = 0.28$ $e_b = 1.28$	$\alpha_2 = 6.48$ $e_f = 0.23$ $e_b = 1.33$
	$\alpha_2 = 19.7$ $e_f = 0.96$ $e_b = 0.59$	$\alpha_2 = 12.28$ $e_f = 0.61$ $e_b = 0.94$	$\alpha_2 = 10.4$ $e_f = 0.46$ $e_b = 1.11$	$\alpha_2 = 9.52$ $e_f = 0.37$ $e_b = 1.21$	$\alpha_2 = 9.01$ $e_f = 0.31$ $e_b = 1.28$
0.25	$\alpha_2 = 37.7$ $e_f = 1.2$ $e_b = 0.41$	$\alpha_2 = 17.9$ $e_f = 0.77$ $e_b = 0.81$	$\alpha_2 = 14.21$ $e_f = 0.57$ $e_b = 1.02$	$\alpha_2 = 12.64$ $e_f = 0.46$ $e_b = 1.14$	$\alpha_2 = 11.75$ $e_f = 0.39$ $e_b = 1.23$
	$\alpha_2 = 73.54$ $e_f = 1.44$ $e_b = 0.31$	$\alpha_2 = 25.5$ $e_f = 0.92$ $e_b = 0.7$	$\alpha_2 = 18.73$ $e_f = 0.68$ $e_b = 0.93$	$\alpha_2 = 16.12$ $e_f = 0.55$ $e_b = 1.08$	$\alpha_2 = 14.71$ $e_f = 0.47$ $e_b = 1.18$

Fig. 4-4. Configurations of the various modeled spillway surface irregularities

4.4.3 Numerical modeling

We used ANSYS-Fluent Version 2020 R2 to simplify the computation of the hydraulic parameters over the irregular surfaces of the channel bottom. ANSYS-Fluent converts scalar transport equations into algebraic equations that can be solved numerically using a controlled volume approach. For the analysis, we ran the open-channel submodel in ANSYS-Fluent, which is partially based on the volume of the fluid multiphase model. The k- ϵ turbulence model, with enhanced wall treatment conditions, served as the turbulence model to better evaluate the results at the water-rock interface. For the simulations, Navier-Stokes equations were solved using averaged Reynolds numbers. In the case of stability, pressure-velocity coupling was treated using the widely used COUPLED algorithm. The results were extracted using CFD-Post, a post-processing tool that facilitates the visualization and analysis of CFD data (Ansys Inc. 2009). Table 4-2 presents the model input data for our

2D fluid flow modeling. We applied a $3 \text{ m}\cdot\text{s}^{-1}$ velocity–inlet boundary condition; this value was defined on the basis of a sensitivity analysis. In open channels, the upstream velocity–inlet boundary conditions defined the flow velocity and relevant scalar characteristics of the flow at the flow inlet. At the outflow zone, we specified a pressure–outlet boundary condition. We assumed a no-slip boundary condition at the water–rock interface (Fig. 4-3). The starting point for the simulation calculations was the water surface at the model’s entrance (inlet). Atmospheric pressure and a water depth of 2 m were also set in the model. We investigated grid independence to verify the accuracy of our findings. The outcomes of this evaluation are presented in Table 4-3, and the examination was conducted on the final irregularity, for which we also evaluated the maximum total pressure and water depth. Our grid convergence study determined that the ideal mesh size for our purposes was 10 cm.

Table 4-2. Input parameters used in the computational fluid dynamics (CFD) modeling

Parameters	Value	Description
Initial flow depth	2 m	See point 3 in Fig. 4-4
Initial flow velocity	$3 \text{ m}\cdot\text{s}^{-1}$	See point 1 in Fig. 4-4
Inlet boundary condition	–	Velocity inlet (point 1 in Fig. 4-3)
Outlet boundary condition	–	Pressure outlet (point 4 in Fig. 4-3)
Unlined spillway length	50 m	–
No. of irregularities	32	–
Irregularity height (h)	10, 15, 20, 25, 30 cm	
Irregularity angle (α)	$12^\circ, 19^\circ, 26^\circ, 33^\circ, 40^\circ$	
Channel slope	5°	–

Table 4-3. Grid independence study at the last irregularity

Boundary conditions	Structural schemes				
	20	15	10	5	1
Maximum size of the grid cell (cm)	20	15	10	5	1
Water depth (cm)	82.1	73.3	68.9	67.9	68.1
Maximum total pressure (kPa)	52.63	60.16	63.18	63.6	63.52

4.5 RESULTS AND MODIFICATION OF THE USPD EQUATION

We first examined the effects of surface irregularities on various hydraulic parameters, including velocity, velocity head, pressure head, and position head. To do so, we analyzed 25 irregularity 2D configurations and 4 unique 2D configurations of unlined spillway slope. To examine the effects of irregularities on hydraulic parameters, we assessed each parameter independently. The following subsections detail our findings. We conducted separate analyses of the maximum velocity, average velocity, maximum velocity head, average velocity head, pressure head, and position head. One of our objectives was to observe the differences in energy and, subsequently, the USPD when the average and maximum velocities were considered separately. From Fig. 4-5 and Equations (4-5) – (4-7), the summation of position head and pressure head remains constant, irrespective of the variation in the location of the analysis point within the water depth. Ultimately, in examining the impact of irregularities on position head and pressure head, our analysis focused on their summation rather than analyzing each parameter individually.

In hydraulics, the hydraulic head refers to the sum of the velocity head (H_V), pressure head (H_P), and position head (Z). The relationship among (H_V), (H_P), and (Z) is described by Equations (4-5) – (4-7), respectively.

$$E = H_V + H_P + Z, \quad (4-5)$$

$$H_V = \frac{1}{2g} v^2, \quad (4-6)$$

$$H_P = d, \quad (4-7)$$

where g is the gravitational acceleration, d is the water depth, and v is the local flow velocity.

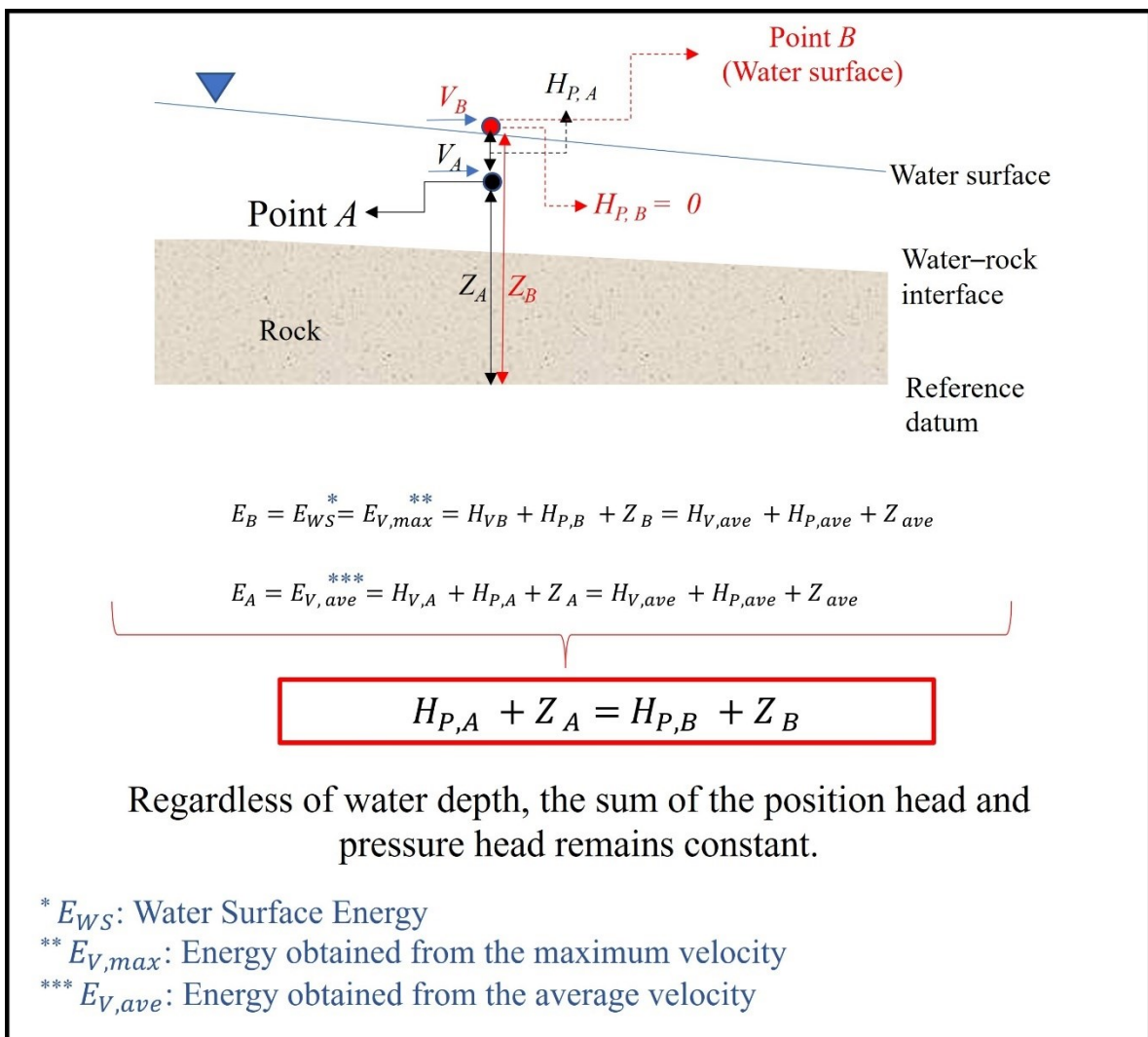


Fig. 4-5. Calculation of energy at the water surface (Point B) and location of the average velocity (Point A) measurement

4.5.1 Effects of irregularities on maximum and average velocities

To estimate the maximum velocity profile, we analyzed 11 vertical cross sections along the spillway by calculating each section's maximum velocity and water depth. Maximum velocity decreased as irregularity angle (α_1) and irregularity height (h) increased (Fig. 4-6). The effect of height on flow velocity was greater than the effect of α_1 ; for instance, when α_1 was held constant ($\alpha_1 = 12$), maximum velocity decreased from approximately $11.5 \text{ m}\cdot\text{s}^{-1}$ at $h = 10 \text{ cm}$ to approximately $8 \text{ m}\cdot\text{s}^{-1}$ at $h = 40 \text{ cm}$. When height was held constant (at 10 cm), changes in α_1 did not necessarily reduce maximum velocity. For example, maximum velocity was approximately $11.5 \text{ m}\cdot\text{s}^{-1}$ for $\alpha_1 = 12$ and approximately $9 \text{ m}\cdot\text{s}^{-1}$ for $\alpha_1 = 40$. Interestingly, the changes in α_1 had no significant effect on the maximum velocity at higher irregularity heights (h), whereas irregularity height produced a greater impact. To estimate the average velocity along the spillway, we applied the identical approach used for our analysis of maximum velocity. To avoid redundancy and minimize the number of figures, we excluded average velocity from this section; The impact of irregularities on velocity heads aligns with the effects observed in velocity profiles, and this relationship is explored in Section 3.3, illustrating the relationship between irregularities and velocity heads.

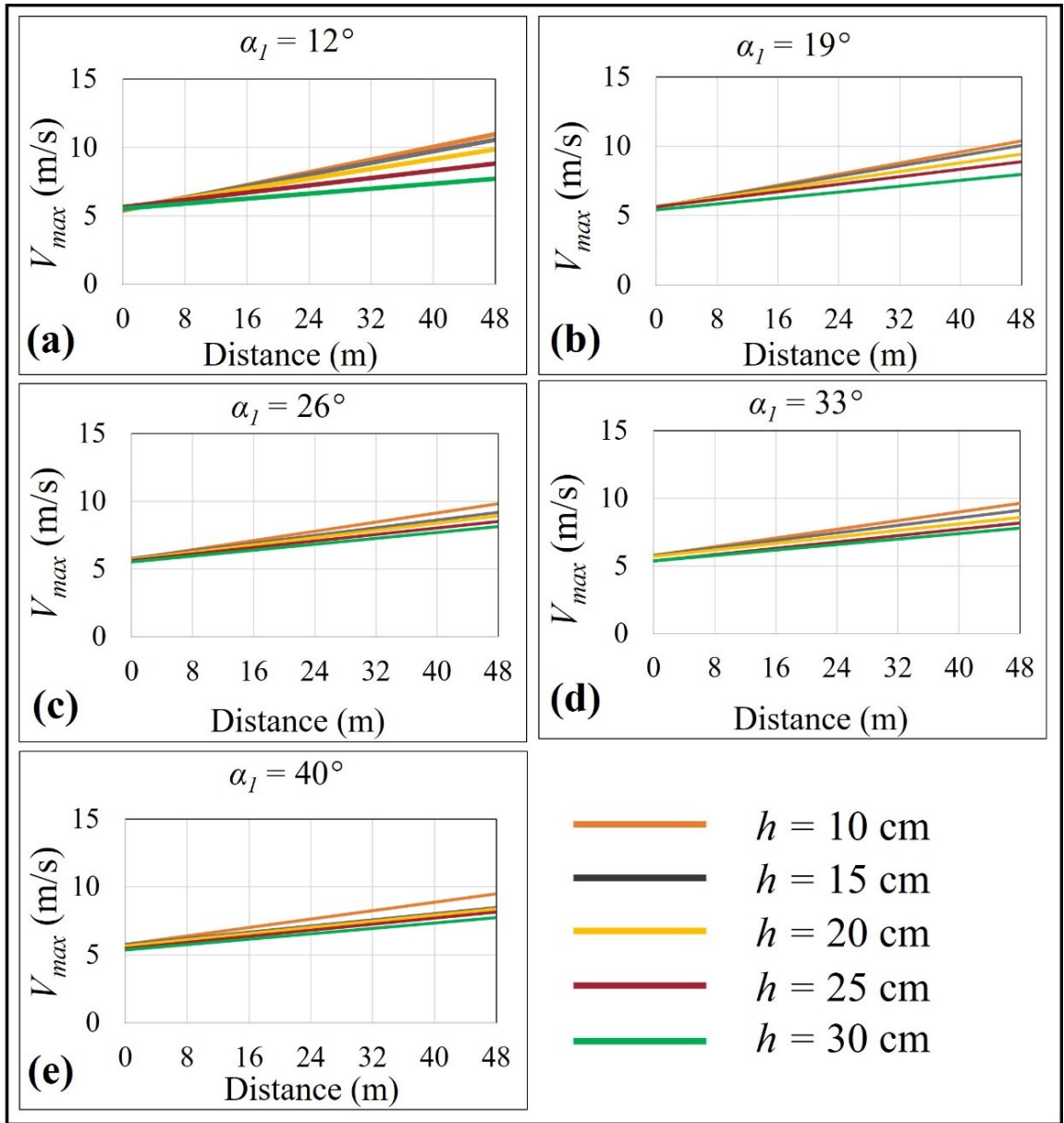


Fig. 4-6. Maximum velocity profiles of flow along the unlined spillway

4.5.2 Effects of irregularities on maximum velocity head ($H_{v, \max}$)

The maximum velocity head is a vital parameter in hydraulic studies. Equation (4-6) served to compute the maximum velocity head, and the related graphs present the numerical simulation results (Fig. 4-7). The effects of irregularities on the maximum velocity head were similar to those illustrating their effect on maximum velocity (Fig. 4-6).

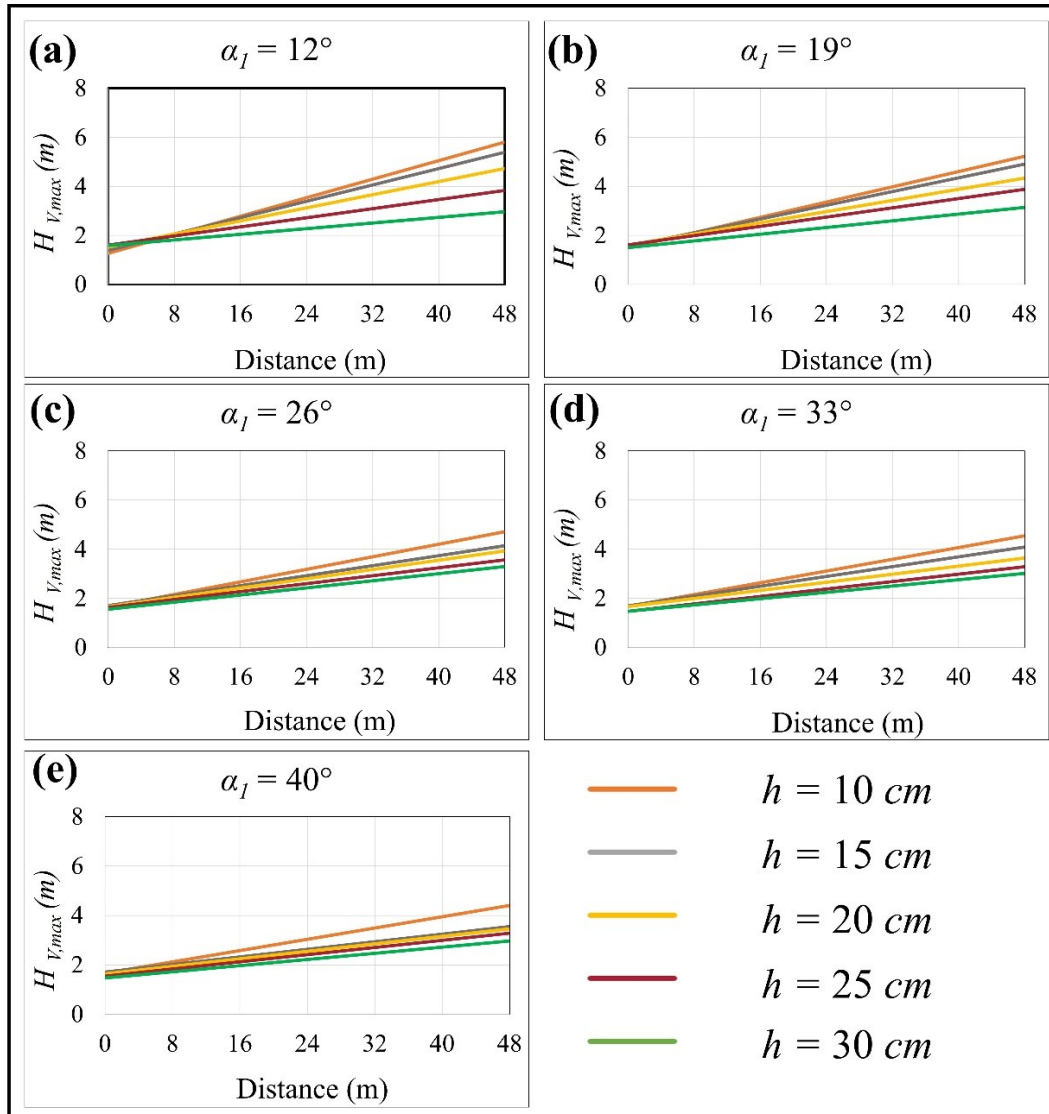


Fig. 4-7. Maximum velocity head profiles of flow along the unlined spillway

4.5.3 Effects of irregularities on average velocity head ($H_{V, ave}$)

The average velocity head was determined on the basis of the average water flow velocity, and Fig. 4-8 displays $H_{V, ave}$ in nonlinear overflows. Comparing Figs. 4-7 and 4-8, we observe that the $H_{V, ave}$ values are approximately 65% of those of $H_{V, max}$. Moreover, as α_1 increases, the impact of h on $H_{V, ave}$ decreases (Fig. 4-8).

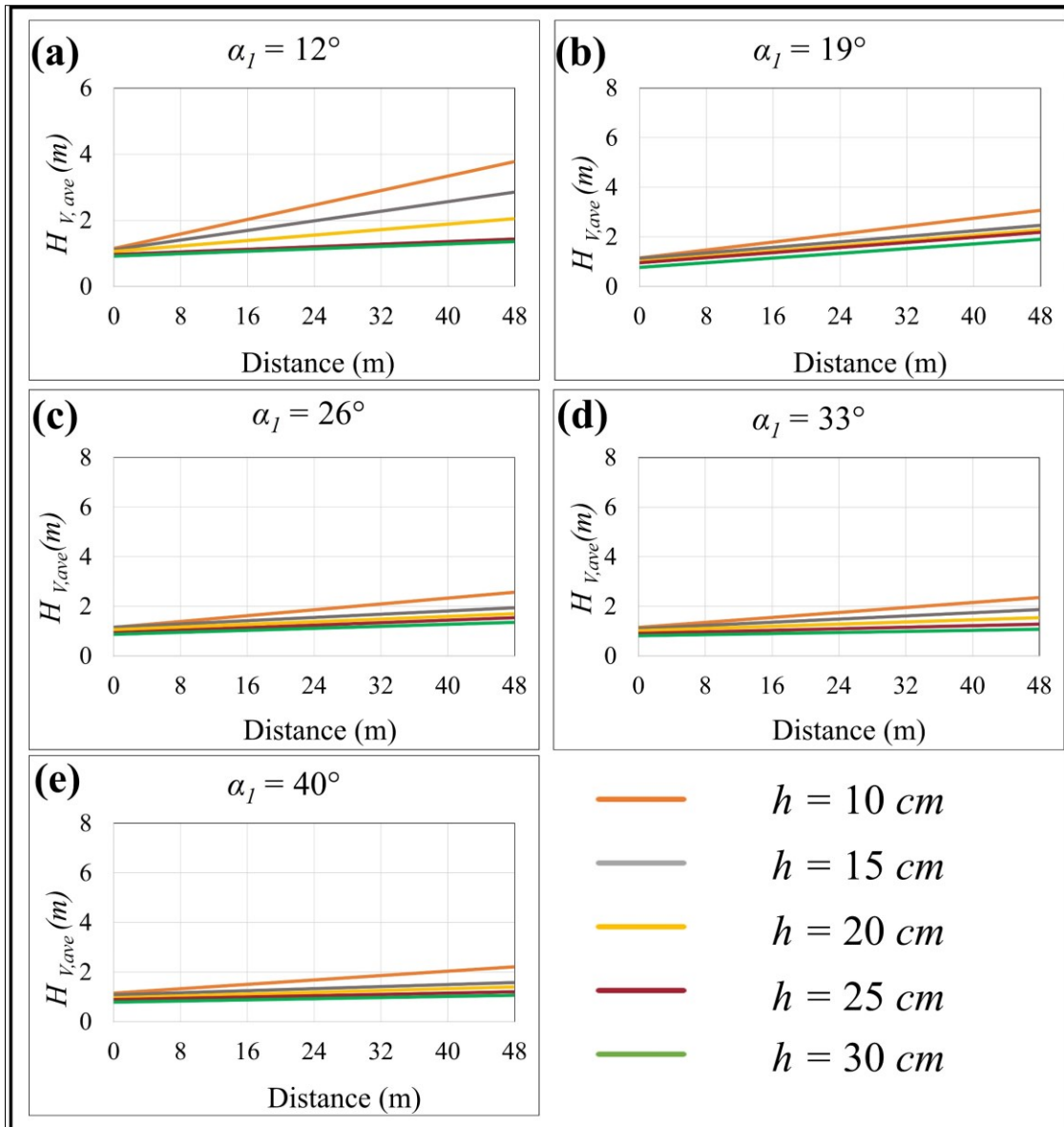


Fig. 4-8. Average velocity head profiles of the flow along the unlined spillway

4.5.4 Effects of irregularities on pressure head and position head ($H_p + Z$)

We then investigated the effects of rock surface irregularities on the hydraulic parameters of the pressure head and elevation head. At a given distance x , the sum of pressure head and elevation head remained constant regardless of irregularity height (see Fig. 4-5). Moreover, the $(H_p + Z)$ graphs in Fig. 4-9 overlapped, indicating an independence from rock surface irregularities and an effect of the distance parameter, which decreases upstream to downstream.

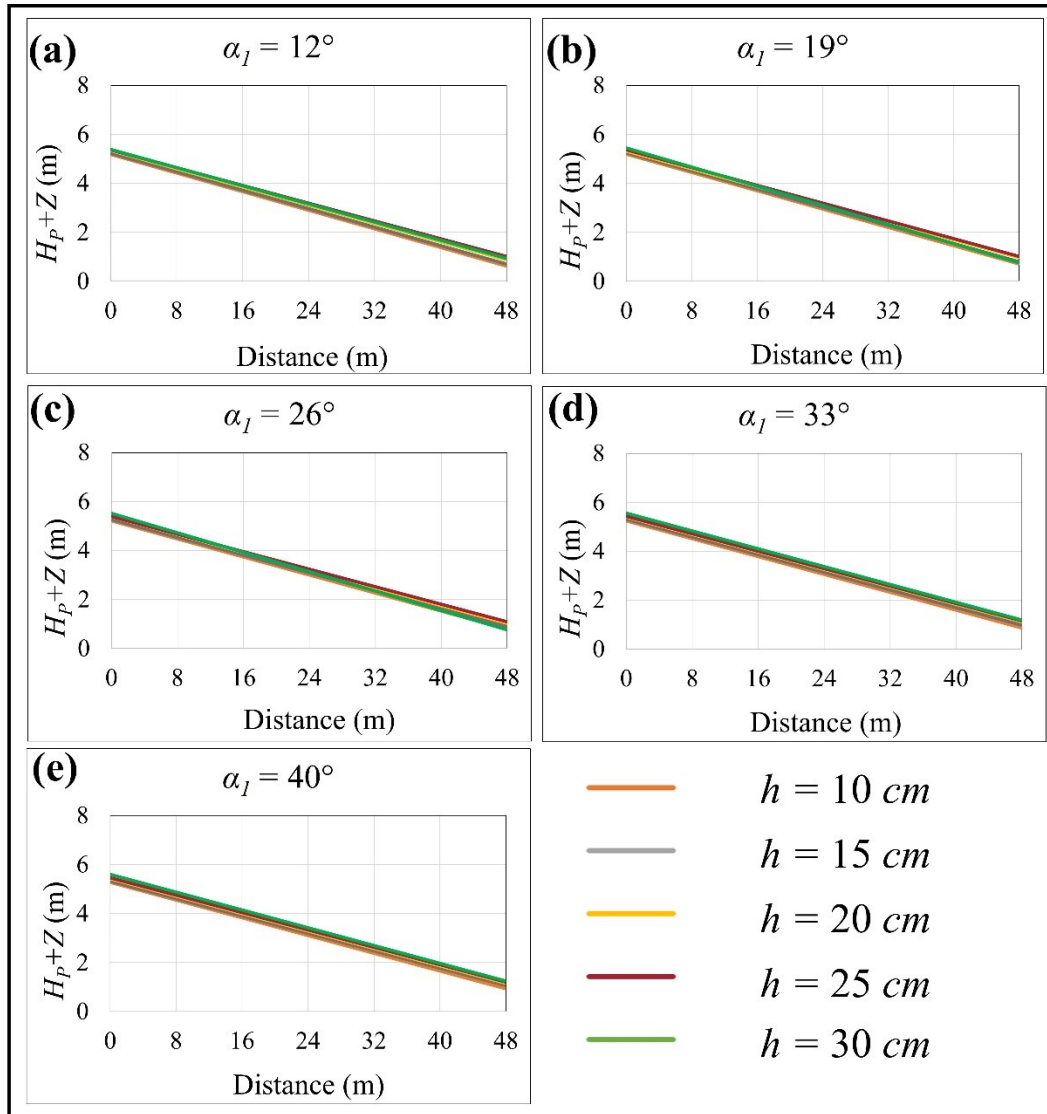


Fig. 4-9. Profiles of the (H_p+Z) along the unlined spillway

4.5.5 Sequential approach for modifying the USPD: A stepwise approach

4.5.5.1 Development of $H_{v, \max}$, $H_{v, \text{ave}}$, and (H_p+Z) equation as functions of α_1 , h , and x , respectively

As stated earlier, we determined $H_{v, \max}$ using maximum velocity.

$$c_{\alpha_1, h} = \frac{H_{v, \max} - H_{vi, \max}}{x}, \quad (4-8)$$

where Equation (4-8) represents the angle coefficient of each graph in Fig. 4-7, with a $c_{\alpha_1, h}$ value for each configuration. Table 4-4 provides the corresponding $c_{\alpha_1, h}$ values for each configuration. $H_{vi, \max}$ represents the maximum velocity at the starting point, which can be calculated using Equation (4-6) with the initial velocity at that point.

Table 4-4. Angle factors of the HV, max graphs

	$\alpha_1 = 12^\circ$	$\alpha_1 = 19^\circ$	$\alpha_1 = 26^\circ$	$\alpha_1 = 33^\circ$	$\alpha_1 = 40^\circ$
h = 0.1 m	0.0944	0.0777	0.064	0.0599	0.0571
h = 0.15 m	0.0833	0.0698	0.051	0.0499	0.0384
h = 0.2 m	0.0667	0.0569	0.0472	0.0412	0.0379
h = 0.25 m	0.0463	0.0541	0.0404	0.0379	0.0363
h = 0.3 m	0.0286	0.0473	0.0364	0.0322	0.0312

We used our results (Table 4-4) to plot the best-fit curves (and the associated equations) for $c_{\alpha_1, h}$ against irregularity height (h). The equations are equivalent to Equation (4-9).

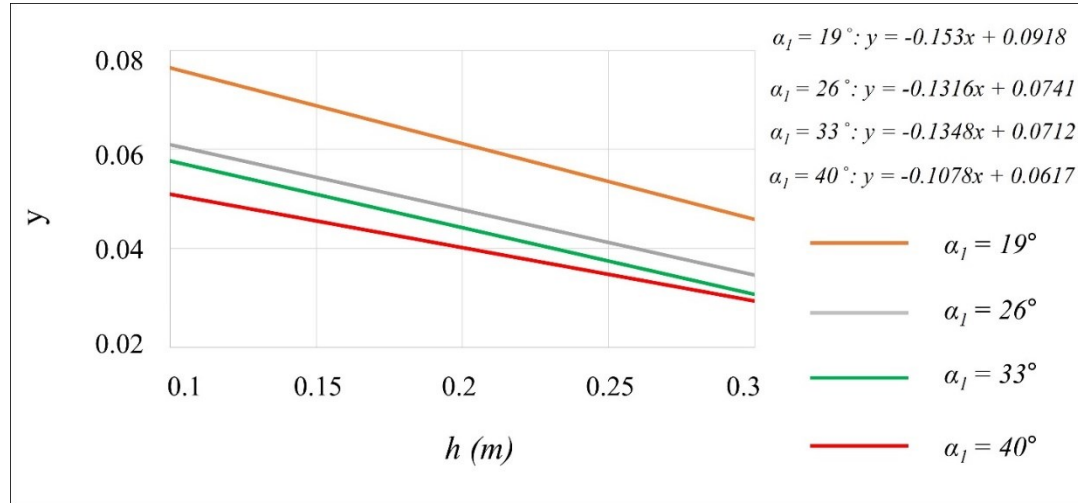


Fig. 4-10. Relationship between $c_{\alpha_1, h}$ and irregularity height (h)

The angle coefficients of the graphs depicted in Fig. 4-10 were nearly equal and graphs are almost parallel. Therefore, we calculated the average angle coefficient (a_{ave}) for the graphs and developed new equations for $c_{\alpha_1, h}$ related to the average value (a_{ave}). Following the substitution of the average value, we determined a corresponding set of $b_{\alpha_1, n}$ values (Table 4-5).

$$y = c_{\alpha_1, h} = \left(\frac{H_{v, max} - H_{vi, max}}{x} \right)_{\alpha_1} = a_{\alpha_1} h + b_{\alpha_1} \quad (4-9)$$

Table 4-5. New y-intercepts produced on the basis of a_{ave}

Tan α_1	0.34432	0.48773	0.64940	0.8391
b_{α_1}	0.0918	0.0741	0.0712	0.0617
$b_{\alpha_1, n}$ (produced using $a_{ave} = 0.1318$)	0.08968	0.07412	0.0709	0.0641

Differences among the graphs in Fig. 4-10 relate to the y-intercept ($b_{\alpha_1, n}$) that is altered by changing α_1 . Therefore, we aimed to determine the correlation between $b_{\alpha_1, n}$ and $\tan(\alpha_1)$ using Fig. 4-11 [Equation (4-10)]. After obtaining Equation (4-10) from the results in Fig. 4-11, using the Equation (4-10) and the value of a_{ave} ($a_{ave} = 0.1318$), we applied them in Equation (4-9) to derive Equation (4-11). Equation (4-11) represents $H_{vi, max}$,

and it is a function of irregularity height (h), irregularity angle (α_1), and the distance from the upstream (x). Fig. 4-12 depicts the steps followed in developing Equation (4-11).

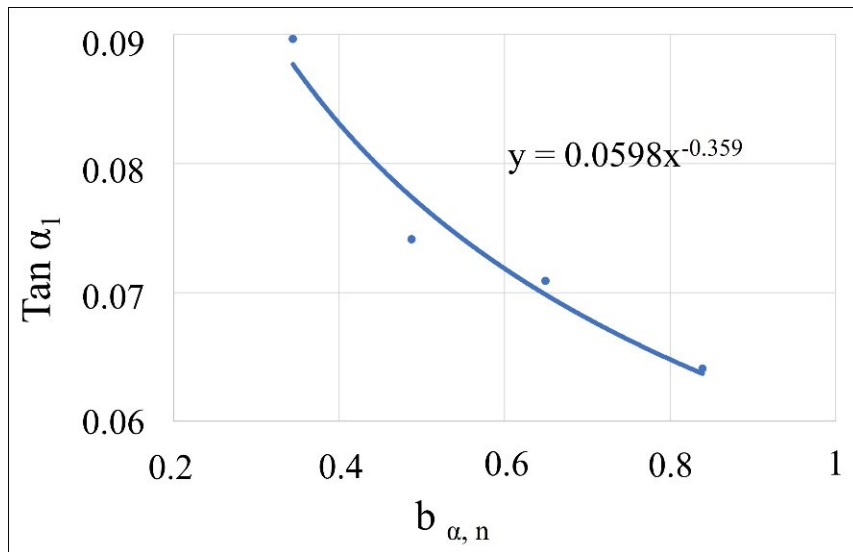


Fig. 4-11. Correlation between $\tan(\alpha_1)$ and the new y-intercepts of the angle factor graphs

$$b_{\alpha_1, n} = 0,0365 \tan \alpha_1^{-0,526}, \text{ and} \quad (4-10)$$

$$H_{v, \max} = \left(\frac{0,0365}{\sqrt{\tan \alpha_1}} - 0,1318h \right) x + H_{vi, \max} \cdot \quad (4-11)$$

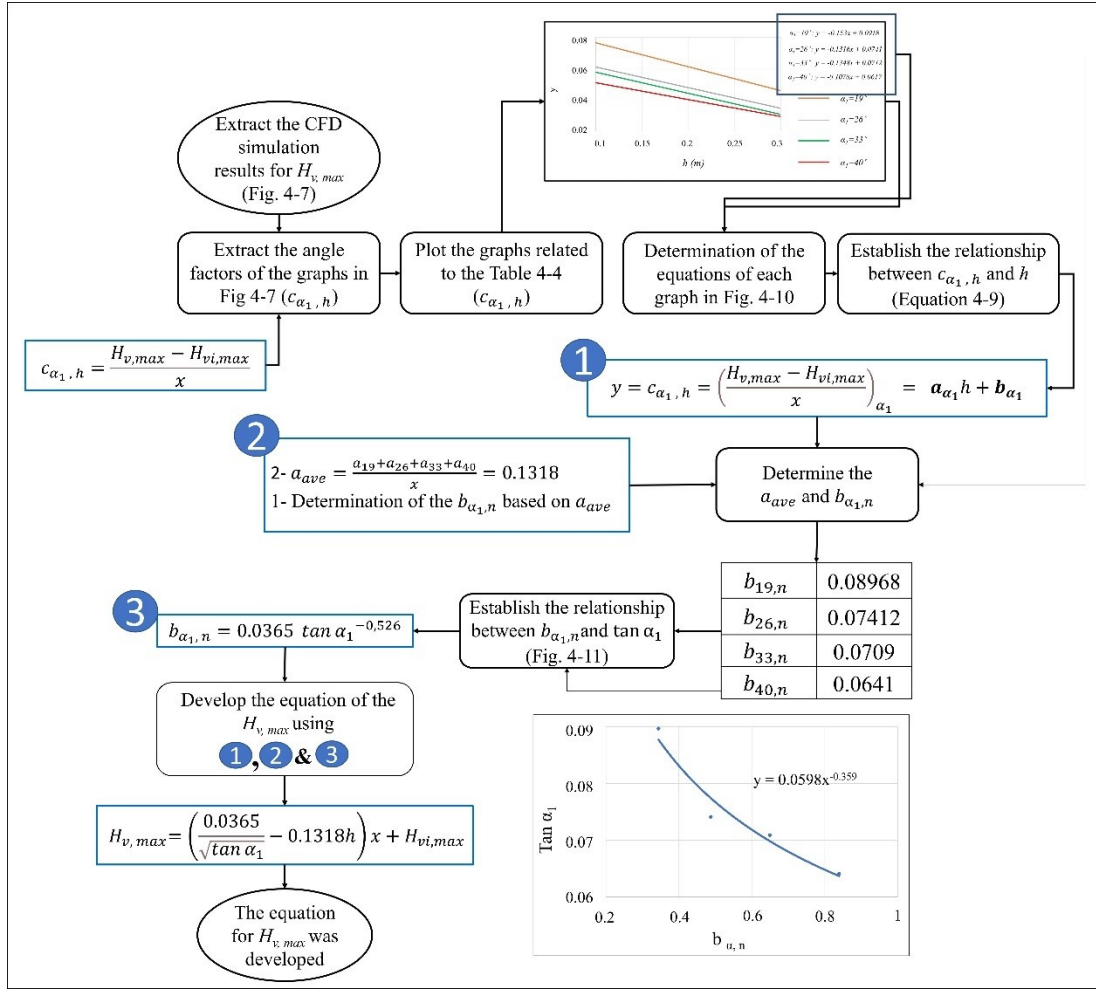


Fig. 4-12. Methodology for modifying the USPD on the basis of irregularity height and angle (α_1 and h)

We applied the same approach to derive the $H_{v, ave}$ equation, which relied on the results obtained from the Ansys-Fluent software. The resulting equation, denoted by Equation (4-12), expresses $H_{v, ave}$ as a function of α_1 , h , and x . As discussed above, Equation (4-13) ($H_p + Z$) is independent of surface irregularities (α_1 and h) because the impact of irregularities on ($H_p + Z$) can be neglected. Referring to Fig. 4-9, ($H_p + Z$) as a function of x is illustrated by Equation (4-13).

$$H_{v, ave} = \left(\frac{0.0234}{\sqrt{\tan \alpha_1}} - 0.08h \right) x + H_{vi, ave} , \text{ and} \quad (4-12)$$

$$(H_p + Z) = [-0.09 x + (H_{pi} + Z_i)] \quad (4-13)$$

4.5.5.2 Effects of the spillway slope (β) on developed equations for $H_{V, \max}$, $H_{V, \text{ave}}$, V_{\max} , V_{ave} , and $(H_P + Z)$

In the previous section, the equations for $H_{V, \max}$, $H_{V, \text{ave}}$, and $(H_V + Z)$ are regardless of the overall slope of the unlined spillway (β). To investigate further, we simulated additional models using spillway slopes (β) ranging from 2.5° to 15° while maintaining a smooth surface. We extracted the results of these simulations for $H_{V, \max}$, $H_{V, \text{ave}}$, and $(H_V + Z)$ and presented those of $H_{V, \max}$ in Fig. 4-13. Despite the differences in β , the coefficient of the angle for each graph remained the same, as depicted in Equation (4-8). However, as we had already obtained the effects of irregularities on the hydraulic parameters for $\beta = 5^\circ$, we divided the angle coefficients of the graphs in Fig. 4-13 by the angle coefficient of the normalizer, $\beta = 5^\circ$, as shown in Equation (4-14).

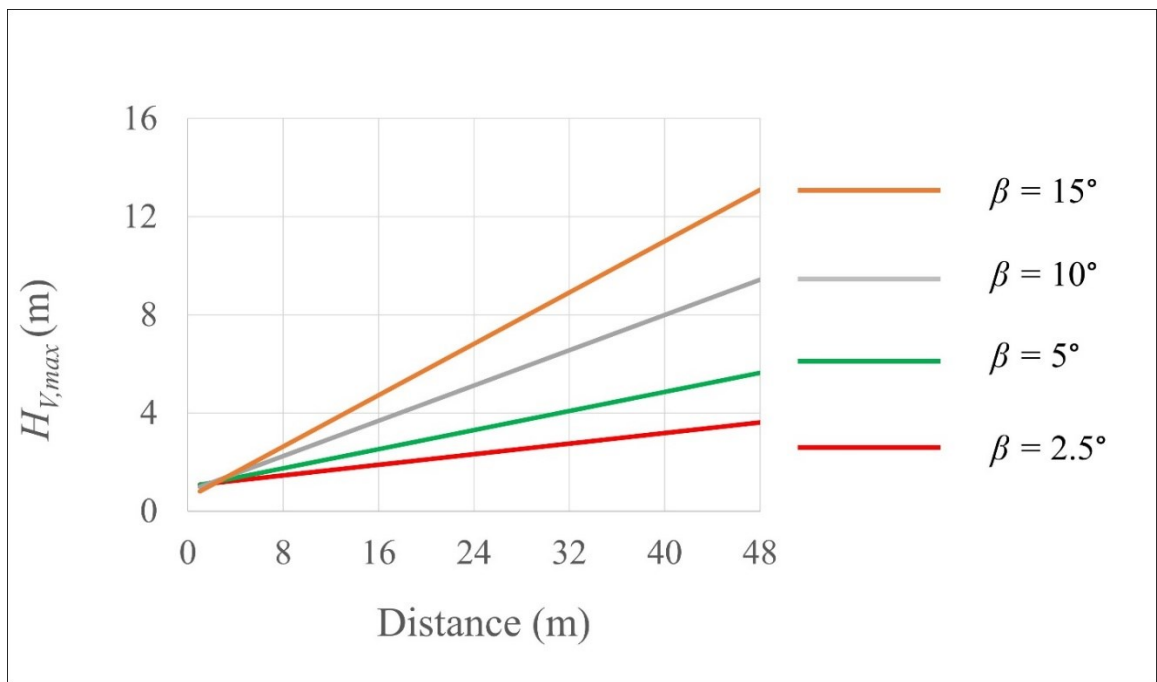


Fig. 4-13. Simulation results for $H_{V, \max}$ as a function of distance

Table 4-6 presents the coefficients of various normalized angles using the tangent function of the slope angle, β . The corresponding diagram (Fig. 4-14) has the horizontal axis representing $\tan(\beta)$ and the vertical axis representing the coefficient of the normalized angle factors obtained from the graphs in Fig. 4-13. After obtaining the graphical equation of Fig. 4-14, we equated it with Equation (4-14a), where the denominator is identical to that of Equation (4-11). By substituting the Equation (4-11) and graphical equation of Fig. 4-14 in Equation (4-14a) (see point 1 and 2 in Fig. 4-15), we obtained a new equation [Equation (4-14)] for $H_{V, \max}$, which is a function of β , α_1 , h , and x .

Table 4-6. The coefficients of various normalized angles on the basis of the tangent function of the slope angle, β

β (°)	2.5	5	10	15
$\tan \beta$	0.04366	0.08749	0.17633	0.26795
Angle factor (before normalization)	0.0538	0.097	0.18	0.261
Angle factor (after normalization)	0.5546	1	1.8557	2.6907

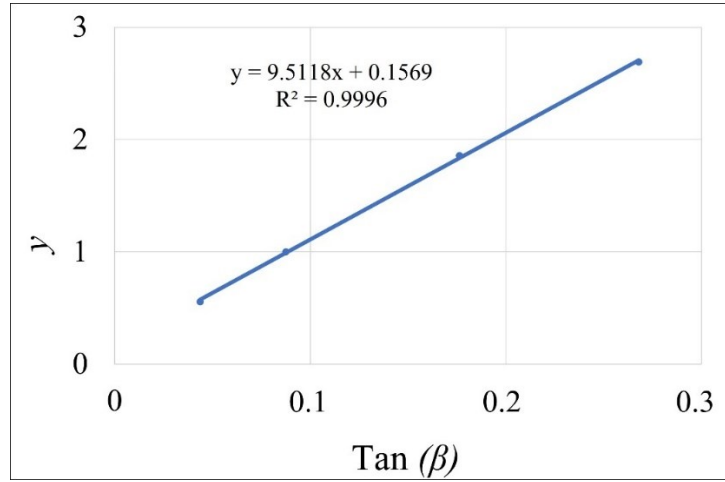


Fig. 4-14. Relationship between the coefficient of the normalized angle factors of H_V, \max and the unlined spillway slope (β)

Similarly, by applying the same technique, we could also derive new equations for (H_p+Z) and $H_{V, \text{ave}}$ as a function of β [Equations (4-15) and (4-18), respectively]. Using Equations (4-6), (4-14), and (4-15), we obtained equations for the maximum and average velocities [Equations (4-16) and (4-17), respectively] along the unlined spillway (Fig. 4-15 presents how we modified the equation).

$$y = \frac{\left(\frac{H_{v, \max} - H_{vi, \max}}{x}\right)_{\beta}}{\left(\frac{H_{v, \max} - H_{vi, \max}}{x}\right)_{\beta=5}} \quad (4-14a)$$

$$H_{v, \max} = (9.51 \tan \beta + 0.16) \left(\frac{0.0365}{\sqrt{\tan \alpha_1}} - 0.1318h \right) x + H_{vi, \max} \quad (4-14)$$

$$H_{v, \text{ave}} = (7.94 \tan \beta + 0.34) \left(\frac{0.0234}{\sqrt{\tan \alpha_1}} - 0.08h \right) x + H_{vi, \text{ave}} \quad (4-15)$$

$$V_{\max} = \sqrt{\left[(9.51 \tan \beta + 0.16) \left(\frac{0.0365}{\sqrt{\tan \alpha_1}} - 0.1318h \right) x + H_{vi, \max} \right] 2g} \quad (4-16)$$

$$V_{\text{ave}} = \sqrt{\left[(7.94 \tan \beta + 0.34) \left(\frac{0.0234}{\sqrt{\tan \alpha_1}} - 0.08h \right) x + H_{vi, \text{ave}} \right] 2g} \quad (4-17)$$

$$(H_p + Z) = (H_{p_i} + Z_i) - (\tan \beta + 0.01)x \quad (4-18)$$

*where H_{p_i} is the initial water depth and Z_i is the difference between levels of the analyzed section: $(X_2 - X_1) \cdot \sin \beta$.

$$\Delta E = (H_{v, \max} + H_p + Z)_2 - (H_{v, \max} + H_p + Z)_1 \quad (4-19)$$

$$USPD = \rho g q \frac{\Delta E}{\Delta x}$$

(4-20)

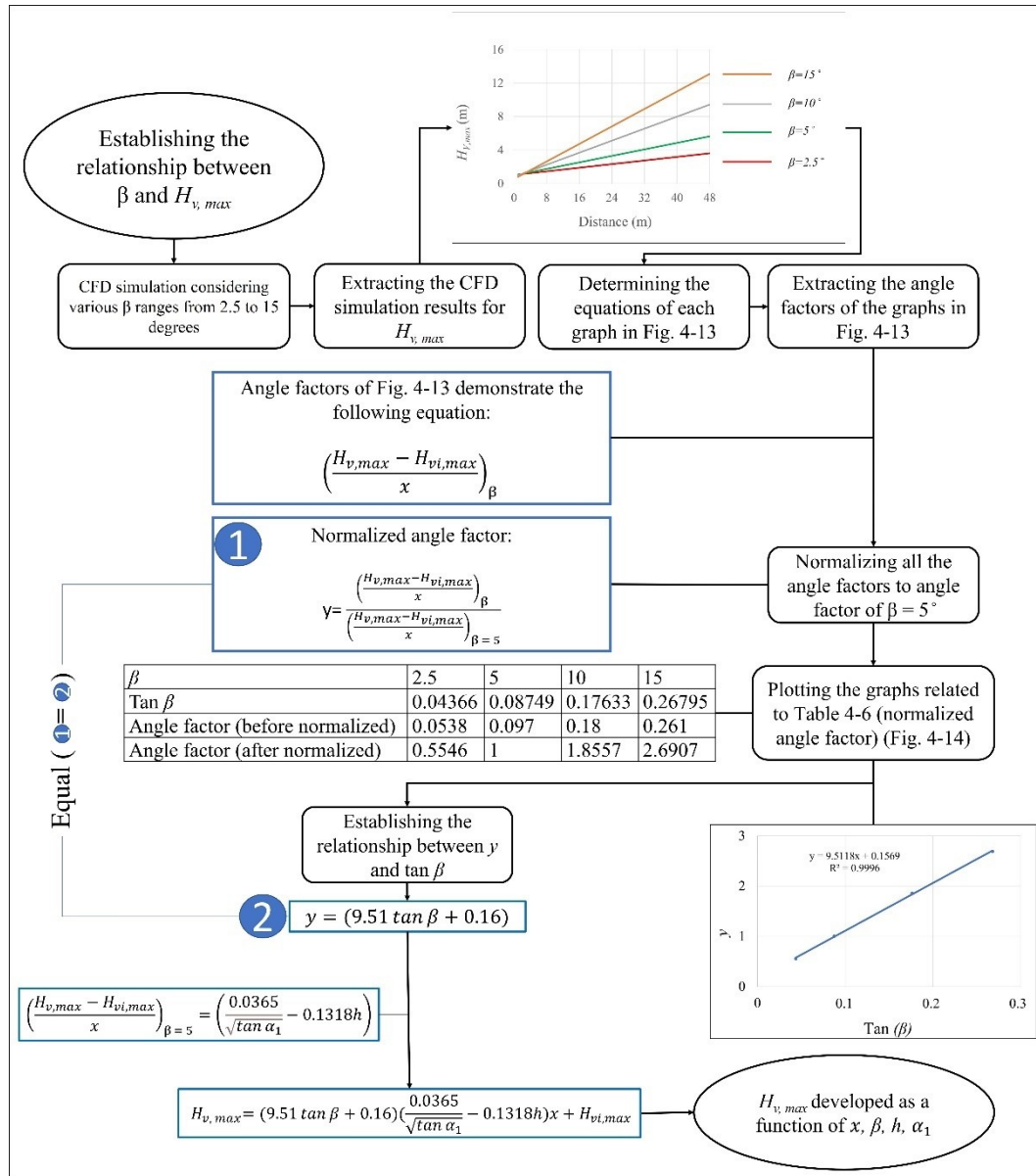


Fig. 4-15. Methodology to modify the USPD for application on an unlined spillway slope (β)

We could then derive a new equation for $H_{v, max}$ by considering spillway slope, irregularity height, and position along the spillway. The equation is a function of $\alpha_1, h,$ and x to permit a more comprehensive analysis of hydraulic parameters under various conditions. Equation (4-19) shows the energy loss from upstream to downstream, and Equation (4-20) presents our modified equation for the USPD. Notably, the abovementioned equations cannot be used with $\alpha_1 = 0^{\circ}$ because no natural rock surfaces possess an α_1 value of absolute zero.

4.6 CROSS VALIDATION, COMPARISON, AND PRACTICALITY

To verify the accuracy of the developed equations, we ran a cross-validation test using the data obtained from the ANSYS-Fluent simulations. We simulated another model in ANSYS-Fluent using the configuration $\beta = 8^\circ$, $\alpha_1 = 20^\circ$, and $h = 0.17$ m and compared the simulation results with those of the developed equation for USPD. We calculated the equation's root mean squared error (RMSE) by applying Equation (4-21). The RMSE for the total energy was 0.034 when average velocity was considered and 0.237 when maximum velocity was taken into account. The cross-validation process demonstrated a consistent match between the developed equations and simulation results. Furthermore, we validated our simulations against analytical models, specifically for smooth surfaces configurations. Ultimately, our findings indicate that this equation is capable of predicting hydraulic parameters for unlined spillways across various irregularities.

$$RMSE = \sqrt{\frac{\sum_{i=1}^n (USPD_{equation} - USPD_{ANSYS})^2}{n}} \quad (4-21)$$

We then compared these newly developed equations, which consider the effects of irregularities on the hydraulic parameters, with existing equations to predict the USPD of unlined spillways having irregularities. We used the equations to estimate the total energy in the upstream and downstream regions using a configuration of $\beta = 5^\circ$, $\alpha_1 = 20^\circ$, $h = 0.17$ m, and $L = 50$ m. This configuration closely resembles the initial 50 m of unlined spillway of the Anthony dam in Australia, considering an initial velocity of $3 \text{ m}\cdot\text{s}^{-1}$ [1]. The energy values obtained using the Pells equation did not incorporate the surface irregularities of the rock formation (Table 4-7). In contrast, our equation considers these irregularities, enabling the calculation of energy on the basis of either the maximum or average flow velocity. There is a clear disparity in the head loss between the upstream and downstream sections when comparing the Pells and our novel equations (Table 4-7). Interestingly, our method produces a slightly higher head loss. This discrepancy can be attributed to the presence of irregularities in the rock, which facilitate the transfer of energy to the rock surface, consequently leading to hydraulic erosion.

Table 4-7. Comparison of the energy results as determined using our novel equation and those of the Pells (2016) equation

	Location	Maximum	Average
$E_{\text{modified}} \text{ (m)}$	Upstream	7.66	6.06
	Downstream	4.8	2.61
$E_{\text{Pells}} \text{ (m)}$	Upstream	5.05	5.05
	Downstream	2.25	2.25

Engineers and designers can use these developed equations to predict the hydraulic parameters of unlined spillways with irregularities and optimize the design of such structures. These novel equations can help engineers better predict the hydraulic parameters (e.g., erosion and overflow) of the spillway. We also conducted simulations using heterogeneous irregularities (unlined spillway surface with various irregularity

angles and heights, i.e., surfaces with irregular irregularities) to test the practicality of our equations. Despite assuming homogeneous surface irregularities, we attempted to include various irregularities in the new model; however, the energy results for heterogeneous and homogeneous models were nearly identical (Fig. 4-16).

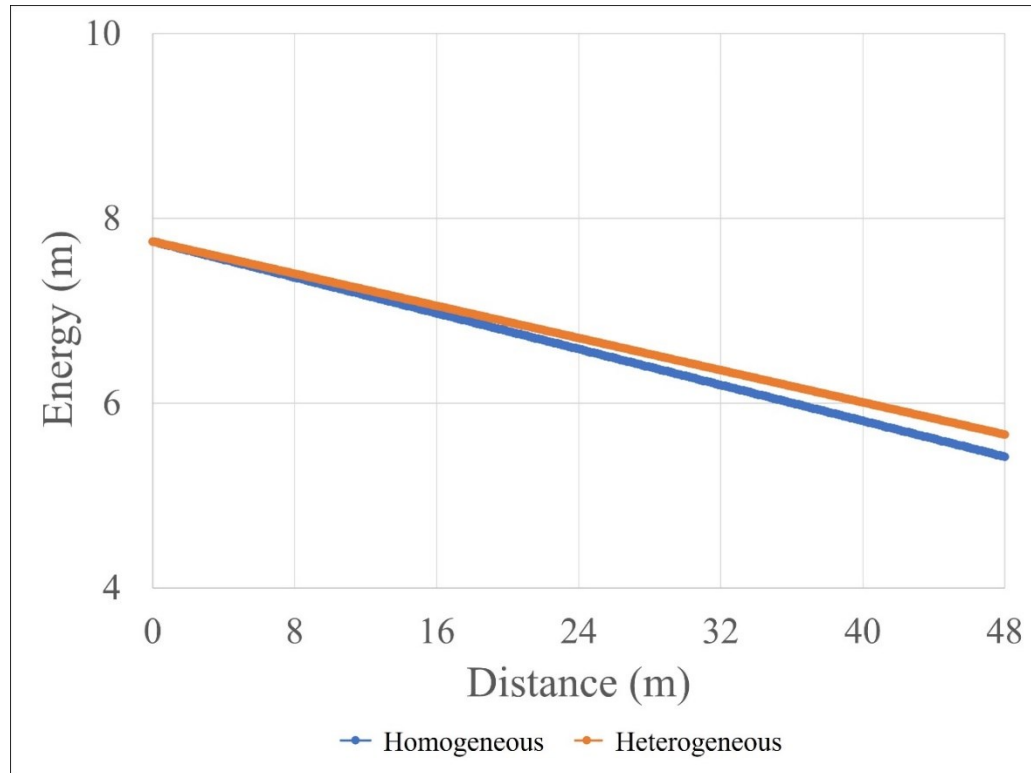


Fig. 4-16. Comparison of model outputs run using heterogeneous and homogeneous irregularities

4.7 CONCLUSIONS

We developed novel equations to predict the hydraulic parameters of unlined spillways characterized by surface irregularities. Cross validation verified the accuracy of the equations and confirmed their ability to predict the hydraulic parameters of unlined spillways having irregularities. We also demonstrated that our equations, when run compared against other existing equations in the literature, predicted the USPD of unlined spillways more accurately when considering irregularities on the rock mass surface. These novel equations account for the effects of irregularities on the hydraulic parameters, an effect neglected by other existing equations. We found that irregularities along the spillway surface affect various hydraulic parameters, and changes in irregularity height have a marked effect on hydraulic parameters. In the design of hydraulic structures, particularly unlined spillways, a pivotal aspect is delineating the erosive and resistive elements. The fundamental parameter in characterizing the erosive aspect is defining the unit stream power dissipation (USPD). It is advisable for designers to employ the developed equations in this thesis to determine the USPD, enabling a subsequent comparison with the resistive part of the phenomenon. The utilization of these equations contributes to heightened accuracy, as they take into account the geometrical parameters of the rock surface,

including irregularities. Consequently, by considering a more comprehensive set of parameters, these equations enhance precision and optimize the overall design process. Future research should address the 2D nature of the simulations, steady-state simulations, and the effect of geometric characteristics of the spillway.

CHAPTER 5

DISCUSSION AND CONCLUSION

5.1 DISCUSSION

The study of hydraulic erodibility prediction has traversed academic landscapes since the early 1930s, yielding a diverse array of methodologies encompassing theoretical, semi-theoretical, numerical, and semi-analytical approaches. This thesis comprises three main objectives: firstly, a comprehensive review of methodologies assessing hydraulic erodibility downstream of dam spillways to identify their advantages and drawbacks; secondly, an investigation into how surface irregularities affect hydraulic parameters in unlined dam spillways; and lastly, a modification of the unit stream power dissipation (USPD) equation for unlined spillways by incorporating geometric parameters and surface irregularities to improve predictions of energy dissipation in water flow over these spillways. This work progresses from reviewing existing methods, understanding the impact of irregularities, to refining the USPD equation for more accurate results in practical engineering applications.

In the assessment of existing methodologies aimed at evaluating hydraulic erodibility in dam spillways, a diverse array of theoretical, semi-theoretical, numerical, and semi-analytical approaches has been identified. The predominant focus of these methodologies has been the prediction of erodibility across a spectrum of contexts, encompassing substrates like soils, granular materials, and plunging jets. Semi-theoretical methods, often reliant on erodibility indices such as the Kirsten index, offer insights into the geomechanical facets of erosion processes. Conversely, Bollaert's Comprehensive Scour Method (CSM) integrates dynamic pressure, fracture toughness, and stress intensity as contributing factors to approximate the depth of scour. In a parallel vein, Dasgupta's numerical approach melds 2D UDEC modeling with 3D Computational Fluid Dynamics (CFD) to furnish a more comprehensive viewpoint. Nonetheless, persistent challenges arise due to limitations in available data and disparities between projected and observed outcomes. These methodologies are not exempt from limitations: semi-theoretical methods grapple with confined applicability, well-established approaches prove insufficient within diverse scenarios, the role of spillway geometry, notably surface roughness, remains insufficiently explored, and the intricate interplay between various forces and rock properties presents a complex enigma. The combination of geomechanical, geometrical and hydraulic knowledge requires a comprehensive method that can bridge gaps effectively, possibly benefiting from emerging technologies like Computational Fluid Dynamics (CFD). In summation, the trajectory of erodibility prediction is undergoing a transformative phase characterized by the convergence of geomechanical, geometrical, and hydraulic considerations, poised to yield more resilient methodologies amenable to the intricate realities of erodibility phenomena in hydraulic systems. Moreover, these methodologies have also ventured into the domain of addressing the erodibility of rock formations within the intricate context of unlined spillways – a domain that

necessitates a nuanced understanding of geomechanical, geometrical, and hydraulic dynamics. Table 5-1 illustrates the advantages and disadvantages of various approaches.

Table 5-1. Advantages and disadvantages of the various approaches.

Approaches		Advantages	Disadvantages
Semi-theoretical	Kirsten	Easy to use Quick	The committed error of these methods is high Lack of consideration of effective geomechanical parameters Lack of estimation of the scour depth and the approximate location of erosion
	Annandale		
	Van Schalkwyk		
	RMEI	Easy to use Quick	The committed error of these methods is high Lack of consideration of effective geomechanical parameters Lack of estimation of the scour depth and the approximate location of erosion
eGSI	Consideration of various geometries Consideration of representative hydraulic erosive parameter		
Semi-analytical	CSM	Estimation of the ultimate scour depth and the approximate location of erosion Has a physical, experimental, and mechanical background Consideration of various geometries Consideration of some geomechanical parameters	Confusing and ambiguous Requires in situ tests Practical for plunge pools Consideration of various hydraulic erosive parameters
Numerical		Estimation of the ultimate scour depth and the approximate location of erosion Good accuracy Easy to extract the results of various parameters	Estimation of the ultimate scour depth and the approximate location of erosion Lack of unit software to consider hydraulic and geomechanical aspects at the same time Requires a highly skilled workforce Long processing time

Our second study effectively demonstrated the application of ANSYS-Fluent software and 2D steady-state simulations within computational fluid dynamics to investigate the influence of unlined spillway surface irregularities, specifically their height and angle, on hydraulic parameters. This investigation revolved around varying irregularity height and angle to assess their impact on key hydraulic factors including flow velocity, dynamic pressure, static pressure, total pressure, shear stress, velocity head, pressure head, elevation, energy, and energy loss. The findings unveiled several observations: firstly, irregularities affected hydraulic parameters, a consideration absent in prevailing methodologies for establishing hydraulic erosive parameters. Secondly, altering the angle did not consistently lead to a linear velocity decrease at a constant height (α_1), often resulting in negligible alterations. Thirdly, while angle (α_1) changes minimally influenced maximum flow velocity at greater heights, height adjustments significantly impacted it. Fourthly, variations in irregularity height induced substantial shifts in total pressure along the channel bottom, whereas angle adjustments had more limited effects. Additionally, the total pressure, assessed using maximum dynamic pressure, saw a 2.5–3 times increase relative to channel bottom pressure. Furthermore, a significant energy loss of approximately 70% was observed along the water-rock interface profile from upstream to downstream. Notably, the energy demonstrated an approximately 30% increase upstream and a substantial 250%–350% increase downstream along this interface when compared to the energy at the water surface. Moreover, higher flow velocity correlated with elevated energy and reduced energy loss. However, it is crucial to acknowledge certain study limitations, including the

confinement to a 2D context and a focus on steady-state simulations rather than transient ones. Furthermore, the geometric characteristics of the unlined spillway, including channel shape, channel length, water depth, and channel width, were not considered in the present study. This underscores the necessity for future research to address these constraints and achieve a more comprehensive understanding of the subject matter.

The study's third phase was dedicated to the modification of the unit stream power dissipation (USPD) equation to incorporate the combined impact of both rock surface irregularities and the geometry of unlined spillways. This approach encompassed adapting the equation to capture the mutual influences of irregularities and the geometric attributes inherent to unlined spillways. Building upon the outcomes of phase two and further simulations, we refined the USPD equation to incorporate these variables. To evaluate the accuracy of the proposed equation, a cross-validation process was conducted using ANSYS-Fluent simulations. This entailed a comparison between outcomes from a distinct model, featuring parameters $\beta = 8^\circ$, $\alpha_l = 20^\circ$, and $h = 0.17$ m, and results derived from the modified USPD equation. Accuracy assessment utilized the root mean squared error (RMSE), yielding values of 0.034 and 0.237 for average and maximum velocity scenarios. This validation substantiated the precision of the adapted equations in predicting hydraulic parameters within irregularity-affected unlined spillways. A comparison with existing equations for predicting USPD demonstrated the novel equations' capacity to accommodate the effects of irregularities. Furthermore, these equations were applied to estimate total energy in scenarios resembling the initial segment of the Anthony dam's unlined spillway, revealing disparities between the newly proposed and conventional equations. The adjusted equations effectively accounted for irregularities, shedding light on their role in energy transfer and hydraulic erosion. In conclusion, a set of equations for velocity, dynamic pressure, velocity head, energy, and USPD were proposed as a result of this phase. In the designing of hydraulic structures, especially unlined spillways, a crucial consideration involves distinguishing between erosive and resistive factors. The key parameter for characterizing the erosive component is the definition of unit stream power dissipation (USPD). Designers are encouraged to utilize the equations developed in this thesis to calculate the USPD, allowing for a subsequent comparison with the resistive aspect of the phenomenon. The application of these equations enhances accuracy by incorporating the geometric parameters of the rock surface, including irregularities. As a result, with a more inclusive set of parameters considered, these equations improve precision and streamline the overall design process. Future research should confront the constraints posed by 2D simulations and steady-state conditions to achieve a more comprehensive grasp of the subject [149].

5.2 CONCLUSION

In conclusion, this research offers a comprehensive summary of the key findings derived from the analysis of scientific papers in Chapters 2 through 4. These findings significantly deepen our understanding of the research topic. The study commences by thoroughly reviewing existing approaches to hydraulic erodibility,

pinpointing their limitations. It then systematically categorizes crucial parameters, focusing on how geometric characteristics of the rock surface and unlined spillways impact hydraulic parameters. Leveraging these insights, the study refines the hydraulic erosive equation, aligning it with observed relationships. Additionally, the study provides suggestions for future research, highlighting areas that warrant further exploration. These suggestions aim to inspire and guide future researchers in advancing the field and addressing existing knowledge gaps.

The findings emphasize the importance of conducting detailed evaluations of individual geomechanical parameters in semi-analytical methods and the necessity for a unique approach to determine the erosive parameter of water. It is evident that the existing semi-analytical methods developed for plunge pool cases may not be directly applicable to spillway cases, highlighting the significance of considering site-specific factors. In the developed equations of this study, the inputs predominantly rely on parameters commonly used in the design and geometry of unlined spillways. Site-specific parameters are not necessary for these equations. To define the geometric parameters of irregularities, readily available data such as blasting patterns can be utilized. This study serves as an essential establishment in the domain of hydraulic erodibility. This investigation constitutes a seminal contribution to the domain of hydraulic erodibility, offering engineers distinctive methodologies for appraising the hydraulic facets of erodibility, particularly addressing the erosive agent in open channels and unlined spillways. In the evolution of scientific understanding, significant shifts necessitate collective engagement. The present study lays the cornerstone for further advancements, with the foresight that forthcoming research initiatives will iteratively amplify and refine the preliminary foundational insights expounded within this scholarly work.

Using ANSYS-Fluent software and 2D steady-state simulations, this study investigated the influence of surface irregularities on hydraulic parameters in unlined spillways. The results revealed that irregularities affect hydraulic parameters, including flow velocity, dynamic pressure, static pressure, total pressure, and energy. For the quantified outcomes, kindly refer to the analysis presented in the Discussion (section 5-1). The analysis offered insights into the correlation between irregularity height and angle, illuminating the influence of geometrical parameters of both the unlined spillway and rock surface on hydraulic parameters.

While previous studies have focused on relative roughness in hydraulic engineering, it is important to note that this study specifically addresses 2D irregularities. The distinguishing aspect lies in the scale of irregularities examined, ranging from centimeters to even meters, as opposed to the millimeter-scale typically associated with roughness. Acknowledging the limitations of the study, such as its 2D nature, steady-state simulations, and the absence of geometric characteristics of the spillway, future research should aim to overcome these limitations. This can be achieved through investigating transient behavior, utilizing 3D modeling techniques, and considering the influence of spillway geometry. These aspects lay beyond the scope of this thesis, given the constraints of time. However, their relevance prompts their inclusion as potential directions for future research endeavors.

One significant outcome of this research is the development of novel equations for predicting hydraulic parameters, particularly the unit stream power dissipation (USPD), in unlined spillways with 2D surface irregularities. The modified equations offer engineers and designers a valuable tool for optimizing the design and maintenance of unlined spillways considering more geometrical parameters comparing to the existing equations. It is noteworthy that comparing computational results for irregular surfaces with real-world irregularities poses challenges, primarily stemming from the commonly disregarded rock surface irregularities in analytical evaluations. This oversight impedes direct comparisons. Our confidence in the findings is fortified through the comprehensive cross-validation of computational models, involving the comparison of smooth surfaces in both scenarios. This methodical assessment unveils disparities, signifying the influence of irregularities on hydraulic parameters. This study represents a foundational contribution to the field of hydraulic erodibility, guiding engineers toward distinctive methodologies to assess the hydraulic aspect of erodibility, particularly the erosive agent in open channels and unlined spillways.

In light of our research findings, a comprehensive exploration of hydraulic erodibility has revealed noteworthy insights. Hydraulic erodibility is thoroughly involved in two key dimensions: erosive and resistive aspects. The erosive dimension pertains to hydraulics, while the resistive aspect delves into geomechanics in the context of hydraulic erodibility. Our research significantly emphasizes the erosive impact through the modification of the unit stream power dissipation equation, a crucial factor in the design of hydraulic structures. Based on this research, the assessment of hydraulic erodibility in unlined dam spillways can be improved by considering irregularities in the rock surface (angle and height) and the slope of unlined spillways. This refinement brings calculations closer to reality, reducing uncertainty and mitigating project risks economically and in terms of safety. This optimization empowers hydraulic engineers to refine and optimize their designs. Furthermore, the outcomes of our research can be used to modify various parameters in existing methodologies. For instance, the NPES parameter in the Pells method can be adjusted, providing researchers with greater flexibility to employ our equations and research outcomes for more precise evaluations. By enhancing and refining existing methods, a substantial step can be taken toward aligning these methodologies more closely with real-world scenarios.

In conclusion, this research advances our understanding of rock mass erosion in hydraulic structures. The findings underscore the importance of considering surface irregularities, provide guidance for future research endeavors, and present improved equations for more accurate predictions of hydraulic parameters. By incorporating these advancements, engineers and designers can enhance the safety and efficiency of water management systems.

5.3 PERSPECTIVES FOR FUTURE RESEARCH

In order to advance the field of hydraulic erodibility assessment, several potential avenues for future research can be explored. These include:

- It is strongly recommended to complement these analytical and numerical approaches with laboratory and field (in-situ) investigations for comprehensive verification and validation of the results. Integrating experimental data obtained from laboratory studies and real-world field conditions would not only strengthen the reliability of the mathematical analyses but also contribute to a more holistic understanding of the hydraulic erodibility dynamics in unlined spillways.
- Analysis of spillway geometry: Further investigation into the impact of spillway geometry on the hydraulic erosive parameter is warranted. Analyzing various spillway shapes, dimensions, and cross-sectional profiles can provide valuable insights into how these geometric factors influence erosion behavior. This analysis can contribute to the refinement of erosion prediction models.
- Evaluation of geometrical and geomechanical parameters: It is crucial to assess the effect of both geometrical and geomechanical parameters of the rock mass on the hydraulic erosive parameter. This entails a comprehensive examination of factors such as joint characteristics, rock mass stability, and material properties to gain a deeper understanding of their influence on erosion potential.
- Assessment of shear stress within joints: A thorough evaluation of shear stress within joints can enhance understanding of the role of joint characteristics in erosion processes. This assessment can help identify critical locations and contribute to the development of more accurate erosion prediction models.
- Examination of pressure and uplift forces: Analyzing the pressure and uplift forces applied on rock blocks can provide valuable insights into their stability and vulnerability to erosion. Understanding these forces is crucial for assessing erosion risks and designing appropriate mitigation measures.
- Creation of 3D models: Developing three-dimensional models can enable a more comprehensive evaluation of additional parameters that influence hydraulic erosive behavior. By incorporating the third dimension, a more realistic representation of flow patterns and erosion mechanisms can be achieved.
- Utilization of Fluid-Structure Interaction (FSI) methods: The application of Fluid-Structure Interaction (FSI) methods can facilitate the development of a representative hydraulic erosive parameter that considers all relevant geometrical and geomechanical parameters of spillways and rock masses. These methods allow for a coupled analysis of fluid flow and structural response, enabling a more accurate assessment of erosion potential.
- By pursuing these research directions, the field can advance in terms of accurately assessing hydraulic erosive parameters in relation to spillway irregularities, geometric factors, and rock mass characteristics. These advancements will contribute to the refinement of erosion prediction models, ultimately aiding in the design and management of hydraulic structures.

REFERENCES

1. Pells, S. Erosion of Rock in Spillways. Ph.D. Thesis, UNSW Sydney, Sydney, Australia, 2016. Available online (09 November 2021): <http://handle.unsw.edu.au/1959.4/56008>.
2. Rock, A.J. *Semi-Empirical Assessment of Plunge Pool Scour: Two-Dimensional Application of Annandale's Erodibility Index Method on Four Dams in British Columbia, Canada, A*; Colorado School of Mines. Arthur Lakes Library: Golden, CO, USA, 2015.
3. Bollaert, E. The Comprehensive Scour Model: Theory and Feedback from Practice. In Proceedings of the 5th International Conference on Scour and Erosion, San Francisco, CA, USA, 7–10 November, 2010.
4. Atkinson, B.K. *Fracture Mechanics of Rock*; Academic Press: Cambridge, MA, USA, 1987.
5. Mason, P.J.; Arumugam, K. Free Jet Scour Below Dams and Flip Buckets. *J. Hydraul. Eng.* **1985**, *111*, 220–235. [https://doi.org/10.1061/\(asce\)0733-9429\(1985\)111:2\(220\)](https://doi.org/10.1061/(asce)0733-9429(1985)111:2(220)).
6. Akhmedov, T.K. Calculation of the depth of scour in rock downstream of a spillway. *Int. Water Power Dam. Constr.* **1988**, *40*, 25–27.
7. Breusers, H.; Raudkivi, A. *Scouring. IAHR Hydraulic Structures Design Manual 2*; AA Balkema: Rotterdam, The Netherlands, 1991.
8. Aderibigbe, O.; Rajaratnam, N. Erosion of loose beds by submerged circular impinging vertical turbulent jets. *J. Hydraul. Res.* **1996**, *34*, 19–33. <https://doi.org/10.1080/00221689609498762>.
9. Tan, S.; Raudkivi, A. *Erosion of Cohesive Soils: A Report Submitted to the National Water and Soil Conservation Authority*; Department of Civil Engineering, University of Auckland: Auckland, New Zealand, 1984.
10. Kamphuis, J.W. Influence of sand or gravel on the erosion of cohesive sediment. *J. Hydraul. Res.* **1990**, *28*, 43–53. <https://doi.org/10.1080/00221689009499146>.
11. Hanson, G.J. Surface Erodibility Of Earthen Channels at High Stresses Part I—Open Channel Testing. *Trans. ASAE* **1990**, *33*, 0127–0131. <https://doi.org/10.13031/2013.31305>.
12. Hairsine, P.B.; Rose, C.W. Modeling water erosion due to overland flow using physical principles: 1. Sheet flow. *Water Resour. Res.* **1992**, *28*, 237–243. <https://doi.org/10.1029/91wr02380>.
13. Moren, L.; Sjoberg, J. Rock Erosion In Spillway Channels—A Case Study of the Ligga Spillway. In *11th ISRM Congress*; OnePetro: Lisbon, Portugal, 2007.
14. Hahn, W.; Drain, M. Investigation of the erosion potential of kingsley dam emergency spillway. In Proceeding of the Joint Annual Meeting and Conference of AIPG, AGWT, and the Florida Section of AIPG, Orlando, FL, USA, 2010.
15. Pells, S.E.; Pells, P.J.; Peirson, W.L.; Douglas, K.; Fell, R. Erosion of unlined spillways in rock—Does a “scour threshold” exist? In *Contemporary Challenges for Dams. Proceedings of the Annual Australian National Committee on Large Dams Conference*; ANCOLD, Brisbane, Australia. vol. 4, no. 8. 4–8 November 2015.
16. Annandale, G.W.; Wittler, R.J.; Ruff, J.F.; Lewis, T.M. Prototype validation of erodibility index for scour in fractured rock media. International Water Resources Engineering Conference (ASCE), Memphis, Tennessee, United States. August 3–7, 1998.

17. Annandale, G.W.; Kirsten, H.A. On the erodibility of rock and other earth materials. In *Hydraulic Engineering*; ASCE: 1994.
18. Kirsten, H.A.; Moore, J.S.; Kirsten, L.H.; Temple, D.M. Erodibility criterion for auxiliary spillways of dams. *Int. J. Sediment Res.* **2000**, *15*, 93–107.
19. Cengel, Y.A.; Cimbala, J.M. *Fluid Mechanics: Fundamentals and Applications*, 3rd ed.; CRC Press: Boca Raton, FL, USA, 2015
20. Kirsten, G.W. *Scour Technology: Mechanics and Engineering Practice*; McGraw-Hill: New York, NY, USA, 2006.
21. Annandale, G. Erodibility. *J. Hydraul. Res.* **1995**, *33*, 471–494.
22. Pitsiou, S. *The Effect of Discontinuities on the Erodibility of Rock in Unlined Spillways of Dams*; University of Pretoria, South Africa 1990.
23. Moore, J. The Characterization of Rock for Hydraulic Erodibility. In *Technical Release*; USDA: 1991; Volume 78.
24. Van Schalkwyk, A.; Jordaan, J.; Dooge, N. Erosion of rock in unlined spillways. *Int. Comm. Large Dams, Paris Q* **1994**, *71*, 555–571.
25. Bieniawski, Z. Engineering classification of jointed rock masses. *Civ. Eng. South Afr.* **1973**, *15*, 335–343.
26. Barton, N.; Lien, R.; Lunde, J. Engineering classification of rock masses for the design of tunnel support. *Rock Mech. Rock Eng.* **1974**, *6*, 189–236, <https://doi.org/10.1007/bf01239496>.
27. Kirsten, H. A classification system for excavating in natural materials. *Civ. Eng. = Siviele Ing.* **1982**, *24*, 293–308.
28. Kirsten, H. Case histories of groundmass characterization for excavatability. In *Rock Classification Systems for Engineering Purposes*; ASTM International; 1988.
29. Van Schalkwyk, A.; Jordaan, J.; Dooge, N. *Die Erodeerbaarheid Van Verskillende Rotsformasies Onder Varierende Vloeitoestande (No. WNK Verslag No. 302/1/95). Verslag Aan Die Waternavorsingskommissie Deur Die Departement of Geologie, Universiteit Van Pretoria, South Africa*; Universiteit Van Pretoria: Pretoria, South Africa, 1994.
30. Dooge, N. *Die Hidrouliese Erodeerbaarheid Van Rotsmassas in Ombelynde Oorlope Met Spesiale Verwysing Na Die Rol Van Naatvulmateriaal*; University of Pretoria: Pretoria, South Africa, 1993.
31. Moore, J.S.; Temple, D.M.; Kirsten, H. *Headcut advance threshold in earth spillways*. In Bulletin of the Association of Engineering Geologists; (United States); Volume 31(2), pp. 277-280, Jun 1994;
32. Jennings, J.; Brink, A.B.A.; Williams, A. Revised guide to soil profiling for civil engineering purposes in Southern Africa. *Civil Eng. = Siviele Ing.* **1917**, *15*, 3–13.
33. CECIL III, OWEN SINCLAIR. *Correlations of Rock Bolt-Shotcrete Support and Rock Quality Parameters in Scandinavian Tunnels*; University of Illinois at Urbana-Champaign: 1970.
34. Bandpey, A.K.; Shahriar, K.; Sharifzadeh, M.; Marefvand, P. Validation of 3D discrete fracture network model focusing on areal sampling methods—A case study on the powerhouse cavern of Rudbar Lorestan pumped storage power plant, Iran. *Geomech. Eng.* **2018**, *16*, 21–34.

35. Boumaiza, L.; Saeidi, A.; Quirion, M. Determining relative block structure rating for rock erodibility evaluation in the case of non-orthogonal joint sets. *J. Rock Mech. Geotech. Eng.* **2018**, *11*, 72–87. <https://doi.org/10.1016/j.jrmge.2018.06.010>.
36. Hoek, E.; Kaiser, P.; Bawden, W. *Support of Underground Excavations in Hard Rock AA BALKEMA; ROTTERDAM/BROOKFIELD: 1995*.
37. Bieniawski, Z. Rock mass classification in rock engineering applications. In Proceedings of the a Symposium on Exploration for Rock Engineering, Johannesburg, South Africa, 1–5 November 1976.
38. Saeidi, A.; Eslami, E.; Quirion, M.; Seifaddini, M. Assessment of rock mass erosion in unlined spillways using developed vulnerability and fragility functions. *Georisk Assess. Manag. Risk Eng. Syst. Geohazards* **2019**, *14*, 280–292. <https://doi.org/10.1080/17499518.2019.1660796>.
39. Douglas, K.; Pells, S.; Fell, R.; Peirson, W. The influence of geological conditions on erosion of unlined spillways in rock. *Q. J. Eng. Geol. Hydrogeol.* **2018**, *51*, 219–228. <https://doi.org/10.1144/qjegh2017-087>.
40. Jaeger, C. Über die Aehnlichkeit bei flussaulichen Modellversuchen. *Wasserkr. Wasserwirtsch.* **1939**, *34*, 269.
41. Yu, C. Investigation of scour and air entrainment by falling jets downstream of dam. *J. Hydraul. Eng.* **1963**, *2*.
42. Damle, P.; Venkatraman, C.; Desai, S. Evaluation of scour below ski-jump buckets of spillways. In *CWPRS Golden Jubilee Symposia*; Poona, India, 23–25 January 1966.
43. Mirtskhulava, T.E., Mechanism and Computation of Local and General Scour in Non-Cohesive, Cohesive Soils and Rock Beds, International Association for Hydraulic Research, No. XII, vol. 3, pp. 169-176, Fort Collins, Colorado, USA, September 1967.
44. Martins, R. Scouring of rocky river beds by free jet spillways. *Int. Water Power Dam. Constr.* **1975**, *27*, 152–153.
45. Taraimovich, I.I. Deformations of channels below high-head spillways on rock foundations. *Power Technol. Eng.* **1978**, *12*, 917–923. <https://doi.org/10.1007/bf02322089>.
46. Mason, P.J. Effects of Air Entrainment on Plunge Pool Scour. *J. Hydraul. Eng.* **1989**, *115*, 385–399. [https://doi.org/10.1061/\(ASCE\)0733-9429\(1989\)115:3\(385\)](https://doi.org/10.1061/(ASCE)0733-9429(1989)115:3(385)).
47. Liu, P. *Mechanism of Free Jet's Scour on Rocky River-Beds*; Higher Education Press: Beijing, China, 1994.
48. Chen, J.; Shi, B.; Wang, Q. 3-D network numerical modeling technique for random discontinuities of rock mass. *Chin. J. Geotech. Eng. Chin. Ed.* **2001**, *23*, 397–402.
49. Bombardelli, F.A.; Gioia, G. Scouring of granular beds by jet-driven axisymmetric turbulent cauldrons. *Phys. Fluids* **2006**, *18*, 088101. <https://doi.org/10.1063/1.2335887>.
50. Castillo, L.G.; Carrillo, J.M. Scour, Velocities and Pressures Evaluations Produced by Spillway and Outlets of Dam. *Water* **2016**, *8*, 68. <https://doi.org/10.3390/w8030068>.
51. Hartung, W. Die kolkbildung hinter überstromen wehren im hinblick auf eine beweglich sturzbettgestaltung. *Die Wasser Wirtsch.* **1959**, *49*, 309–313.
52. Chee, S.; Padiyar, P. Erosion at the base of flip buckets. *Eng. J. Can.* **1969**, *52*, 22–24.

53. Bisaz, E.; Tschopp, J. Profundidad de erosión al pie de un vertedero para la aplicación de corrección de arroyos en quebradas empinadas. In *Proceedings of the Fifth Congreso Latinoamericano de Hidraulica (IAHR)*, Lima, Peru, 23–28 October 1972.
54. Machado, L. O Sistema de Dissipacao de Energia Proposto para a Barragem de Xingo. In *Transactions of the International Symposium on the Layout of Dams in Narrow Gorges*; ICOLD: Rio de Janeiro, Brazil, 1982.
55. Ervine, D.; Falvey, H.; Withers, W. Pressure fluctuations on plunge pool floors. *J. Hydraul. Res.* **1997**, *35*, 257–279. <https://doi.org/10.1080/00221689709498430>.
56. Bollaert, E. Wall jet rock scour in plunge pools: A quasi-3D prediction model. *Intl. J. Hydropower Dams* **2012**, *2012*.
57. Bollaert, E.; Munodawafa, M.; Mazvidza, D. Kariba Dam Plunge Pool Scour: Quasi-3D Numerical Predictions. *La Houille Blanche* **2013**, *1*, 42–49, <https://doi.org/10.1051/lhb/2013007>.
58. Maleki, S.; Fiorotto, V. Blocks Stability in Plunge Pools under Turbulent Rectangular Jets. *J. Hydraul. Eng.* **2019**, *145*, 04019007. [https://doi.org/10.1061/\(asce\)hy.1943-7900.0001573](https://doi.org/10.1061/(asce)hy.1943-7900.0001573).
59. Bollaert, E.; Schleiss, A. *Transient Water Pressures in Joints and Formation of Rock Scour Due to High-Velocity Jet Impact*; EPFL-LCH: 2002.
60. Bollaert, E.F.; Lesleighter, E.J. Spillway rock scour experience and analysis—the Australian scene over the past four decades. In *11th National Conference on Hydraulics in Civil Engineering & 5th International Symposium on Hydraulic Structures: Hydraulic Structures and Society-Engineering Challenges and Extremes*; Engineers: Australia, 2014.
61. Bollaert, E.F.R.; Schleiss, A.J. Physically Based Model for Evaluation of Rock Scour due to High-Velocity Jet Impact. *J. Hydraul. Eng.* **2005**, *131*, 153–165. [https://doi.org/10.1061/\(asce\)0733-9429\(2005\)131:3\(153\)](https://doi.org/10.1061/(asce)0733-9429(2005)131:3(153)).
62. Bollaert, E.; Schleiss, A. Scour of rock due to the impact of plunging high velocity jets Part I: A state-of-the-art review. *J. Hydraul. Res.* **2003**, *41*, 451–464. <https://doi.org/10.1080/00221680309499991>.
63. Bollaert, E. A comprehensive model to evaluate scour formation in plunge pools. *Int. J. Hydropower Dams* **2004**, *11*, 94–101.
64. Bollaert, E.; Harris, J.; Whitehouse, R.; Moxon, S. Simplified comprehensive scour model compared to erodibility index method. **2016**, 549–558. <https://doi.org/10.1201/9781315375045-68>.
65. Ewalds, H.; Wanhill, R. *Fracture Mechanics-Delft*; Delftse UM: London, 1986.
66. Paris, P.C. A rational analytic theory of fatigue. *Trend Eng.* **1961**, *13*, 9.
67. Atkinson, B.K. Subcritical crack growth in geological materials. *J. Geophys. Res. Space Phys.* **1984**, *89*, 4077–4114. <https://doi.org/10.1029/jb089ib06p04077>.
68. Bollaert, E.; Morel, F.; Blancher, B.; Lucquiaud, P. Scour potential at Laouzas Dam. In *Proceedings of the ICSE 8th International Conference on Scour and Erosion*, Oxford, UK, 12–15 September 2016.
69. Pan, Y.-W.; Li, K.-W.; Liao, J.-J. Mechanics and response of a surface rock block subjected to pressure fluctuations: A plucking model and its application. *Eng. Geol.* **2014**, *171*, 1–10. <https://doi.org/10.1016/j.enggeo.2013.12.008>.

70. Bollaert, E.; Annandale, G.; Schleiss, A. *Scour of Rock Due to High-Velocity Jet Impact: A Physically Based Scour Model Compared to Annandale's Erodibility Index Method*; Lisse, Netherlands, Swets & Zeitlinger; ISBN: 90-5809-518-5, pp. 187–199, 2002.
71. Annandale, G.W. Rock Plunge Pools: A Design Approach for Limiting Scour Extent. In Proceedings of the 2nd International Conference on Scour and Erosion (ICSE-2), Singapore, 14–17 November 2004.
72. Manso, P.F.D.A. *The Influence of Pool Geometry and Induced Flow Patterns in Rock Scour by High-Velocity Plunging Jets*; EPFL: 2006.
73. Xavier Meriade Duarte, R. *Influence of Air Entrainment on Rock Scour Development and Block Stability in Plunge Pools*; EPFL: 2014.
74. Duarte, R.; Pinheiro, A.; Schleiss, A.J. An Enhanced Physically Based Scour Model for Considering Jet Air Entrainment. *Engineering* **2016**, *2*, 294–301. <https://doi.org/10.1016/j.eng.2016.03.003>.
75. Asadollahi, P. *Stability Analysis of a Single Three Dimensional Rock Block: Effect of Dilatancy and High-Velocity Water Jet Impact*; The University of Texas at Austin: 2009.
76. Federspiel, M.; Bollaert, E.; Schleiss, A. Response of an intelligent block to symmetrical core jet impact. In *33rd IAHR Congress "Water Engineering for a Sustainable Environment"*; IAHR: 2009.
77. Federspiel, M.P.E.A.; Bollaert, E.; Schleiss, A. Dynamic response of a rock block in a plunge pool due to asymmetrical impact of a high-velocity jet. In *Proceedings of the 34th World Congress of the International Association for Hydro-Environment Research and Engineering: 33rd Hydrology and Water Resources Symposium and 10th Conference on Hydraulics in Water Engineering*; Engineers: Australia, 2011.
78. Asadollahi, P.; Tonon, F.; Federspiel, M.P.; Schleiss, A.J. Prediction of rock block stability and scour depth in plunge pools. *J. Hydraul. Res.* **2011**, *49*, 750–756. <https://doi.org/10.1080/00221686.2011.618055>.
79. Martins, R. Contribution to the knowledge on the scour action of free jets on rocky river beds. In Proceedings of the 11th Congress on Large Dams, 1973.
80. Tonon, F. Analysis of single rock blocks for general failure modes under conservative and non-conservative forces. *Int. J. Numer. Anal. Methods Géoméch.* **2007**, *31*, 1567–1608. <https://doi.org/10.1002/nag.608>.
81. Bollaert, E.F.R. Numerical Modeling of Scour at Bridge Foundations on Rock. *Scour Eros.* **2010**, 767–776. [https://doi.org/10.1061/41147\(392\)76](https://doi.org/10.1061/41147(392)76).
82. Reinius, E. Rock erosion. *Int. Water Power Dam. Constr.* **1986**, *38*, 43–48.
83. George, M.F. *3D Block Erodibility: Dynamics of Rock-Water Interaction in Rock Scour*; UC Berkeley: 2015.
84. Beltaos, S.; Rajaratnam, N. Plane turbulent impinging jets. *J. Hydraul. Res.* **1973**, *11*, 29–59. <https://doi.org/10.1080/00221687309499789>.
85. Hartung, F.; Häusler, E. Scours, Stilling Basins and Downstream Protection under Free Overfall Jets at Dams; 11th ICOLD: Madrid, Spain, 1973; Volume 12.
86. Reich, F. Umlenkung eines Freien Flüssigkeitsstrahles an einer ebenen Platte. *Z. Ver. Dtsch. Ing.* **1927**, *71*, 261–264.

87. Lesleighter, E.; Bollaert, E.; McPherson, B.; Scriven, D. Spillway Rock Scour Analysis-Composite of Physical & Numerical Modelling; Paradise Dam, Australia, In B. Crookston & B. Tullis (Eds.), Hydraulic Structures and Water System Management. 6th IAHR International Symposium on Hydraulic Structures, Portland, OR. doi:10.15142/T300628160716 (ISBN 978-1-884575-75-4). (pp. 343-352), 27-30 June 2016.
88. Wibowo, J.; Lin, J. Stability Analysis of Spillways: Toward a Computational Approach. In *Powerpoint Presentation Taken from the Internet*; 2009.
89. Goodman, R.E.; Shi, G.-H. *Block Theory and Its Application to Rock Engineering*; 1985.
90. Li, A.; Liu, P. Mechanism of rock-bed scour due to impinging jet. *J. Hydraul. Res.* **2010**, *48*, 14–22, <https://doi.org/10.1080/00221680903565879>.
91. Dasgupta, B.; Basu, D.; Das, K.; Green, R. Development of computational methodology to assess erosion damage in dam spillways. In Proceedings of the 31st Annual United States Society on Dam Conference, 2011.
92. George, M.F.; Sitar, N. *Block Theory Application to Scour Assessment of Unlined Rock Spillways*; Report No UCB GT; University of California: Los Angeles, CA, USA, 2012; p. 12-02.
93. George, M.F.; Sitar, N. System reliability approach for rock scour. *Int. J. Rock Mech. Min. Sci.* **2016**, *85*, 102–111.
94. Gardner, M.H. *Development of a Coupled 3-D DEM-LBM Model for Simulation of Dynamic Rock-Fluid Interaction*; University of California: Berkeley, CA, USA, 2018.
95. Franke, P. *L'affouillement: Mécanisme et Formes*; Oesterreichische Wasserwirtschaft: 1960.
96. Mih, W.C. Equations for Axisymmetric and Twodimensional Turbulent Jets. *J. Hydraul. Eng.* **1989**, *115*, 1715–1719. [https://doi.org/10.1061/\(asce\)0733-9429\(1989\)115:12\(1715\)](https://doi.org/10.1061/(asce)0733-9429(1989)115:12(1715)).
97. Hoffmans, G.J. Jet scour in equilibrium phase. *J. Hydraul. Eng.* **1998**, *124*, 430–437.
98. Arnaboldi, C.; Artusa, D.; Avignone, F. III; Balata, M.; Bandac, I.; Barucci, M.; Beeman, J.; Brofferio, C.; Bucci, C.; Capelli, S. New Limit on the Neutrinoless $\beta\beta$ Decay of Te 130. *Phys. Rev. Lett.* **2005**, *95*, 142501.
99. Pagliara, S.; Amidei, M.; Hager, W.H. Hydraulics of 3D Plunge Pool Scour. *J. Hydraul. Eng.* **2008**, *134*, 1275–1284. [https://doi.org/10.1061/\(asce\)0733-9429\(2008\)134:9\(1275\)](https://doi.org/10.1061/(asce)0733-9429(2008)134:9(1275)).
100. Pagliara, S.; Hager, W.H.; Unger, J. Temporal Evolution of Plunge Pool Scour. *J. Hydraul. Eng.* **2008**, *134*, 1630–1638. [https://doi.org/10.1061/\(asce\)0733-9429\(2008\)134:11\(1630\)](https://doi.org/10.1061/(asce)0733-9429(2008)134:11(1630)).
101. Hoffmans, I.G.J. Closure problem to jet scour. *J. Hydraul. Res.* **2009**, *47*, 100–109.
102. Bollaert, E. Penstock Scour Formation At Bluestone Dam. In Proceedings of the 31st Annual USSD Conference and Exhibition, San Diego, CA, USA, 11-15 April 2011.
103. Pan, H.; Wang, R.; Huang, J.; Ou, G. Study on the ultimate depth of scour pit downstream of debris flow sabo dam based on the energy method. *Eng. Geol.* **2013**, *160*, 103–109. <https://doi.org/10.1016/j.enggeo.2013.03.026>.

104. Huang, M.; Liao, J.; Pan, Y.; Cheng, M. Modifications of the Erodibility Index Method for the Evaluation of the Soft Bedrock Erosion. In *47th US Rock Mechanics/Geomechanics Symposium*; American Rock Mechanics Association: 2013.
105. Tanaka, N.; Sato, M. Scoured depth and length of pools and ditches generated by overtopping flow from embankments during the 2011 Great East Japan Tsunami. *Ocean Eng.* **2015**, *109*, 72–82. <https://doi.org/10.1016/j.oceaneng.2015.08.053>.
106. Lai, X.; Yin, D.; Finlayson, B.; Wei, T.; Li, M.; Yuan, W.; Yang, S.; Dai, Z.; Gao, S.; Chen, Z. Will river erosion below the Three Gorges Dam stop in the middle Yangtze? *J. Hydrol.* **2017**, *554*, 24–31.
107. Wüthrich, D.; Chamoun, S.; Bollaert, E.; De Cesare, G.; Schleiss, A.J. Hybrid Modelling Approach to Study Scour Potential at Chancy-Pougny Dam Stilling Basin. In *Advances in Hydroinformatics*; Springer: Singapore, 2018; pp. 869–884.
108. Wu, T.; Pan, C.; Li, C.; Luo, M.; Wang, X. A field investigation on ephemeral gully erosion processes under different upslope inflow and sediment conditions. *J. Hydrol.* **2019**, *572*, 517–527. <https://doi.org/10.1016/j.jhydrol.2019.03.037>.
109. Bi, N.; Sun, Z.; Wang, H.; Wu, X.; Fan, Y.; Xu, C.; Yang, Z. Response of channel scouring and deposition to the regulation of large reservoirs: A case study of the lower reaches of the Yellow River (Huanghe). *J. Hydrol.* **2018**, *568*, 972–984. <https://doi.org/10.1016/j.jhydrol.2018.11.039>.
110. Dong, Y.; Xiong, D.; Su, Z.; Duan, X.; Lu, X.; Zhang, S.; Yuan, Y. The influences of mass failure on the erosion and hydraulic processes of gully headcuts based on an in situ scouring experiment in Dry-hot valley of China. *Catena* **2019**, *176*, 14–25. <https://doi.org/10.1016/j.catena.2019.01.004>.
111. Rong, G.; Tan, J.; Zhan, H.; He, R.; Zhang, Z. Quantitative evaluation of fracture geometry influence on nonlinear flow in a single rock fracture. *J. Hydrol.* **2020**, *589*, 125162. <https://doi.org/10.1016/j.jhydrol.2020.125162>.
112. Palermo, M.; Pagliara, S.; Bombardelli, F.A. Theoretical Approach for Shear-Stress Estimation at 2D Equilibrium Scour Holes in Granular Material due to Subvertical Plunging Jets. *J. Hydraul. Eng.* **2020**, *146*, 04020009. [https://doi.org/10.1061/\(asce\)hy.1943-7900.0001703](https://doi.org/10.1061/(asce)hy.1943-7900.0001703).
113. Palermo, M.; Bombardelli, F.A.; Pagliara, S.; Kuroiwa, J. Time-dependent scour processes on granular beds at large scale. *Environ. Fluid Mech.* **2021**, *21*, 791–816. <https://doi.org/10.1007/s10652-021-09798-2>.
114. Gioia, G.; Bombardelli, F.A. Localized Turbulent Flows on Scouring Granular Beds. *Phys. Rev. Lett.* **2005**, *95*, 014501–014501. <https://doi.org/10.1103/physrevlett.95.014501>.
115. Boumaiza, L.; Saeidi, A.; Quirion, M. A method to determine relevant geomechanical parameters for evaluating the hydraulic erodibility of rock. *J. Rock Mech. Geotech. Eng.* **2019**, *11*, 1004–1018. <https://doi.org/10.1016/j.jrmge.2019.04.002>.
116. Boumaiza, L.; Saeidi, A.; Quirion, M. A method to determine the relative importance of geological parameters that control the hydraulic erodibility of rock. *Q. J. Eng. Geol. Hydrogeol.* **2021**, *54*. <https://doi.org/10.1144/qjgeh2020-154>.
117. Koulibaly, A.S.; Saeidi, A.; Rouleau, A.; Quirion, M. Identification of Hydraulic Parameters Influencing the Hydraulic Erodibility of Spillway Flow Channels. *Water* **2021**, *13*, 2950.
118. Jalili Kashtiban, Y., et al., A Review on Existing Methods to Assess Hydraulic Erodibility Downstream of Dam Spillways. *Water*, 2021. 13(22): p. 3205.

119. Jalili Kashtiban, Y., Saeidi, A., Farinas, M.-I., and Patarroyo, J., (2022b, 2-5 October). Evaluation of the effect of rock surface irregularities on the hydraulic parameters of water in unlined dam spillways, *GeoCalgary 2022*, Calgary, Canada.
120. Darcy, H., *Recherches expérimentales relatives au mouvement de l'eau dans les tuyaux*. Vol. 1. 1857: Mallet-Bachelier.
121. Weisbach, J.L., *Lehrbuch der Ingenieur-und Maschinen-Mechanik: Theoretische Mechanik*. Vol. 1. 1845: Druck und Verlag von Friedrich Vieweg und Sohn.
122. Manning, R., et al., *On the flow of water in open channels and pipes*. 1890.
123. Khodashenas, S.R. and A. Paquier, A geometrical method for computing the distribution of boundary shear stress across irregular straight open channels. *Journal of Hydraulic Research*, 1999. 37(3): p. 381-388.
124. Prasad, B.V.R. and M.J. Russell, Discussion of "Diffusional Mass Transfer at Sediment-Water Interface" by Nancy Steinberger and Midhat Hondzo. *Journal of Environmental Engineering*, 2000. 126(6): p. 576-576.
125. Yang, S.-Q. and S.-Y. Lim, Boundary shear stress distributions in trapezoidal channels. *Journal of Hydraulic Research*, 2005. 43(1): p. 98-102.
126. Guo, J. and P.Y. Julien, Shear stress in smooth rectangular open-channel flows. *Journal of hydraulic engineering*, 2005. 131(1): p. 30-37.
127. Seckin, G., N. Seckin, and R. Yurtal, Boundary shear stress analysis in smooth rectangular channels. *Canadian Journal of Civil Engineering*, 2006. 33(3): p. 336-342.
128. Severy, A. and S. Felder. *Flow Properties and Shear Stress on a Flat-Sloped Spillway*. in *Proceedings of the 37th IAHR World Congress*, Kuala Lumpur, Malaysia. 2017.
129. Kashtiban, Y.J., K. Shahriar, and E. Bakhtavar, Assessment of blasting impacts on the discontinuities in a salt stope and pillar mine using a developed image processing. *Bulletin of Engineering Geology and the Environment*, 2022. 81(4): p. 1-14.
130. Lopez Jimeno, C.L.J.E.A.C.F.J., *Drilling and blasting of rocks*. 1995, Rotterdam, Netherlands; Brookfield, VT: A.A. Balkema.
131. Manual, U., *ANSYS FLUENT 12.0. Theory Guide*, 2009.
132. Hirt, C.W. and B.D. Nichols, Volume of fluid (VOF) method for the dynamics of free boundaries. *Journal of computational physics*, 1981. 39(1): p. 201-225.
133. Bombardelli, F.A., et al., Computations of curved free surface water flow on spiral concentrators. *Journal of Hydraulic Engineering*, 2001. 127(7): p. 629-631.
134. Lee, C.-H., C. Xu, and Z. Huang, A three-phase flow simulation of local scour caused by a submerged wall jet with a water-air interface. *Advances in Water Resources*, 2019. 129: p. 373-384.
135. Imanian, H. and A. Mohammadian, Numerical simulation of flow over ogee crested spillways under high hydraulic head ratio. *Engineering Applications of Computational Fluid Mechanics*, 2019. 13(1): p. 983-1000.
136. Li, Y., et al., Numerical Simulations of Hydraulic Characteristics of A Flow Discharge Measurement Process with A Plate Flowmeter in A U-Channel. *Water*, 2019. 11(11): p. 2382.
137. Laursen, E. M. (1958). The total sediment load of streams. *Journal of Hydraulic Engineering*, 84, 1-36.
138. Lacey, G. (1930). Stable channels in alluvium. *Minutes of the Proceedings of the Institution of Civil Engineers*, 229(1930), 259-292. doi:10.1680/imotp.1930.15592.
139. Bakhmeteff, B. A. (1932). *Hydraulics of open channels* (1st ed.). New York: McGraw-Hill.

140. Blench, T. (1952). Regime theory for self-formed sediment-bearing channels. *Transactions of the American Society of Civil Engineers*, 117(1), 383–400. doi:10.1061/TACEAT.0006641.
141. Laursen, E. M., & Toch, A. (1956). *Scour around bridge piers and abutments*.
142. Yalin, M. S. (1972). *Mechanics of sediment transport* (1st ed.): Pergamon Press.
143. Ackers, P., & White, W. R. (1973). Sediment transport: New approach and analysis. *Journal of the Hydraulics Division*, 99(11), 2041-2060. doi:10.1061/JYCEAJ.0003791.
144. Chanson, H. (1995). *Hydraulic design of stepped cascades, channels, weirs and spillways*. Oxford, UK: Pergamon Press.
145. Knighton, A. D. (1998). *Fluvial forms and processes: A new perspective*. London: Arnold.
146. Khodashenas, S. R., & Paquier, A. (1999). A geometrical method for computing the distribution of boundary shear stress across irregular straight open channels. *Journal of Hydraulic Research*, 37(3), 381-388. doi:10.1080/00221686.1999.9628254.
147. Jalili Kashtiban, Y., Shahriar, K., & Bakhtavar, E. (2022b). Assessment of blasting impacts on the discontinuities in a salt stope and pillar mine using a developed image processing. *Bulletin of Engineering Geology and the Environment*, 81(4), 151. doi:10.1007/s10064-022-02638-7.
148. Lopez, J. C., Lopez, J. E., & Ayala, C. F. J. (1995). *Drilling and blasting of rocks*. Boca Raton, FL: CRC Press.
149. Jalili Kashtiban Y, Saeidi A, Farinas M-I, Patarroyo J. Evaluation of the Effect of Surface Irregularities on the Hydraulic Parameters within Unlined Dam Spillways. *Water*. 2023; 15(16):3004. <https://doi.org/10.3390/w15163004>.

PUBLICATIONS

JOURNAL ARTICLES

A review on existing methods to assess hydraulic erodibility downstream of dam spillways. *Water*, 13(22), 3205, <https://doi.org/10.3390/w13223205>

Evaluation of the effect of surface irregularities on the hydraulic parameters within unlined dam spillways, *Water* 2023, 15(16), 3004; <https://doi.org/10.3390/w15163004>

Modification of the unit stream power dissipation (USPD) equation for unlined spillways considering geometrical parameters and surface irregularities, *Acta Geotechnica* (Under review)

CONFERENCE PAPERS

Evaluation of the effect of rock surface irregularities on the hydraulic parameters of water in unlined dam spillways, *GeoCalgary Conference*, October 2022, Calgary, Canada (Published)

Evaluation of the effect of rock surface irregularities on energy gradient in unlined dam spillways, *15th International ISRM Congress 2023*, October 2023, Salzburg, Austria (Accepted)

Appendix A: Supplementary data of article 1

Table A1. Result of the application of various semi-theoretical approaches on several case studies.

Name	H_{UD} (KW/m ²)	N	<i>eGSI</i>	<i>RMEI</i>	Kirsten et al. (2000) [18]	Van Schalkwyk et al. (1994b) [29]	Annandale (1995) [21]	Pells [1] (<i>eGSI</i>)	Pells [1] (<i>RMEI</i>)	Observed
Ant.1	1.7	867	47	1188	No Scour	Minor	Negligible	Negligible	Minor	Minor
Ant.2	0.8	575	47	243	No Scour	Negligible	Negligible	Negligible	Negligible	Negligible
Ant.3	0.7	867	47	1440	No Scour	Negligible	Negligible	Negligible	Minor	Minor
Ant.4	6.3	1902	42	1080	No Scour	Negligible	Negligible	Minor	Minor	Moderate
App.1	2.6	206	45	648	No Scour	Minor	Negligible	Minor	Negligible	Negligible
App.2	15	206	43	648	No Scour	Minor	Minor	Moderate	Minor	Minor
Bro.1	6.4	3720	67	1440	No Scour	Negligible	Negligible	Negligible	Moderate	Minor
Bro.2	28	2753	67	1296	No Scour	Negligible	Minor	Minor	Moderate	Moderate
Bro.3	42	2232	55	1152	No Scour	Minor	Minor	Moderate	Moderate	Moderate
Bro.4	56	2232	53	1080	No Scour	Minor	Minor	Moderate	Moderate	Moderate
Bro.5	28	5634	65	432	No Scour	Negligible	Negligible	Negligible	Minor	Negligible
Bro.6	37	7018	77	144	No Scour	Negligible	Negligible	Negligible	Negligible	Minor
Bro.7	56	2423	55	1440	No Scour	Negligible	Minor	Moderate	Large	Large
Bur.1	165	11413	82	252	No Scour	Negligible	Minor	Negligible	Negligible	Negligible
Bur.2	165	7855	80	288	No Scour	Negligible	Minor	Negligible	Minor	Negligible
Bur.3	165	6087	60	972	No Scour	Negligible	Minor	Moderate	Moderate	Moderate
Bur.4	165	3652	40	1890	No Scour	Negligible	Minor	Extensive	Extensive	Large
Cat.1	60	3709	72	567	No Scour	Negligible	Minor	Negligible	Minor	Minor
Cat.2	60	3709	72	126	No Scour	Negligible	Minor	Negligible	Negligible	Negligible
Cat.3	60	3709	72	567	No Scour	Negligible	Minor	Minor	Minor	Large
Cop.1	5.7	723	35	1620	No Scour	Minor	Negligible	Minor	Moderate	Moderate
Cop.2	4.7	8379	70	1755	No Scour	Negligible	Negligible	Negligible	Moderate	Minor
Cop.3	14	8379	65	1620	No Scour	Negligible	Negligible	Negligible	Moderate	Moderate
Cop.4	34.7	3724	32	1755	No Scour	Negligible	Minor	Large	Large	Large

Cop.5	76.1	3724	32	1755	No Scour	Negligible	Minor	Extensive	Extensive	Extensive
Cop.6	47.1	3724	25	1755	No Scour	Negligible	Minor	Extensive	Extensive	Extensive
Cop.7	66.1	3724	32	1755	No Scour	Negligible	Minor	Moderate	Extensive	Moderate
Cop.8	95	7914	67	1485	No Scour	Negligible	Minor	Minor	Large	Moderate
Cop.9	168	3724	32	1755	No Scour	Negligible	Minor	Extensive	Extensive	Large
Cop.10	650	3724	25	1755	Scour	Negligible	Extensive	Extensive	Extensive	Extensive
Cop.11	10	723	35	1620	No Scour	Minor	Minor	Moderate	Moderate	Minor
Cop.12	97	8379	70	1350	No Scour	Negligible	Minor	Minor	Large	Moderate
Cop.13	145	8379	65	1350	No Scour	Negligible	Minor	Moderate	Large	Moderate
Dar.1	18	4510	52	504	No Scour	Negligible	Negligible	Minor	Minor	Minor
Dar.2	18	4510	52	1080	No Scour	Negligible	Negligible	Moderate	Moderate	Moderate
Dar.3	18	4510	52	972	No Scour	Negligible	Negligible	Moderate	Minor	Moderate
Dar.5	9	4539	60	648	No Scour	Negligible	Negligible	Minor	Minor	Minor